Improving Surface and Materials Properties of Distillation Membranes for Water Desalination

by

Elizabeth Hjelvik-Warren

B.S., University of New Mexico, 2018

M.S., University of Colorado at Boulder, 2023

A thesis submitted to the

Faculty of the Graduate School of the

University of Colorado in partial fulfillment

of the requirement for the degree of

Doctor of Philosophy

Material Science and Engineering

2025

Committee Members:

Anthony Straub, Ph.D.

Michael Toney, Ph.D.

Yifu Ding, Ph.D.

Chunmei Ban, Ph.D.

Mark Hernandez, Ph.D.

Abstract

Hjelvik, Elizabeth (Ph.D., Materials Science and Engineering)

Improving Surface and Materials Properties of Distillation Membranes for Water Desalination

Thesis directed by Professors Anthony Straub and Michael Toney

There is an increased interest in implementing distillation membranes in desalination technologies due to their potential for high chemical resistance and ability to reject nonvolatile contaminants. Distillation membranes are typically hydrophobic in nature therefore, when they are submerged into a wastewater stream, an air liquid interface is formed and driving forces such as heat, pressure or concentration cause the water to evaporate at the interface and transport through the membranes as vapor water. This mechanism allows for full rejection of nonvolatile contaminants from the feed stream. While distillation membranes have benefits over commercial membranes, they also suffer drawbacks. Like most membranes distillation membranes are susceptible to the buildup of material on their surface, otherwise called fouling. This causes the eventual decline of the membrane's performance through either clogging of the membranes pores or water penetrating through the air-gap leading to pore wetting and eventual loss of the highly selective nature of these membranes. The purpose of this dissertation research is to understand the surface and materials properties of distillation membranes for their eventual application as air-gap membranes in desalination technologies. As a first objective, we aim to understand the full extent of commercial distillation membranes chemical resistance to oxidative disinfection chemicals. From this information, we probe methods to modify commercially available distillation membranes to prevent fouling and

wetting. We investigate how low power plasma technologies can create omniphobic surfaces to prevent pore wetting. Then we explore utilizing an atomic layer deposition process to create self-cleaning catalytically active distillation membranes to prevent fouling. Lastly, we explored ways to improve the flux of distillation membranes in pressure driven processes through the informed design of their pore structures. Overall, this dissertation research provides insight into the design and subsequent fabrication of highly oxidative resistant distillation membranes that can resist fouling and wetting.

Table of Contents

List of Figures

List of Tables

List of Equations

List of Supplementary Figures

List of Supplementary Tables

List of Supplementary Equations

Acknowledgements

To start off, I want to thank my advisors, Professors Anthony Straub and Michael Toney.

Tony, you took a chance on me by welcoming me into your group (via Zoom) during the COVID19 pandemic and I will forever be grateful for the multiple virtual writing sessions that supported me during my NSF GRF application.

Mike, thank you for advocating for me and helping me through the toughest of times during my graduate career, I would not be in graduate school still if it weren't for you.

My thesis committee members: Yifu Ding, Chunmei Ban and Mark Hernandez. Thank you for the time you are taking out of your busy schedules to serve on my committee and provide input on my research.

The brilliant researchers that offered me technical support through my Ph.D.: Tomoko Borsa, Adrian Gestos and David Bergsman.

Tomoko and Adrian, from your expertise, training, and technical advice I have become an absolute SEM and XPS wizard. David, my vacuum chamber simply would not exist if it weren't for your willingness to chat and advise (all the way from Washington) as I designed and built the chamber on my own. I will miss our surface science chats at conferences.

My Straub lab coworkers: Hannah Cairney, Trisha Nickerson, Omar Larris, Mohammad Allouzi, Yukai Tomosovic, Kian Lopez, and Sangsuk Lee.

Hannah you are and always will be my favorite collaborator. Trisha there are not enough words in the world to describe the impact your advocacy and support have had on my graduate career.

My Toney lab coworkers, there are way too many of you to list in this section. I will miss regular group lunches and office banter. A special shout out to my Toney group collaborators Samuel Marks and Bryce Knutson.

My countless mentors I have had throughout my science career: Paul Durfee, Aaron Anderson, Achraf Noureddine, Christina Salas, and Dale Huber

My wonderful friends who have stuck by my side, believed in me, and provided me unwavering support through every failed experiment and challenging time in graduate school: Hunter Simonson, Chris Torres, Matt Ticknor, Samuel Johnson, and many more.

My mom, dad, brother and nephew. Your support through my career has helped me get to this point.

My husband Michael, you have been my calm in this storm and have always been my hand to hold in the dark. Thank you for being my weirdo in this wild, wild journey. And finally, my little terror cats Renfri and Tortilla, your cuddles and chaos have kept my mind sane.

*“It is not only the steps forwar**d** that we must accept. It is the stumbles. The trials. The knowledge th**a**t we will fail…. But if we stop, if we accept the pe**r**son we are when we fall, the journey ends. That failure becomes our destination. To lo**v**e the journey is to accept no such end. I have found, through painful experience, that the most important step a person can take is always the next **o**ne**.”***

-Brandon Sanderson, Oathbringer

1. Motivation and outline

There is an increased interest in implementing distillation membranes in desalination technologies due to their potential for high chemical resistance and ability to reject nonvolatile contaminants. To realize the benefits of distillation membranes in desalination, they must be sufficiently designed to address their propensity for fouling and wetting while retaining their high selectivity and their high chemical resistance. The purpose of this dissertation research is to understand the surface and materials properties as well as the design parameters of distillation membranes for their eventual application as air-gap membranes in desalination technologies.

As a first objective, we aim to understand the full extent of commercial distillation membranes chemical resistance to oxidative disinfection chemicals. Water treatment trains integrate chemicals and membranes into a multistep process. However, current commercial membranes such as polyamide have been found to suffer severe degradation from chemicals primarily due to the amide bond present in polyamide. Distillation membranes are often believed to have high chemical resistance due to their chemical structure being comprised of fluorocarbons or hydrocarbons. However, their chemical resistance to pretreatment chemicals has yet to be tested. Therefore, we probed how high exposure of chemical oxidants would impact performance, materials, and chemical properties of commercial distillation membranes. From this study, we found that fluoropolymer membranes yielded higher oxidation resistance than membranes comprised of only hydrocarbons.

Once we understood the chemical resistance of commercially available distillation membranes, we wanted to probe methods to modify distillation membranes to prevent

fouling and wetting. Fouling is a universal issue in membranes systems, fouling on distillation membranes can lead to the eventual intrusion of water into the membrane pores leading to catastrophic failure. Therefore, we were interested in probing surface modification methods that could improve distillation membranes anti-fouling and anti-wetting ability.

As a step to address wetting, we demonstrated a quick and efficient method to create nanostructures on a PTFE membrane utilizing a low power oxygen plasma process. The plasma modified membranes showed higher wetting resistance to low surface tension liquids. Then to further inform surface design processes for antiwetting membranes we probed into the nanotexture formation mechanism and found that plasma is locally heating the top surface thus leading to the texture formation. Then as a step to prevent fouling, we explored creating catalytic coatings on the membrane top surface with atomic layer deposition. We found that we were able to successfully coat a PTFE membrane with TiO_2 without impacting the membrane's overall wettability. Additionally, the TiO_2 coated membranes demonstrated catalytic degradation of a model dye molecule after exposure to UV light.

Finally, we explored how to increase water fluxes in distillation membranes. Overall, design parameters such as pore size, shape, and length can help address the critical need for higher permeability distillation membranes. Overall, this dissertation aimed to improve distillation membrane performance through understanding the oxidation properties of current distillation membranes, improving the surfaces for antiwetting and antifouling properties and probing how the membranes physical parameters such as pore size, shape and length can improve overall permeability of the membrane.

2. Water scarcity, desalination, and membrane technologies.

2.1. Water scarcity and current desalination technologies

In recent years, the ability to provide clean water to global populations has become a substantial challenge. With freshwater sources declining due to declining water sources and increasing water demand, populations across the world have begun to experience critical water stress.[1] Due to this global water scarcity, there has become a significant need in developing technologies that are able to create clean water outside of the natural hydrological cycle.[2]

Presently, membrane-based technologies have been widely implemented in water purification and desalination to treat unconventional water sources.[3] Membrane desalination is defined as the process in which salt and minerals are removed from water through a semi-permeable membrane. Current membrane technologies include microfiltration, nanofiltration, and reverse osmosis (RO) processes, with RO being widely used in brackish and seawater desalination.[4] In RO, the thin film composite membranes, commonly polyamide, Figure 1A, and historically cellulose acetate, are able to achieve rejections of monovalent ions, such sodium and chloride, that are greater than 99%.[4,5] In addition to their high rejection, polyamide membranes have been shown to have relatively high performance in recovering clean water.

Desalination membranes technologies can be broadly separated into liquid-filled or air-gap membranes, with RO membranes being considered liquid-filled membranes.[6] Transport through the membrane's has been suggested to follow the solution- diffusion model, Figure 1B. According to this model, for water to move across the membrane it first

must absorb into the polymer network, then diffuse through the membrane and eventually experiencing desorption on the permeate side. [4,6]

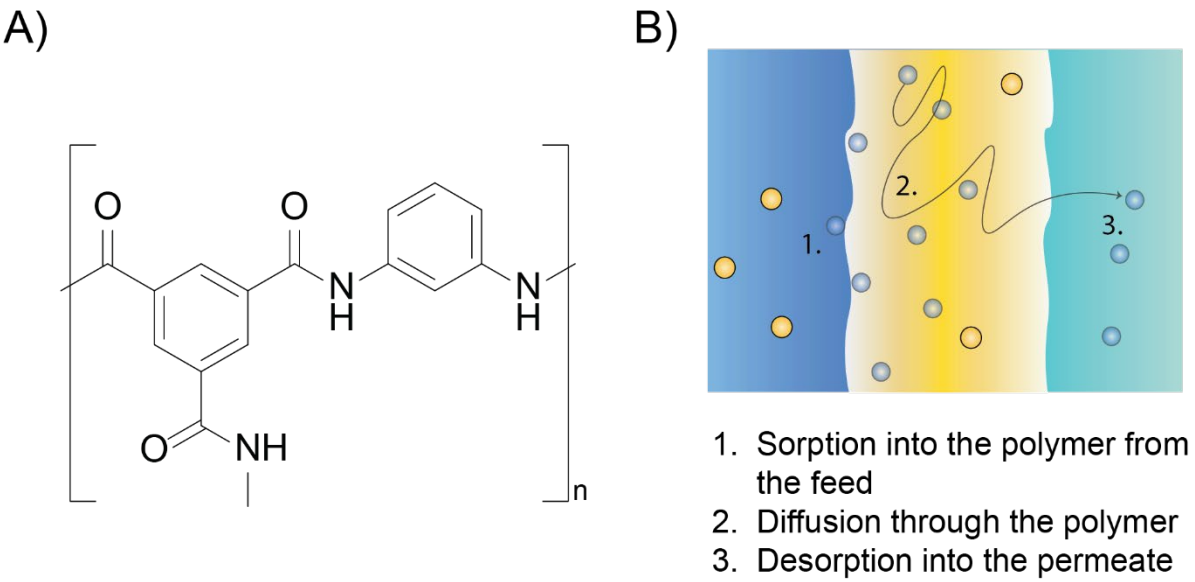

Figure 1: A) Polyamide structure B) Schematic of transport of water through liquid filled (PA) membrane.

Equation 1 explains the parameters that impact flux through an liquid filled membrane, where $J_{w,l}$ is defined as liquid flux through the membrane, L is the permeability coefficient, p is the transmembrane pressure difference, and π is the osmotic pressure difference between the feed and product water (permeate). The permeability coefficient is defined in equation 1.1, where D is the water diffusivity, S is water solubility, V is water partial molar volume, and l is the membrane thickness.

$$J_{w,l} = L(\Delta p - \Delta \pi) \qquad \text{Eq 1.0}$$

$$L = \frac{DSV}{RTl} \qquad \text{Eq 1.1}$$

$$\pi = CRT \qquad \text{Eq 1.2}$$

Equation 1: Liquid filled membrane flux equations.

Osmotic pressure is reliant upon the solution concentration and temperature and for simplicity we simplify osmotic pressure to a thermodynamically ideal solution, defined in equation 1.2, where C is the ion concentration, R is the ideal gas constant and T is the operating temperature. RO processes typically operate at high pressure to account for the difference in osmotic pressure between the feed and permeate side. RO technologies have found significant use in processing seawater and brackish water. In seawater, osmotic pressure can range from 23-35 barr and brackish water 1-3 barr. Therefore, to overcome the osmotic pressure and drive transport through RO membranes, feed pressures can range from 60-80 and 6-30barr, for seawater and brackish water respectively.

Permeability in liquid filled membranes is inversely proportional to membrane thickness and can be theoretically higher than current observed values. However, even though in theory, RO membranes can reach higher water permeabilities, it has been found that through increasing the permeability there is a loss in selectivity due to a permeability-selectivity trade-off.[6]

While RO has been widely implemented in desalination plants worldwide, there are significant issues with the membranes used. Polyamide RO membranes are faced with an inevitable decline in performance due to fouling or the buildup of materials on the surface. Presently in desalination, pretreatment steps that add oxidative or chlorine containing chemicals to feed streams have been pursued to help reduce fouling. However, it has been found these chemicals interact with the amide linkage thus leading to unfavorable degradation of the polyamide membrane and a loss in performance. [7,8] Additionally, while there is a high rejection of salts in RO, low molecular weight neutral

compounds have low rejections. This is believed to be due to these compounds having smaller hydrodynamic radius's than hydrated ions.[9] Therefore, new membrane materials must be pursued to address these drawbacks and a potential alternative that has been found is hydrophobic distillation membranes.

2.2. Distillation membranes

Distillation membranes are different from RO membranes in that they are considered air-gap because of their hydrophobic nature. When submerged into a wastewater stream, an air-liquid interface is formed at the entry of the pore. Driving forces such as heat (membrane distillation) pressure (pressure driven distillation) or concentration (osmotic distillation) cause the water to evaporate at the interface and travel through the membranes as vapor water.[6] Eventually the water condenses on the permeate side as pure water. This mechanism allows for full rejection of nonvolatile contaminants from the feed stream. It has been shown that air-gap membranes can reject contaminants such as urea, boron, and N-Nitrosodimethylamine (NDMA) all of which have low selectivity in RO technologies.[10] Additionally, the rejection of salt with distillation membranes remains high like salt rejection in RO. In addition to their high selectivity of nonvolatile contaminants, distillation membranes are believed to be highly resistant to chemical degradation, which stems from their chemical structures. Commercial distillation membranes that have been studied for desalination include polytetrafluoroethylene (PTFE), polyvinylidene fluoride (PVDF) and polypropylene (PP), Figure 2B.[11]

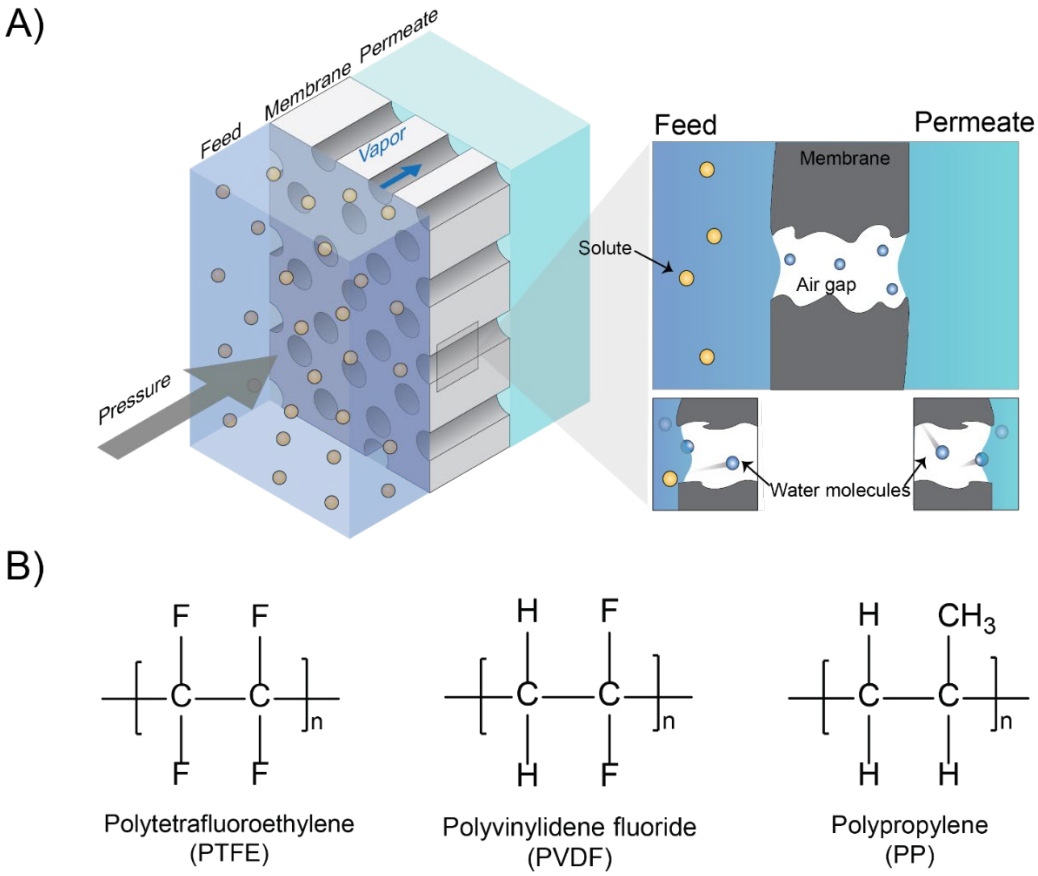

Figure 2: A) Schematic of water transport through air-gap membranes. B) Structures of common polymeric air filled membranes.

In polyolefin polymers like polypropylene, they are comprised of carbon-carbon and carbon-hydrogen bonds. Since carbon and hydrogen have similar electronegativities they are less prone to breaking especially in comparison to the amide linkage in polyamide. For carbon-hydrogen bonds, the ability to break the bond, bond dissociation energy, is reliant upon the number of pendant groups attached to the carbon. For instance, carbons that are bound to four hydrogens have a bond energy of 493.3 kJ/mol where carbons bound to one hydrogen have a bond energy of 403.8 kJ/mol.[12] Then for fluoropolymers, PTFE and PVDF, they are comprised of a carbon-carbon backbone decorated with

fluorine pendant groups. The size of the fluorine atom provides uniform coverage over the carbon-carbon backbone and therefore protects the backbone from chemical attack.[13,14] Within the carbon-fluorine bond, the electron density is concentrated around the fluorine since it is a high electron withdrawing atom. This in turn leaves carbon electron poor which introduces an ionic character via the partial charges of the carbon and fluorine.[15,16] Since carbon and fluorine are covalently bound the addition of the partial ionic character leads to a large overall bond dissociation energy of 544 kJ/mol. [17,18] Table 1 summarize the structures and bond dissociation energies (BDE) of the different polymer membranes used in desalination. Overall, distillation membranes address the two main drawbacks of RO membranes, however there is still a need to sufficiently understand and design distillation membranes where they can perform similarly to RO while also retaining long term performance.

Table 1: Desalination membranes and the bond energies

Membrane	Structure	Bond	BDE (kJ/mol)
Polyamide	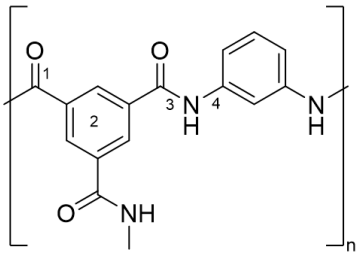	1	749
		2	473
		3	386
		4	305
Polypropylene	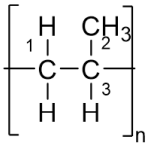	1	452
		2	473
		3	337.5
Polyvinylidene fluoride	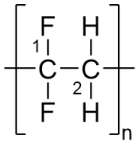	1	414.5
		2	481
Polytetrafluoroethylene	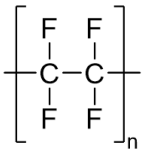	1	481

2.3. Design issues in distillation membranes:

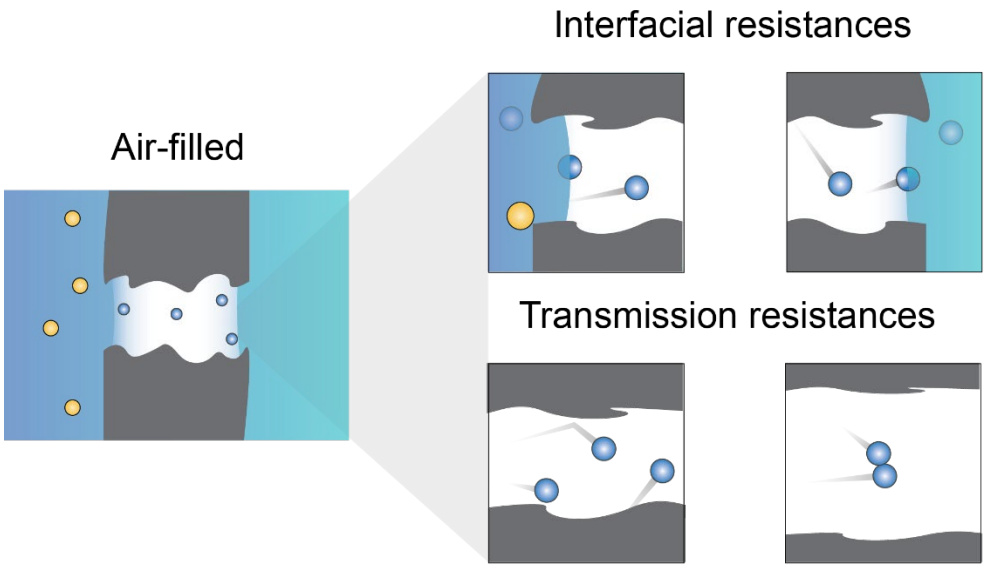

Figure 3: Schematic of liquid versus air filled membranes and associated resistances in air filled membranes

$$J_{w,v} = B_w(p_f - p_p) \qquad \text{Eq. 2.0}$$

$$B_w = \varepsilon\sqrt{\frac{M_w}{2\pi RT}}\left[R_t + R_{i,f} + R_{i,p}\right]^{-1} \qquad \text{Eq. 2.1}$$

$$R_i = \frac{1-\sigma(T)}{\sigma(T)} \qquad \text{Eq. 2.2}$$

$$R_t = \frac{\left(1-\frac{p_0(T)}{p_t}\right)v_w l}{4D_{wa}} + \frac{1}{\eta} \qquad \text{Eq. 2.3}$$

Equation 2: Air filled membranes flux equations.

When compared to liquid filled membranes, air filled membranes have significantly lower permeabilities. For air filled membranes to match liquid filled membranes

permeability performance they must be sufficiently designed to address their low fluxes. Vapor transport is well described by theory and the flux through vapor gap membranes is defined in equation 2.0, as a product of the vapor permeability coefficient (Bw, eq 2.1) and the partial vapor pressure difference between the feed and permeate sides of the membrane (p_f and p_p respectively). Vapor permeability, eq 2.1, is based off membrane porosity (ε), the molar mass of water (M_w), the universal gas constant (R), temperature of the system (T), and the inverted sum of the system resistances. R_t corresponds to the transmission resistances in the system, and $R_{i,f}$ and $R_{i,p}$ correspond to the interfacial resistances that occur on the feed and permeate side of the membrane respectively.[6,19] Interfacial resistances, R_i (eq. 2.2), occur on the vapor-liquid interfaces. These resistances stem from the required phase changes, evaporation on the feed and condensation on the permeate, that the water molecules undergo on each side of the membrane. In equation 2.2 the value of interfacial resistance is reliant upon the condensation coefficient, or the fraction of molecules that condense when they hit a gas-liquid interface.[6,19–21] Since this coefficient is reliant upon the phase changes that occur on the liquid-air interfaces it is difficult to lower the resistances that occur due to the interfacial resistances. Therefore, distillation membranes may be inherently limited in their water permeabilities.[6]

Transmission resistances, R_t, are the resistances that molecules encounter as they transmit through the membrane and are defined in equation 2.3 where $p_0(T)$ is the vapor pressure of water at temperature T, p_t is the pressure of gas in the membrane pores, v_w is mean molecular speed of water vapor, $D_{w,a}$ is diffusion coefficient of water in air, l is membrane thickness and η is transmission probability.[20] The transmission probability

term, η, describes the probability of a gas molecule leaving one liquid-vapor interface of the membrane and arriving at the liquid-vapor interface on the other side of the membrane. Previous studies related η to the pore aspect ratio, which is defined as the length of the pore, l, divided by the pore radius, a.[22] Namely it was found that as the pore aspect ratio increases, the transmission probability decreases which in turn leads to an increase in transmission resistance. As a result, it has been suggested that altering membrane pore shape and structure can help reduce resistance thus increasing the overall permeability.[21]

Fouling in distillation membranes

Fouling is a universal issue amongst membranes, but it particularly impacts hydrophobic membranes as it leads to pore wetting, the penetration of water penetrating through the air-gap pores, leading to a catastrophic loss of selectivity. Foulants can be broadly separated into inorganic, organic or biological compounds, Figure 4.[23,24] There are five theorized mechanisms in which fouling can occur: pore blocking, cake formation, ligand exchange reaction, charge interaction and hydrophobic interaction[23,25].

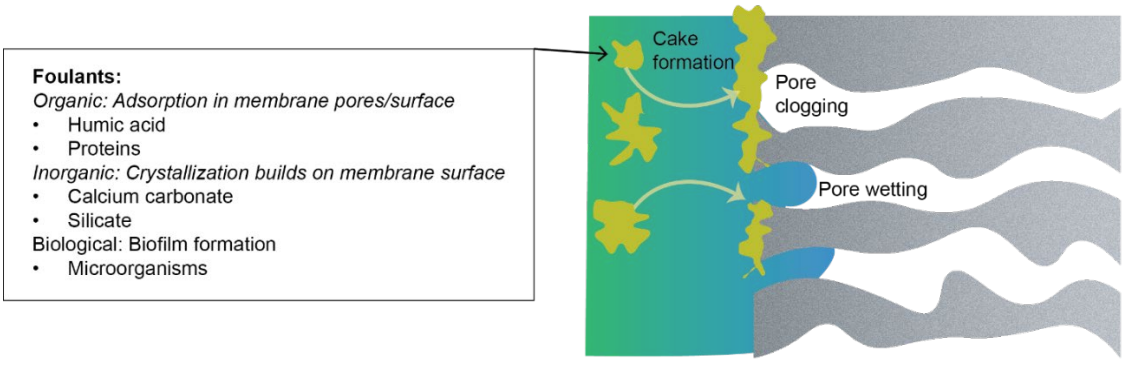

Figure 4: Schematic of fouling on membrane and list of common inorganic, organic and biological foulants.

Amongst these five, hydrophobic interactions have been generally accepted as a primary fouling mechanism. In hydrophobic interactions, foulants with hydrophobic tail moiety's such as amphiphilic organic materials or biological molecules will absorb on the surface and pores of distillation membranes due to hydrophobic-hydrophobic interactions.[24,26–28] The impact of hydrophobicity on fouling propensity has been debated, as some studies report contradicting results stating hydrophobic surface resist fouling more readily than hydrophilic surfaces.[29–31] However, even with the conflicting results there is to be a general understanding that hydrophobic membranes are less likely to have fouling layer reversibility than hydrophilic membranes[25], and increasing their hydrophilicity can aid in anti-fouling behaviors. [32–36]

However, hydrophobic membranes offer a unique challenge in introducing antifouling behavior to their surface, in that they may also retain their overall hydrophobicity after being coated with hydrophilic coatings. Several groups have explored methods to reduce fouling in MD membrane by physically depositing a hydrophilic thin film on the top surface through methods such as casting, dip coating, and spin coating.[37–40] While these methods provide a facile means to deposit antifouling layer, their long-term robustness is questioned as they rely on weak chemical interactions such as van der Waals forces to ensure attachment.[41] To address the potential lack of robustness in these films, there has been interest in utilizing chemical surface chemistry methods such as chemical vapor deposition or atomic layer deposition, where chemistries will be covalently bound to the membrane surface.[42] Chapter 5 explores more in depth the benefits of these surface chemical methods. While these chemical methods are an attractive means to create

antifouling coatings, they have also been found to unfavorably change the polymer mechanical properties and change the overall hydrophobicity.[43–45]

Wetting in distillation membranes

Wetting in porous materials can be experimentally understood through the Young-LaPlace liquid entry pressure (LEP) equation, eq 3.0, where γ_{LV} is defined as the surface energy between the liquid and gas phases, θ_{eq} correspond to the equilibrium water contact angle on the membrane surface and r is the membrane pore radius. Per equation 3.0, a decrease in LEP can occur due to a loss of hydrophobicity, an increase in pore size, and a decrease in surface tension of a feed solution. [46]

$$LEP = \frac{2\gamma_{LV} cos\theta_{eq}}{r} \qquad \text{Eq. 3.0}$$

Equation 3: Liquid entry pressure (LEP) equation.

While the Young-Laplace offers a simplified means to understand the parameters that impact wetting, it is typically more accurate for membranes with cylindrical continuous pores. For polymeric membranes such as PTFE, PVDF, and PP where the pore is considered voids between fibers, models such as the Purcell model, SI equation 1.0, are more accurate.[47] Pore wetting and fouling are often interrelated as fouling can lead to a decrease in hydrophilicity, thus decreasing a membrane overall LEP. However, wetting can also occur due to the inclusion of low surface tension liquids in a solution. There has been significant research done into creating surfaces that can help resist wetting due to low surface tension liquids, and it primarily focuses on creating omniphobic structures on the membrane surface[48,49], which will be discussed in Chapter 4. However, similar to creating antifouling coatings, methods to creating robust omniphobic structures need to

be centralized to the top surface and not impact the distillation membranes overall properties.

Overall, distillation membranes are an attractive alternative to current RO polyamide. However, while they excel in selectivity and oxidation resistance, they also suffer in their low fluxes and their susceptibility to catastrophic failure due to pore wetting which can occur from fouling on the surface. To meet their full potential, there is a need to explore methods that can aid in creating robust antifouling and antiwetting distillation membranes. Additionally, even though commercial hydrophobic membranes are comprised of chemical oxidation resistance, there is interest in understanding the extent of their oxidation resistance.

3. Oxidation resistance of hydrophobic porous membranes used in membrane distillation

This section is adapted from a submitted and published manuscript in the American Chemical Society Applied Engineering Materials Journal by Elizabeth A. Hjelvik, H.T. Cairney and A.P. Straub titled Impact of Oxidative Chemicals on Hydrophobic Porous Membranes Used in Membrane Distillation. H.T. Cairney performed the experiments presented section 3.3.3 Desalination performance testing and the contact angle data presented in Figure 3.

3.1. INTRODUCTION

Anthropogenic climate change has contributed to worsening drought conditions and decreased the reliability of water supplies.[50] Water reuse and desalination offer secure and consistent water supplies outside the natural hydrological cycle that can supplement existing water resources. [51] Membrane-based technologies have been increasingly implemented for advanced water treatment due to their high energy efficiency and ease-of-implementation. [3,6] However, fouling from contaminants in feedwater is a persistent challenge that limits the performance of membrane-based systems, increasing the cost of water treatment by necessitating intensive pre-treatment processes and reducing membrane lifetime.

The use of oxidative disinfectants upstream of a membrane process is an effective technique to reduce fouling and enhance water treatment performance. [52] Chlorination or ozonation of feedwater inactivates microbes before they reach the membrane surface, preventing biofilm formation and the associated performance decline due to biofouling.[53]n Strong oxidants can also transform organic matter into more hydrophilic materials that

have a lower fouling propensity. [54] Furthermore, strong oxidation combined with membrane processes may enhance removal of contaminants in the feed water. [55] Therefore, implementing strong oxidation upstream of, or directly in contact with, membranes used in advanced water treatment is highly desirable.

Although strong oxidants have the potential to enhance membrane performance, materials commonly used in salt-rejecting membranes, such as polyamide and cellulose acetate, degrade when exposed to strong oxidizing agents such as chlorine and ozone. [5,56–58] Disinfection pretreatment strategies upstream of these membranes are therefore limited to the use of chloramines, weaker disinfectants that reduce the effectiveness of downstream ultraviolet treatment processes and are associated with the formation of highly toxic disinfection byproducts, including N-nitrosodimethylamine.[59,60]Alternatively, chlorine is sometimes used upstream of membrane systems, but a costly dechlorination step must be implemented prior to reverse osmosis (RO) to protect the membranes. The development of membrane materials that withstand exposure to strong oxidants is therefore a well-acknowledged need in the field of membrane separations.

Hydrophobic porous membranes used in membrane distillation (MD), osmotic distillation, and pressure-driven distillation have material properties that hold potential to be placed in direct contact with strong oxidants. [10,61–63] Unlike conventional membranes, distillation membranes require hydrophobic materials that can trap air within sub-micron scale pores. Water vapor can then travel through the membrane driven by a partial vapor pressure gradient resulting from a temperature or concentration difference. A variety of hydrophobic materials have been used in membrane-based distillation systems. Among these, polytetrafluoroethylene (PTFE), polyvinylidene fluoride (PVDF), and polypropylene

(PP) have been the most widely studied.[11] All these polymers have chemical structures that are stable and, in theory, have stronger tolerance towards chemical oxidation than hydrophilic polyamide and cellulose acetate polymers used in conventional salt-rejecting membranes.

Despite the potential of combining membrane-based distillation systems with strong oxidants, the oxidation resistance and long-term stability of hydrophobic porous membranes has not been well-characterized for ozone and chlorine, the two strong oxidizing agents that are most commonly used in water treatment. The perfluorinated C-F bonds in PTFE are not known to react with even very strong oxidants such as hydroxyl radical since no lone pairs for electron transfer or hydrogens available for abstraction exist in the chemical structure of PTFE. [13] Experimentally, PTFE membranes have been used in studies involving ozone without noticeable changes in performance, but the chemical properties of PTFE membranes after exposure were not characterized. [64,65] PVDF membranes have been suspected to swell when exposed to ozone, though materials characterization has been inconclusive regarding any chemical changes to the polymer.[66–68] PP and PVDF membranes also have been observed to react with chlorine, but implications for membrane performance are unclear. [69,70] Prior literature thus indicates that some polymers used in distillation systems have the potential to operate with prolonged exposure to strong oxidants such as chlorine and ozone. However, the impact of such exposure on membrane chemical stability and physical structure has not been well-studied. Studying the chemical resilience of hydrophobic polymer membranes used in distillation systems is particularly relevant because small changes in surface chemistry may result in membrane wetting and compromise membrane performance.

In this work, we investigate the effects of oxidant exposure on hydrophobic membranes commonly used in membrane-based distillation processes. We first examine changes in the chemistry and hydrophobicity of PTFE, PVDF, PP membranes after exposure to varying doses of chlorine and ozone, allowing us to gain insights into degradation mechanisms. We then examine changes in membrane polymer structure and characteristics after exposure to oxidants. Finally, we show changes in water flux and salt rejection that occur after membranes have been exposed to varied doses of oxidants. Overall, this work provides important insights on the limits of different MD membrane materials in resisting damage from strong chemical oxidants.

3.2. MATERIALS AND METHODS

3.2.1. Membranes and chemicals

Three hydrophobic, porous polymer membranes commonly used in distillation processes, PTFE (Sterlitech Corporation, USA), PVDF (Durapore, Millipore, Ireland), and PP (Sterlitech Corporation, USA), were tested. All membranes had a nominal pore diameter of 0.2 μm. Each type arrived as flat sheet membranes in a dry state. Samples were cut from flat sheets prior to oxidation and testing. Deionized (DI) water was obtained using a Millipore Synergy UV Remote Water Purification System. Solutions for chlorine degradation experiments were prepared using a sodium hypochlorite solution (NaOCl 5% w/v, LabChem) and DI water with pH adjusted using hydrochloric acid (HCl 1N, Fisher Chemical). Gaseous ozone was produced by a TG-40 ozone generator (Ozone Solutions, USA) for ozone degradation experiments. Sodium chloride (NaCl, Fisher Chemical) dissolved in DI water was used as the feed solution in desalination testing.

3.2.2. Oxidation of membrane materials

Oxidant exposure occurred in the form of passive treatment in which the membrane samples were submerged in prepared solutions for a specified amount of time. Aqueous ozone was generated by feeding pure oxygen into an ozone generator which was then diffused as gaseous ozone into a beaker containing DI water. Due to the rapid degradation of ozone, a constant flow of gaseous ozone was supplied during membrane exposure. Ozone concentration within the beaker was monitored using a spectrophotometer (HACH DR6000, Colorado, USA). The ozone solution was maintained at a concentration of 15 ppm and a pH of 7 for oxidation experiments. Membrane exposure time for PVDF and PTFE in the ozone solution was 1 h, 2 h, and 3 h. PP membranes were exposed for 10 min, 20 min, and 30 min. PP membranes required significantly lower exposure doses in each oxidant solution due to extreme and rapid degradation compared to the PTFE and PVDF membranes.

NaOCl solutions were prepared by diluting a 5% w/v NaOCl solution with DI water to a concentration of 10,000 ppm. The solution was adjusted to a pH of 4 using hydrochloric acid. The solution was covered and reprepared every 24 hours to maintain a constant concentration and pH. Membrane exposure time for PVDF and PTFE in the chlorine solution was 24 h, 48 h, and 72 h. PP membranes were exposed for 20 min, 40 min, and 60 min. Additional PP membranes were exposed for up to 24 h for material characterization, though severe degradation prevented desalination testing on these samples. Following oxidant exposure, membrane samples were thoroughly rinsed with DI water and left in DI water for 24 h. Membranes were rinsed with methanol to remove

any surface contamination, dried, and stored in a desiccator prior to surface characterization.

3.2.3. Membrane characterization

Contact angle was measured with a Biolin Scientific tensiometer using the sessile drop technique. For all measurements, a droplet of DI water (less than 10 µL) was deposited onto the active side of the membrane surface using a pipette. Contact angle was measured on different areas of each sample and reported values represent an average of at least three measurements.

Membrane morphology and surface topography was viewed with scanning electron microscopy (SEM) on a Hitachi SU8010 microscope. Prior to SEM imaging, platinum was sputtered onto the PTFE, PVDF, and PP surfaces until a thickness of 3 nm was achieved on the surface. SEM images were taken of pristine PTFE, PVDF, and PP and the membranes exposed to the highest doses of chlorine and ozone.

Attenuated total reflectance Fourier transform infrared (ATR-FTIR) spectra were acquired from 400–4000 cm-1 using a ThermoScientific Nicolet iS50 FTIR with a Smart iTX attachment with ATR capacities and an ATR diamond crystal. Measurements were taken of PTFE, PVDF, and PP prior to submersion into the oxidant solution and after subsequent exposures.

X-ray photoelectron survey spectra were acquired from 0–1200 eV using a Kratos Supra X-ray photoelectron spectrometer. Polymer samples were isolated on the sample plate to ensure consistent charging through the samples. The Al K Alpha X-ray source was operated at 1486.7 kV and 15 mA current emission. Charge neutralization parameters were determined through the use of continuous scans of the carbon 1s peak.

Survey spectra were used to calculate the atomic percent of elements on the surface while the high-resolution C 1s spectra were peak fitted to determine the changes in the carbon binding after exposure. High resolution scans of O 1s, F 1s, and C 1s were taken to obtain the chemical state of the polymers after oxidant exposure. A Shirley background was used and a Gaussian-Lorentzian sum function with an added asymmetric parameter were used to fit component peaks for the polymers. All spectra were calibrated using a C-C/C-H peak position of 284.8 eV.

A bench-scale crossflow direct contact MD system was used for performance testing on pristine and oxidized membrane samples. Membranes were placed within a flat sheet membrane module with an active surface area of 20.02 cm^2. PP membranes required the use of mesh spacers on either side of the membrane for support. A 0.05 M NaCl feed solution was circulated at 60 ºC in contact with the active side of the membrane. DI water was simultaneously circulated on the permeate side at 20 ºC. Feed and permeate temperatures were continuously monitored prior to entering and upon exiting the membrane module and regulated using a heater and chiller, respectively. Flow rate was measured upon exiting the membrane module and regulated using pumps. Water velocity through the channels was maintained at 0.14 m s-1 across the membrane surface. Water flux across the membrane during operation was determined by measuring the mass change of the permeate reservoir using an analytical balance. Salt rejection across the membrane was measured using a conductivity probe in the permeate reservoir. Measurements were collected in one-minute intervals after the system reached steady state conditions. Water flux and salt rejection across the membrane were then evaluated as a function of oxidant exposure.

3.3. RESULTS AND DISCUSSION

3.3.1. Oxidation impacts on membrane structure and hydrophobicity

To examine the impact of oxidation on hydrophobic porous membranes, 0.2 µm nominal pore size hydrophobic membranes made from PTFE, PVDF, and PP were acquired and exposed to chlorine at pH 4 and ozone at pH 7. Membranes were then thoroughly characterized for chemical, structural, and performance changes in direct contact MD (Figure 5A). Exposure to chemical oxidants may lead to loss of surface hydrophobicity and pore wetting (Figure 5B) or damage to the bulk polymer membrane structure (Figure 5C). In this Section, we will discuss changes in membrane structure and hydrophobicity that were observed after oxidant exposure. Subsequent sections will further analyze chemical changes and MD performance of the oxidant-exposed membranes.

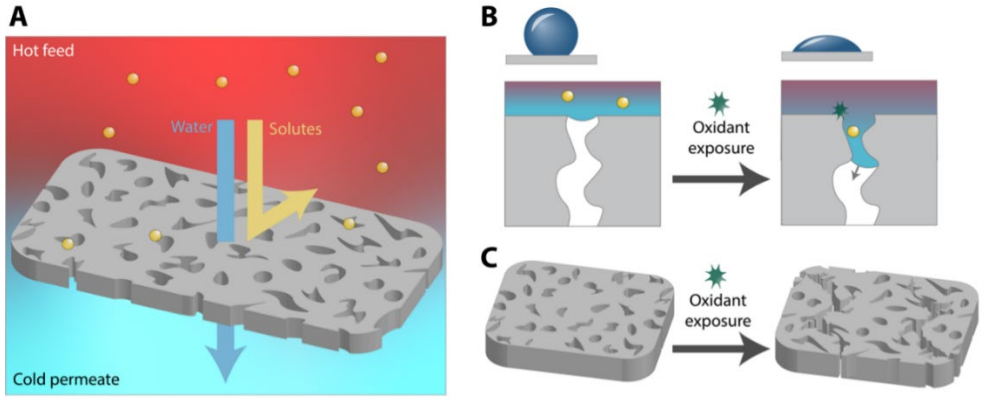

Figure 5: (A) Schematic diagram of membrane distillation. (B) Loss of membrane hydrophobicity as a result of oxidant exposure may lead to pore wetting. (C) Damage to the membrane morphology may also result from exposure to oxidants.

Following oxidant exposure, physical inspection, and SEM imaging were used to examine possible structural degradation in the membranes. After the highest exposures for chlorine (72 h at 10000 ppm) and ozone (3 h at 15 ppm), both PTFE and PVDF showed no changes in their overall morphology in digital and SEM images (Figure 6, Figure S1). Polypropylene, on the other hand, showed significant changes in its macroscale morphology after exposure to lower doses of chlorine (10000 ppm for 24 h), with cracking and tearing occurring on the membrane surface. SEM imaging further revealed that larger than 10 μm cracks were present on the membrane surface and apparent pore sizes at the membrane surface increased from approximately 0.2 μm to 2 μm. For ozone (1 h at 15 ppm), we observed macroscale cracking and debris on the surface of the membrane. Overall, inspection of the membrane samples indicated significant damage to the PP membrane structure after ozone and chlorine exposures.

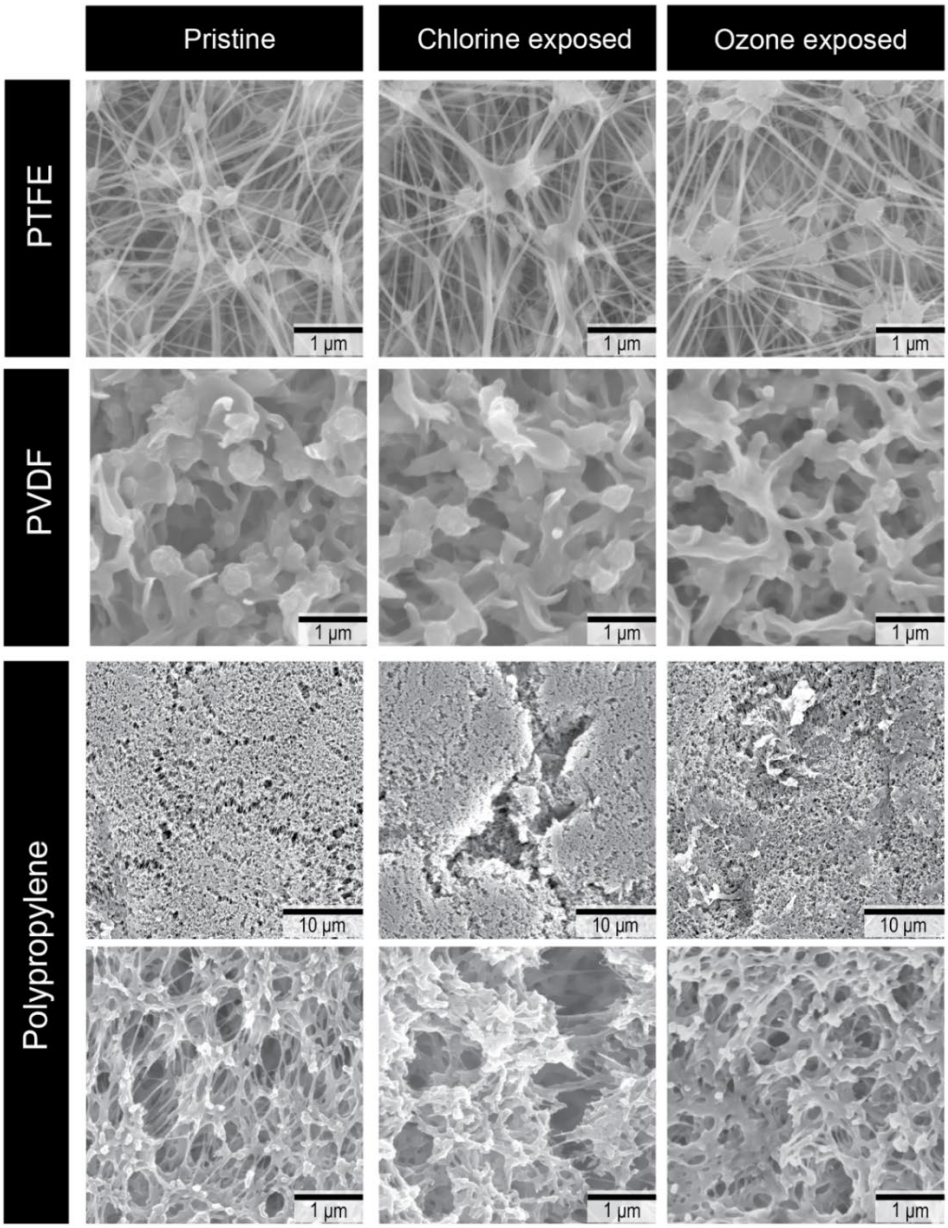

Figure 6: Scanning electron micrographs of polytetrafluorethylene (PTFE), (b) polyvinylidene fluoride (PVDF), and polypropylene membranes before and after exposure to chlorine and ozone oxidants. Polytetrafluoroethylene and polyvinylidene fluoride membranes were exposed to 10000 ppm chlorine for 72 h or 15 ppm ozone for 3 h. Polypropylene membranes were exposed to 10000 ppm chlorine for 24 h or 15 ppm ozone for 1 h.

Measurements of the water contact angles after oxidant exposure showed small changes in the overall hydrophobicity in all cases (Figure 7). After the maximum exposure to chlorine (720000 ppm·h), the contact angle of water on PTFE and PVDF changed from 132° to 117° and 120° to 108°, respectively. After the maximum exposure to ozone (45 ppm· h), the contact angle on PTFE and PVDF decreased from 132° to 111° and 120° to 112°, respectively. PP membranes were exposed to lower doses of chlorine (up to 10000 ppm·h) and ozone (up to 7.5 ppm·h) since they suffered from severe cracking. PP membranes showed more rapid changes in water contact angle during oxidant exposure, experiencing a decrease in contact angle of 140° to 120° and 140° to 117° for chlorine and ozone, respectively. Generally, contact angle measurements showed modest changes in the surface properties across all membranes, with a less than 15% change in contact angle in all cases. Even the PP membranes that showed macroscale membrane cracking showed relatively small changes in contact angle prior to failure.

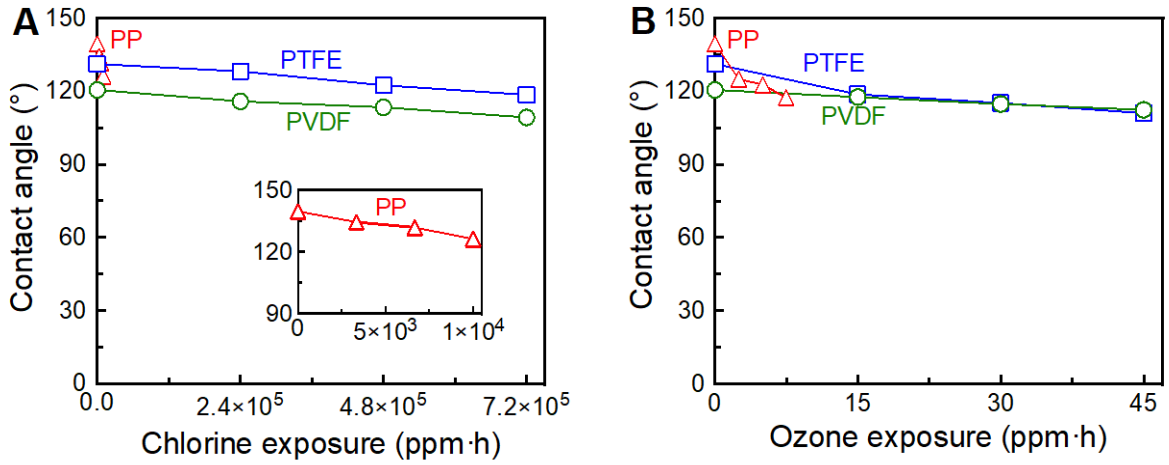

Figure 7: Static water contact angle of polytetrafluroethylene (PTFE), polyvinylidene fluoride (PVDF), and polypropylene (PP) membranes following exposure to (A) 10000 ppm chlorine solution and (B) 15 ppm ozone solution.

3.3.2. Understanding chemical changes in polymers after exposures

The changes in structure and hydrophobicity of membranes after exposure to chlorine and ozone motivated further investigations into membrane surface chemistry. Attenuated total reflectance Fourier transform infrared spectroscopy (ATR-FTIR) was used to gain information on changes in the overall bond structure of membranes before and after oxidation. The PTFE and PVDF membrane showed no changes in ATR-FTIR spectra after exposure to chlorine and ozone. In contrast, PP membranes, which showed significant structural changes after exposure to both chlorine and ozone, also had observable changes in their ATR-FTIR spectra (Figure 8). Following ozonation, we noted the development of a small peak at 1700 cm-1 which corresponds to the presence of a carbonyl group. We saw more significant changes in the chlorinated PP in the region between 4000 cm-1 and 3000 cm-1 where there is a broad peak characteristic of an alcohol group. We also observed the evolution of a broad carbonyl peak between 1800 cm-1 and 1500 cm-1. The formation of similar peaks characteristic of alcohol and carbonyl functional groups is typical in oxidized polyproypylene. [71] The chemical changes in PP are consistent with our understanding that tertiary carbon makes it susceptible to chemical attack. The attached hydrogen is more likely to be abstracted and an alkoxy radical is formed which stabilizes itself through a rearrangement into an alkyl radical and forms a ketone. [12,72]

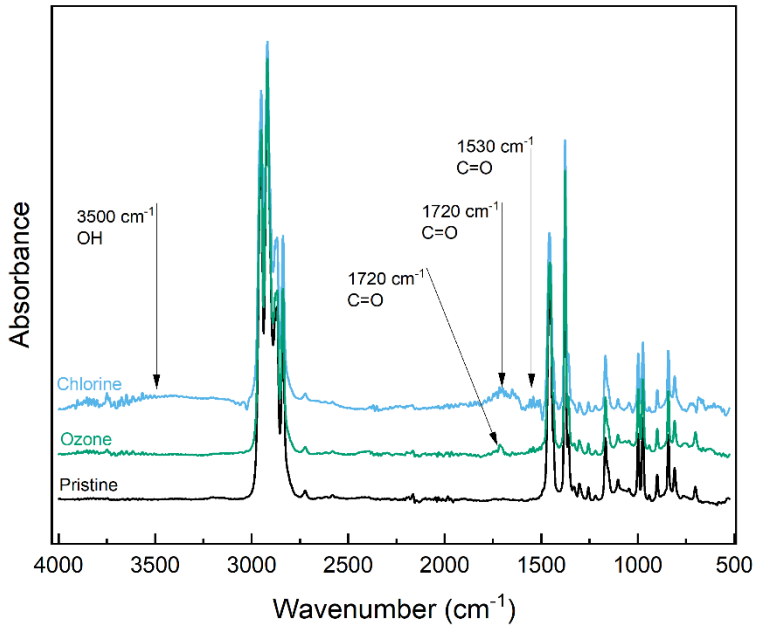

Figure 8: Attenuated total reflectance Fourier transform infrared (ATR-FTIR) spectroscopy scans of polypropylene membranes before and after exposure to ozone and chlorine. Polypropylene membranes were exposed to 10000 ppm chlorine for 24 h or 15 ppm ozone.

XPS was used to gain more information on the atomic compositions of the top surface (approximately 10 nm) of the membrane polymer, where we expected to observe the most chemical changes due to oxidation (Figure 9). For PTFE samples, XPS analysis indicated minor changes in surface chemistry that were likely due to carbon contamination. Pristine PTFE shows the characteristic C-F peak at 291 eV, and following exposures to chlorine and ozone, there are no changes to this peak (Figure 9C). On all three spectra there is an additional peak at 285 eV which corresponds to C-C/C-H bonds and is commonly attributed to carbon contamination. Overall, PTFE membranes showed XPS peaks

characteristic of its highly fluorinated carbon chain that were not affected by chlorine or ozone exposure.

XPS analysis of the PVDF and PP membranes observed more obvious changes to the membrane surface chemistry following oxidation than those seen with PTFE. In pristine PVDF, there are two characteristic peaks: the C-F peak at 291 eV and the C-H peak at 286.4 eV (Figure 9D). Following oxidation with ozone and sodium hypochlorite we see an 8.1% and 17.3%, respectively, decrease in the C-F peak which indicates possible surface defluorination. Additionally, we see an evolution of a peak at 284.8 eV. Since there is indication of defluorination on the PVDF, we believe that the peak at 284.8 eV corresponds to the formation of C=C on the surface which has been suggested to form following defluorination in PVDF.[73,74]

For PP membranes, there is only a peak for C-C/C-H at 285 eV in the pristine membrane (Figure 9E). This structure corresponds to the repeating units of carbon and hydrogen atoms, where the carbon atoms are connected by single bonds. Following oxidation, we observe widening of the carbon peak due to an evolution of carbon oxygen groups on the PP surface. Chlorination of the polypropylene led to a 5.3% and 3.0% increase of C-O and C=O respectively, while ozone led to a 2.5% and 1.5% increase of C-O and C=O respectively on the surface. Thus, oxidation of the PP membranes led to changes in the membranes overall surface chemistry as evidenced by the presence of C-O and C=O following oxidation.

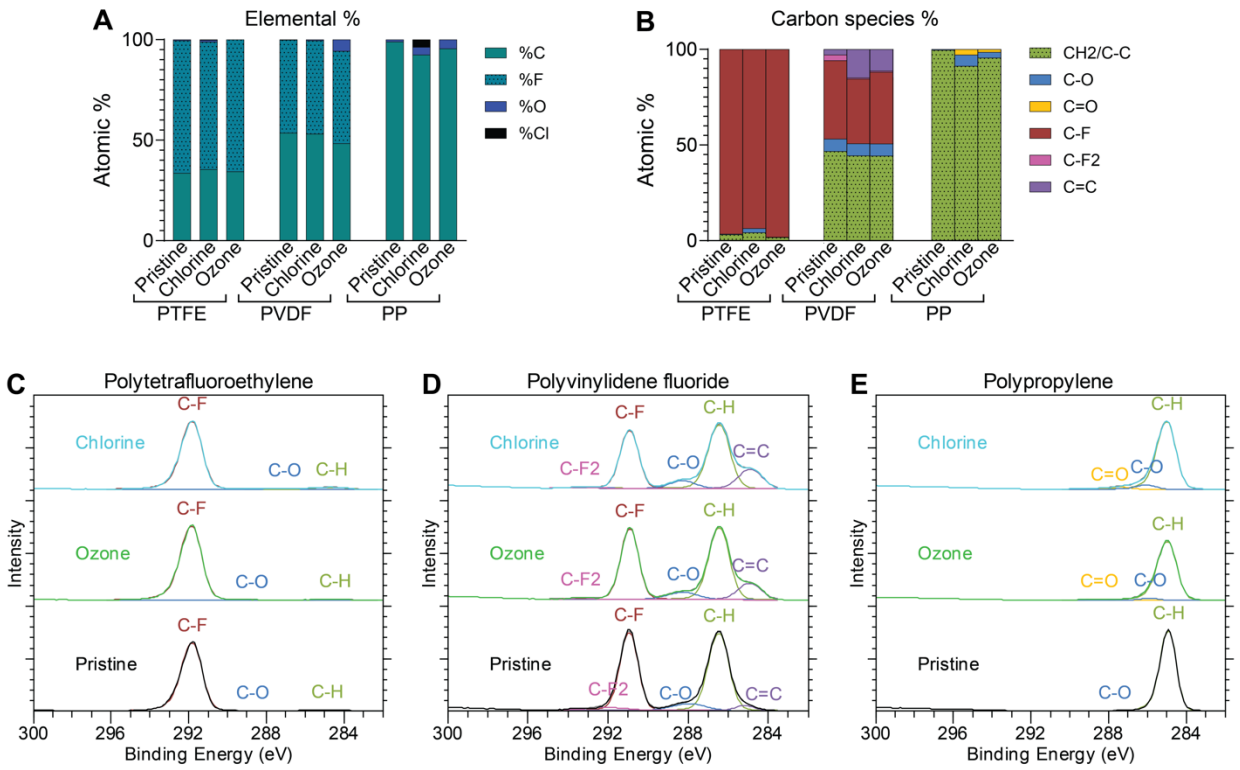

Figure 9: (A) XPS survey spectra show differences in atomic % on the membrane surfaces after oxidant exposures. (B) Carbon core scans show changes in binding environment of the carbon atoms on the surface. (C) We observed no changes in the PTFE structure. (D) (D) PVDF showed changes in its surface chemistry after ozone exposure. (E) PP showed significant changes after both exposures.

3.3.3. Desalination performance testing

Direct contact membrane distillation (MD) testing was used to investigate the impact of chlorine and ozone exposure on the desalination performance of membranes (Figure 10). With a hot temperature of 60 ºC and a cold temperature of 20 ºC, the pristine PTFE, PVDF, and PP membranes showed water fluxes of 35.3 L m-2h-1, 24.5 L m-2h-1, and 47.1 L m-2h-1, respectively. All pristine membranes had salt rejections higher than 99.9%.

After exposure to chlorine and ozone, PTFE and PVDF membranes showed minor changes in water flux and maintained greater than 99.9% salt rejection. The measured water fluxes for PTFE membranes exposed to chlorine or ozone varied from 38.4 L m-2h-1 to 44.7 L m-2h-1. For PVDF membranes, the measure water fluxes of oxidant exposed membranes varied from 26.8 L m-2h-1 to 31.6 L m-2h-1. Although the water fluxes of membranes after oxidant exposure were generally higher than that of the pristine membranes, no clear dependence of water flux on oxidant exposure was observed. These results are consistent with previous data that indicate minor changes in membrane structure and minor differences in hydrophobicity following oxidant exposure.

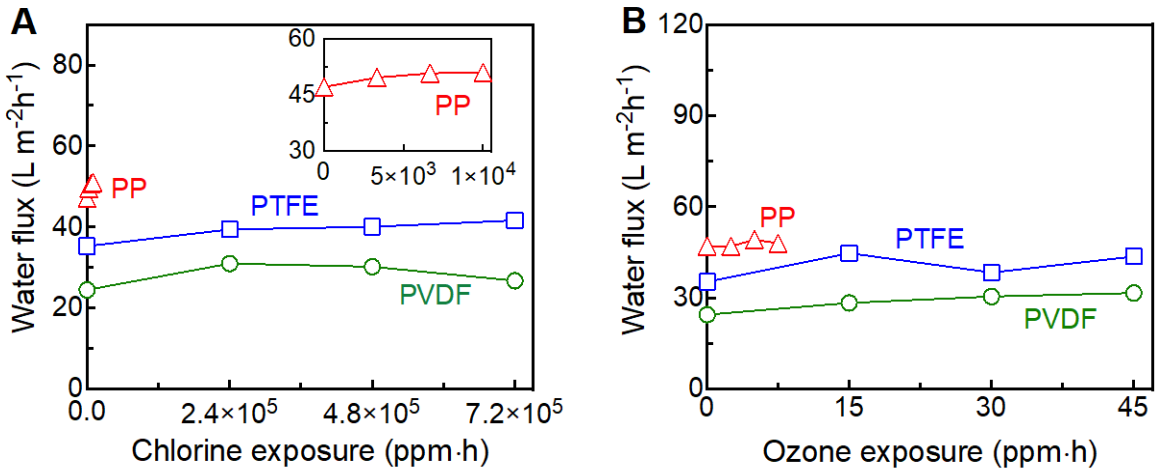

Figure 10: Water flux as a function of oxidant exposure for polytetrafluroethylene (PTFE), polyvinylidene fluoride (PVDF), and polypropylene (PP) membranes after exposure to a 10000 ppm chlorine solution (A) and a 15 ppm ozone solution (B) through a direct contact membrane distillation cell. Temperatures were 60 ºC and 20 ºC through the feed and permeate channels, respectively.

Unlike PTFE and PVDF, PP membranes demonstrated observable cracking which prevented them from being tested in desalination systems at doses higher than 240000

ppm·h chlorine or 15 ppm·h ozone. Within the allowable exposure for PP membranes without reaching catastrophic failure, changes in water flux and salt rejection were minor. Initial water flux was measured to be 47.1 L m-2h-1. Following exposure to chlorine, an 8.3% increase in water flux was observed. Ozone exposure resulted in a 1.7% increase in water flux. Similar to the PVDF and PTFE membranes, changes in salt rejection between pristine membranes and oxidized membranes were negligible during the observed exposures. It should be emphasized that following the exposures used for PP membranes in desalination performance testing, damage to the membrane caused by oxidation resulted in complete failure within the system. This included visible breakage to the membrane resulting in near zero salt rejection and significantly increased water flux through the cell channels.

3.3.4. CONCLUSIONS

The impact of exposure to chlorine and ozone oxidants on three commercial hydrophobic membranes (PTFE, PVDF, and PP) was evaluated by examining changes to structure, surface chemistry, and desalination performance in a crossflow direct contact MD cell. PTFE and PVDF membranes appeared to be minimally impacted by strong oxidants at exposures up to the limit of this study: 720000 ppm·h chlorine and 45 ppm·h ozone. Both membranes experienced slight increases in water flux without compromising selectivity and saw a less than 10% decrease in contact angle. Further characterization revealed no noticeable changes in the structure and chemistry of PTFE, though changes in the chemistry of the PVDF were observed through XPS. PP experienced severe degradation following maximum oxidant exposure of 240000 ppm·h chlorine or 15 ppm·h ozone which was confirmed through surface and structural characterization methods.

Given their high observed oxidation resistance, PTFE and PVDF may be promising options for water treatment applications that involve contact with oxidants or for applications that might benefit from pretreatment using ozone and chlorine. Based on the observed oxidation resistance, pretreatment of water using a typical dose of 4 ppm chlorine would be possible for at least 20 years. With an average continuous ozone dose of 0.1 ppm, both PVDF and PTFE could resist oxidation damage for at least 18 days under these experimental conditions. Past this point, the surface characterization results imply that PVDF could be at risk of failure earlier than the PTFE membranes when in direct contact with ozone.

Polypropylene demonstrates limited oxidation resistance for both chlorine and ozone compared to PTFE and PVDF. Our work indicates that with a typical chlorine dose of 4 ppm, failure of PP membranes may occur within 100 days. Similarly, the use of PP in direct contact with 0.1 ppm ozone would be limited to 9 days. Prior to membrane failure, no noticeable changes in permeability, selectivity, or hydrophobicity were observed. The rapid and unexpected failure of the PP membrane indicate that failure of the membrane may occur without warning in a water treatment system.

Future work should investigate the effects of direct oxidation with additional operational parameters not considered in this study. Desalination performance following oxidant exposure was evaluated with a saline feed stream free of additional organics, salts, and other contaminants that could contribute to membrane fouling or alter membrane surface properties. This work found that membranes made from fluorinated polymers (PTFE and PVDF) showed higher oxidation resistance than non-fluorinated membranes (PP). An additional emerging concern in the practical application of fluorinated membranes is the

release of per- and polyfluoroalkyl substances (PFAS). Additional analysis are necessary to compare the advantages of membrane oxidation resistance with their potential for PFAS release.

4. Plasma-etched nanoporous polytetrafluoroethylene for improved wettability in pressure driven membrane distillation systems

All work was performed by E.A. Hjelvik except for the electrical impedance spectroscopy (EIS) studies which were performed by K.P. Lopez.

4.1. INTRODUCTION:

Omniphobicity

Inspired by surfaces found in nature, such as the lotus flower/springtail/bugs, omniphobic, ability to repel all liquids, surfaces have been suggested to enhance wetting of membranes. The omniphobicity of these surfaces results from the creation of microscopic reentrant structures on membranes. These structures can trap air between them and the liquid thus blocking liquid permeation, and the increased contact area between the structured surface and liquid also leads to an increase in overall.

The increased wetting resistance from omniphobic structures can be understood through Young's equation in terms of contact angle measurements, equation 4.0. Contact angles are typically used to quantify a flat surfaces wettability, or the ability for a liquid to maintain contact with a solid surface. [75] In contact angle, a small droplet of water (less than 10ul) is placed on a surface and if it beads up with a contact angle greater than 90 it is hydrophobic then if it spreads on the surface with a contact angle less than 90 it is hydrophilic, Figure 11A. For a smooth surface, contact angle can be defined in terms of the equilibrium contact angle, $\theta\gamma$, the solid–liquid interfacial energy, γ_S, the solid–vapor interfacial energy, $\gamma_{SV,}$ and the liquid–vapor interfacial energy, $\gamma_{LV.}$

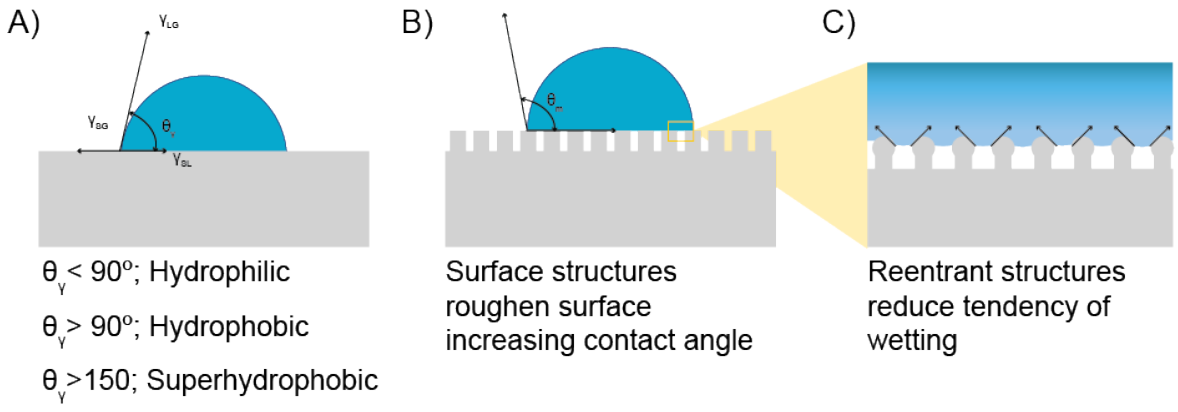

Figure 11: A) Wettability of a liquid on a solid surface. B) Antiwetting Cassie Baxter state as introduced by surface structures C) Reentrant structures resisting wetting from liquid onto solid surface

$$\gamma_{SL} - \gamma_{SV} - \gamma_{LV} \cos\theta_{\gamma} = 0 \qquad \text{Eq. 4.0}$$

$$\cos\theta_m = r \cos\theta_{\gamma} \qquad \text{Eq. 4.1}$$

Equation 4: Surface wettability equations

When looking at textured surfaces like omniphobic surfaces, the Cassie-Baxter states can be used to describe the resulting anti-wetting states. Figure 11B. The measured contact angles on textured surfaces differ from the equilibrium contact angle due to the water droplets having increased contact with the surface. According to the Cassie Baxter model, anti-wetting states occur as textured surfaces lead to the presence of air pockets at the bottom of the interface.[48,75,76] However, it is difficult for a stable Cassie-Baxter state to be achieved when low surface tension liquid is present. Studies have found that in order to maintain this antiwetting state, that in addition to having a superhydrophobic

surface, omniphobic membranes must have surface features that have a concave topography, Figure 11C. [48,75]

Multiple groups have been successful in fabricating this ideal surface for omniphobic membranes. Nanoparticle grafting and functionalization is a popular method in creating reentrant structures on a membrane surface. Membrane surfaces are altered to allow for the electrostatic grafting of inorganic nanoparticles to the surface. The particles are subsequently functionalized with fluorinated compounds such as fluorosilanes, fluoroplasma or fluoropolymers to create a hydrophobic surface.[77] This method has been used as proof of concept of omniphobic membranes and has shown the usefulness of these surfaces for mitigation of wetting, fouling, and scaling in membrane processes. Other methods such as electrospraying and nanolithography have also been implemented to create reentrant structures for an omniphobic surface.[78,79] However, the current processes for creating these surfaces are time consuming, complex, unscalable, and their long-term robustness remains unknown. As a result, the viability of omniphobic surface functionalization strategies for distillation membranes depends on robust and scalable processes. In particular, the ability to etch surfaces with plasma has been shown to create nanoscale structures on polymer surfaces.[80]

Plasma processes

Plasma processes hasverecently found use in being able to alter polymer surface morphology. Plasma was discovered in the 1920's but it was not until the 1980's when plasma was used to modify material surfaces and found application in various fields and eventually became a key technology in the microelectronic industry. [81]

Interactions between plasma and materials surfaces can be separated into ablation or activation. Ablation is the process in which surface contamination is removed from surface through ion bombardment. Activation is the process where new reactive functional groups are created on the material surface to allow for potential surface chemistry reactions. Additional interactions such as deposition and grafting have also been identified but in these cases, plasma interacts with reactive species allowing for thin layers of materials to be deposited on the surface.[81]

The ability to achieve ablation or activation of surfaces is reliant upon a variety of factors, with the predominant one being if the plasma system is set up for remote or direct plasma. The difference between remote and direct plasma is based on where the plasma source is in reference to the material being modified, Figure SI 4. In direct plasma the source of plasma and the material are within the same chamber, which leads to the material experience direct ion bombardment. This can lead to ablation of material but often, the direct ion bombardment also leads to changes in material properties. In most cases, the changes to the overall materials properties are unfavorable.[82,83]

To address these unfavorable material changes, remote plasma is used to maintain the benefits of plasma without impacting the materials properties. Unlike direct plasma, the plasma source in remote plasma is in a separate chamber than the material being modified which allows a higher degree of control of plasma species thus minimizing direct ion bombardment. Remote plasma is commonly used if activation or deposition is desired for the material.[82]

With its ability to clean and activate surfaces, plasma has been pursued to aid in surface chemistry techniques like atomic layer deposition or chemical vapor deposition to

facilitate covalent binding of chemistries to the surface. However, recently plasma has always found utility in creating modifying the surface structures. This was initially looked at to control surface roughening on optical or microelectronic systems but there has been significant interest in its ability to create microstructures on polymer surfaces.[80,83–90]

Plasma texturing on polymers

Xu et al demonstrated the fabrication of nano scale pillar structures on a PTFE surface with oxygen plasma for use as a bactericidal surface.[90] Palumbo et al studied how biased oxygen plasma process can tailor polycarbonate surface properties, chemistry and structures, for controlled wettability properties.[91] Ioannou *et al.* created super hydrophobic PTFE and cellulose acetate for use in MD through the subsequent introductions of oxygen and fluoro plasmas in a quick two-step process. [87]The texturing of polymers with plasma has become of interest for its simplicity and scalability, however, the mechanism by which the membrane surface is modified remains poorly understood. There are several proposed mechanisms for the plasma-induced structural modification report that the initial surface roughness of the polymer will impact the formation of nanotextures on the polymer while suggest that metal contamination on the polymer surface locally screen the plasm resulting in a textured surfaces.

Overall, these studies have shown the potential of plasma processes to create microstructures on polymer surfaces quickly and efficiently. Therefore, we were interested in utilizing plasma to create structures on distillation membranes, probe the resulting structures omniphobic ability, and understand the mechanism in which these structures form to inform future membrane fabrication procedures. In this work, we demonstrate the fabrication of superhydrophobic PTFE membranes through a simple one-step oxygen

plasma process. Following plasma treatment, the PTFE membranes exhibited microstructures on the surface that gave the membrane high rolling contact angles to water, high contact angles to water/ethanol solutions, and demonstrated improved wettability in a high pressure desalination system. Additionally, we propose a new theory of the plasma texturing where we hypothesize that the plasma is inducing localized heating on the top surface of the membrane which in turn melts the polymer fibers.

4.2. MATERIALS AND METHODS

4.2.1. Membranes and Chemicals

Porous PTFE membranes (Pall PTF002LHOP, Lot No: 139403) were modified and tested. Samples were cut into 1 3/8 in circles from flat sheets prior to modification. Deionized (DI) water was obtained using a Millipore Synergy UV Remote Water Purification System. Water ethanol solutions were prepared by increasing the percent of ethanol in a 20 mL solution. Sodium chloride (NaCl, Fisher Chemical) dissolved in DI water was used as the feed solution in impedance and desalination testing.

4.2.2. Plasma treatment of membranes

The membranes were cleaned with nitrogen gas and placed in a Terego barrel plasma cleaner (model). The membranes were modified under direct oxygen plasma (O_2 flow rate: 10 sccm, plasma power 100W). The time of the plasma cleaning was varied from 30 seconds –240 seconds. The first initial 10 seconds of the process stabilized the plasma emission, once stabilized the plasma emission would range from 360-400. Prior to modification, each sample was pumped down to 10-15 to ensure consistent plasma emission between samples.

4.2.3. Membrane characterization

Static contact angle measurements were taken on a Biolin Scientific tensiometer using the sessile drop technique. For all measurements, a droplet of DI water or DI water/ethanol (less than 10 µL) were placed onto the active side of the membrane surface using the automated pipette on the tensiometer. Contact angle measurements were taken in triplicate. Membrane omniphobicity was determined through increasing the concentration of ethanol in the solution.

Membrane morphology and surface topography were viewed with scanning electron microscopy (SEM) on a Hitachi SU8010 microscope. Prior to SEM imaging, membranes were sputtered with platinum until a thickness of 3 nm was achieved on the surface.

Attenuated total reflectance Fourier transform infrared (ATR-FTIR) spectra were acquired from 400–4000 cm-1 using a ThermoScientific Nicolet iS50 FTIR with a Smart iTX attachment with ATR capacities and an ATR diamond crystal.

X-ray photoelectron survey spectra were acquired from 0–1200 eV using a Kratos Supra X-ray photoelectron spectrometer. Polymer samples were isolated on the sample plate to ensure consistent charging through the samples. The Al K Alpha X-ray source was operated at 1486.7 kV and 15 mA current emission. Charge neutralization parameters were determined using continuous scans of the carbon 1s peak. Survey spectra were used to calculate the atomic percent of elements on the surface while the high-resolution C 1s spectra were peak fitted to determine the changes in the carbon binding after exposure. High resolution scans of O 1s, F 1s, and C 1s were taken to obtain the chemical state of the PTFE after plasma treatment.

4.2.4. Applied pressure desalination tests

Pressurized wetting and vapor transport experiments were carried out using a custom-made polycarbonate dead-end filtration cell designed to include two silver electrodes for EIS measurements. Silver wires with a diameter of 1 mm were used as both the working and counter electrodes. Both electrodes were securely positioned on the membrane surface with a 4 mm distance between them to ensure consistency in data. A diagram of the pressure cell can be found in the supplementary material (Figure S1). EIS measurements were performed using a Bio-Logic VMP3 Multichannel Potentiostat. In-situ electrical conductivity measurements in the permeate channel were taken using a calibrated conductivity meter (CQRobot Ocean: TDS Meter) to measure salt rejection.

Time-dependent impedance measurements were taken using a constant frequency of 100 kHz. Nyquist plots were generated by performing EIS at a range of 100 MHz to 1 MHz with a sinusoidal voltage of 10 mV at open circuit potential. The pressure cell was filled with 8.5 mL electrolyte solution of 50 mM NaCl in distilled deionized water. For testing with surfactants, electrolyte solutions included 100 ppm Triton X-100 (Sigma Aldrich). Pressure was applied using compressed nitrogen. A minimum rest time of 5 minutes was implemented following the application of pressure to mitigate the impact of convection on the local electrical field. The permeate side reservoir was equipped with the conductivity probe and filled with a low concentration salt solution (10 mM NaCl) to reduce the magnitude of the impedance measurements. Conductivity was measured every second to determine the rejection of salt across the membrane.

4.3. RESULTS AND DISCUSSION

4.3.1. Plasma treatment creates nanotextures on PTFE surface

Following plasma treatment, we performed basic contact angle tests with 100% DI water. Typically, when a polymer surface is treated with plasma there is a notable decrease in the contact angle due to the introduction of active functional groups on the surface like hydroxyl.[81,92,93] For the untreated PTFE membrane, the contact angle with 100% water is 140°. Following plasma treatment, we observed ultra-high contact angles where the water droplet does not stick to the membrane which is contrary to typically plasma treatment behavior. In fact, the water rolls off the membrane surface when the membrane is tilted at an angle, Figure 12A. This indicates that plasma does not introduce functional groups to the surface but is potentially creating microstructures, as evidenced by higher contact and rolling angles.

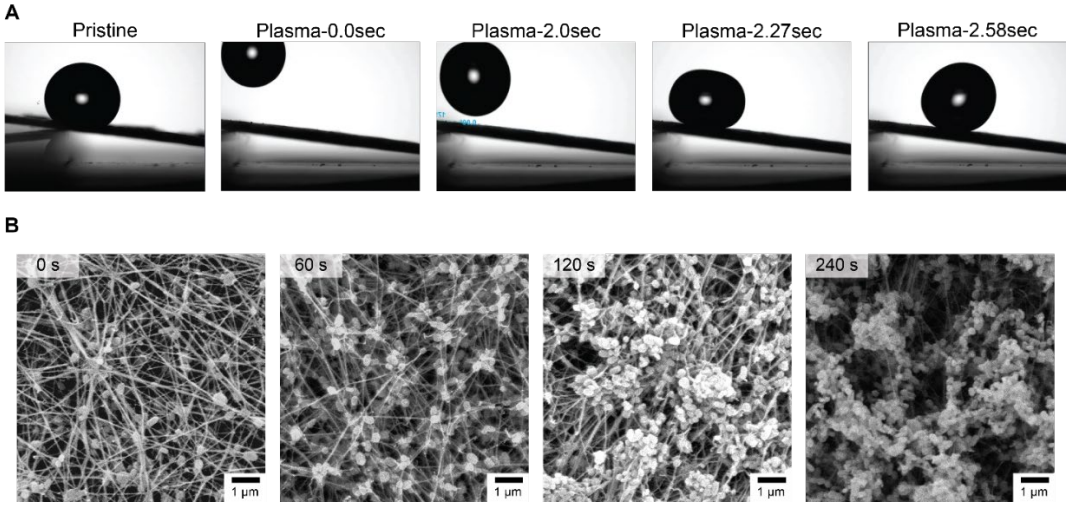

Figure 12: A) Rolling contact angle of 120 seconds of plasma treated PTFE membrane demonstrating high contact angle. B) Progression of texturing on PTFE membrane from 0 seconds to 240 seconds of 100W oxygen plasma

To probe into the changes of the PTFE membrane surface we analyzed their surface structure with scanning electron microscopy, Figure 12B. The PTFE surface undergoes significant morphological changes following plasma treatment. Prior to plasma treatment, pristine PTFE resembles a network of interconnected nodules and fibers. This network evolves during exposure to plasma. After 60 seconds of treatment, there is clear breakage of the fibers in the network and the nodules begin to cluster. At 120 seconds of treatment, there is clear formation of uniform microstructures on the PTFE surface. After 120 seconds, the structures stay relatively the same, however in place of the membrane fibers, there are large voids in the polymer network which may present an issue with selectivity of the membrane when used as a distillation membrane.[46,87]

4.3.2. Plasma treated PTFE membranes have enhanced wetting ability and performance in PD

The high contact and rolling angles in addition to the observed microstructures on the surface indicate the membrane could potentially serve as an omniphobic membrane, Figure 13A. Therefore, we tested the ability of these plasma treated PTFE membranes as anti-wetting surfaces by testing their contact angle with increasing ethanol concentration, Figure 13B. The inclusion of ethanol into the contact angle solution simulates low surface tension liquid conditions and provides a qualitative idea of the omniphobic behavior of the membrane. With increasing ethanol percent, up to 40% ethanol, we see that the plasma treated membranes retain a relatively high contact angle above 120°. On the other hand, untreated membranes contact angle decreases to under 120° when the solution is comprised of 20% ethanol.

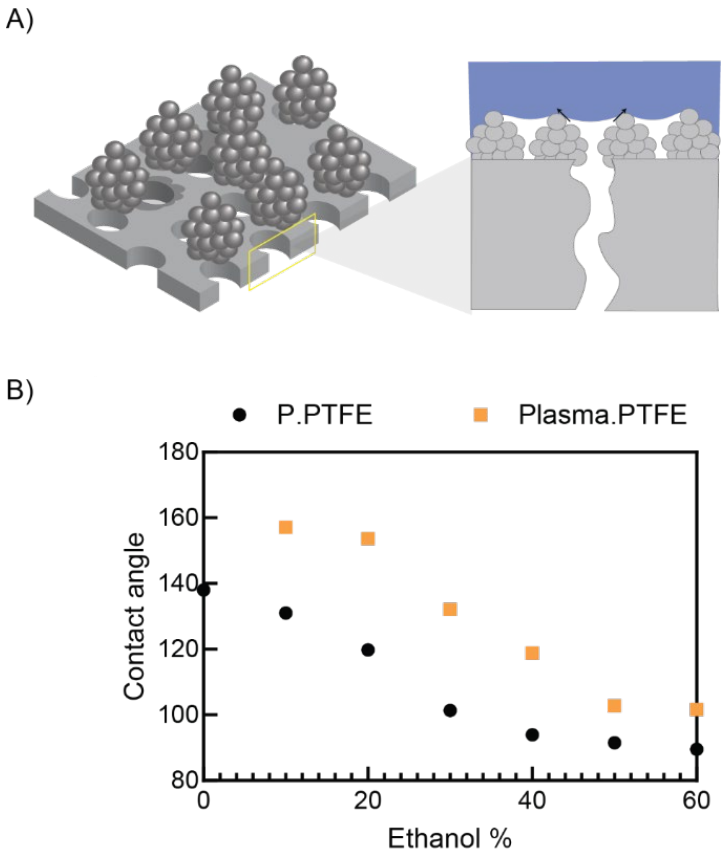

Figure 13: A) Schematic of how microstructures on PTFE achieve concave reentrant structures. B) Contact angle with increasing ethanol content shown with PTFE before and after plasma treatment.

Based off the contact angle measurements, we observed that the plasma PTFE membranes showed an enhanced resistance to low surface tension liquids. From this, we were interested in testing the liquid entry pressure of the membranes in a pressurized system to determine their overall wetting resistance in a desalination system, particularly pressure driven distillation. To investigate how plasma treatment affects liquid entry pressure and performance in PD, electrochemical impedance spectroscopy (EIS) wetting characterization experiments were conducted with pristine, and plasma treated PTFE membranes with 50 mM NaCl and 20% ethanol 80% water feed solutions, Figure 14.

Electrochemical impedance measurements have been used in previous reports to characterize pore wetting in distillation membranes[94–97]. In these studies, the capacitive and resistive impedance elements referred to the length of the airgap and resistance of the membrane material, respectively, such that a decrease in airgap thickness results in a decrease in overall transmembrane impedance.

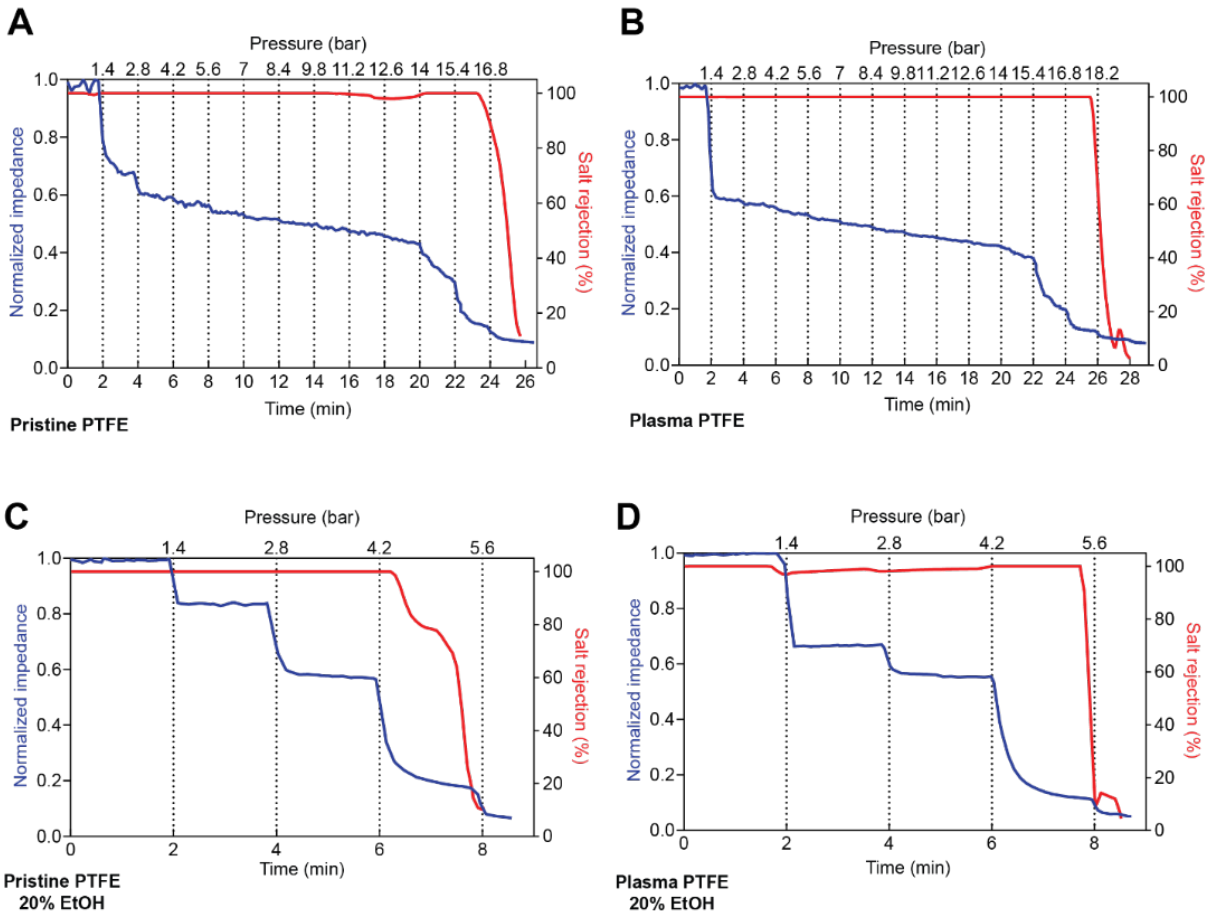

Figure 14: Electrochemical impedance spectroscopy showing wetting behavior of the PTFE before (A and C) and after plasma treatment (B and D). Wetting behavior was studied with feed solutions of 50mM NaCl (A and B) and 50mM NaCl with 20% ethanol (C and D).

Pressure increased by 1.38 bar every 2 minutes with both impedance and salt rejecting being continuously measured. Pressure-induced wetting with a 50mM NaCl feed solution showed LEP values of 16.8 and 18.2 bar (indicated by a gradual drop in impedance, followed by a sharp decline in salt rejection) for the pristine and plasma modified PTFE membranes, respectively (Figure 14A and 14B). Impedance and salt rejection measurements were also used to characterize pore wetting with lower surface tension solutions containing 20% ethanol. For the low surface tension feed solution, the plasma modified PTFE membrane showed an LEP of 5.6 bar compared to the pristine membrane's LEP of 4.2 bar (Figure 14C and 14D). This increase in wetting resistance of low surface tension feed solutions indicates that the plasma membrane displays omniphobic properties.

The higher LEP values indicate that plasma-treated membranes can sustain higher operational pressures without compromising performance, making them suitable for high-pressure water treatment systems. The improved resistance to wetting, even when exposed to low surface tension feed waters, shows the potential for plasma-treated membranes to handle diverse feed compositions, including those containing organic solvents or surfactants. This omniphobic behavior expands the range of feed solutions that can be processed efficiently, enhancing the overall versatility of distillation membranes.

In addition to enhanced wetting behavior, we also tested the plasma PTFE membranes for their performance as potential pressure driven distillation membranes. We saw a general increase in flux performance overall, however, we did see a notable decrease in the salt rejection measurements between tests. We attributed the variation in salt rejection

measurements based off the maximum plasma emission that was observed during plasma treatment, so at higher maximum plasma emission we observed lower salt rejection while with lower emission values we had high salt rejection values.

4.3.3. Understanding how plasma is impacting the PTFE structure

Due to the potential of plasma to enhance distillation membranes wetting resistance, we were interested in understanding how plasma led to microstructure formation on the membrane. In other polymer systems, the formation of textures has been attributed to be a consequence of differential etching[98] which has been hypothesized to occur due to the presence of nanomasks of metal on the surface or the initial roughness of the material. When probing into the mechanism of our treated membranes, we first examined surface chemistry. In our modification, we did not observe any presence of metals on the surfaces of the PTFE with x-ray photoelectron spectroscopy, Figure 15A. We also wanted to probe into any potential bulk changes occurring to the PTFE during plasma. Previous studies have reported that oxygen plasma can lead to the formation of oxygen groups in the PTFE, however in our infrared spectroscopy analysis we saw no significant changes to the PTFE, Figure 15B.

From our XPS studies, our treated membranes agree with the hypothesis that initial surface roughness will impact the ability to texture the membrane with plasma. This is consistent with plasma processing of PTFE films in the literature. Lai et al, observed no texturing following plasma treatment of isotropically expanded PTFE films, films that have relatively low surface roughness.[99] Meanwhile Ioannou et al, reported that membranes with weblike meshes, high surface roughness surfaces, showed texturing.[87] However, we

hypothesize that in addition to initial surface roughness, the surface microstructures being formed are also due to localized heating of the PTFE fibers from the plasma.

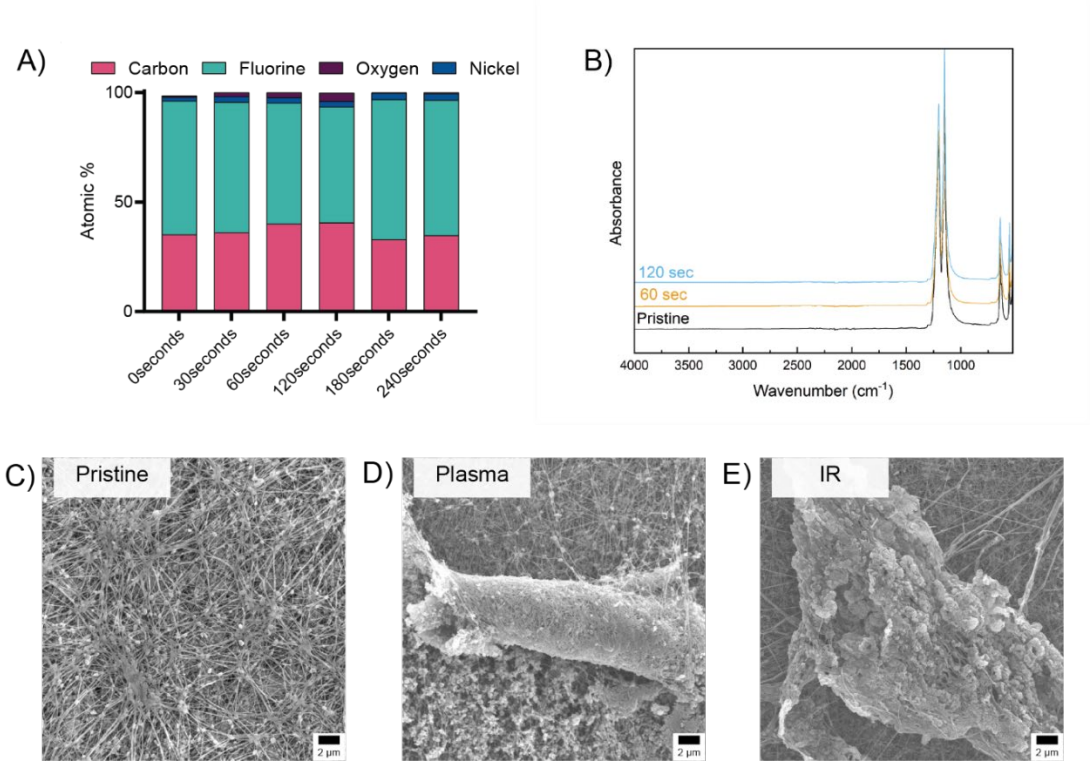

Figure 15: A) Summary of survey x-ray photoelectron spectroscopy. B) Infrared spectroscopy of pristine, 60 second plasma treated and 120 second plasma treated PTFE C)-E) Low magnification SEM images of pristine PTFE, plasma PTFE and infrared heated PTFE.

Following 240 seconds of plasma treatment, we observed that the top layer of the membrane began to delaminate, Figure 15D. From this discovery, we theorized that during plasma treatment, the fibers of the PTFE membrane were in fact melting leading to the clustering of the polymer nodules leading to the microstructures. This tracks with the reported fabrication of the membranes. Per their patent, Sitterer et al, observed that the membranes having “fused” and “non fused” structures on the membrane was based

off heat treatment of the membranes and through the application of an indirect heat treatment the membrane exhibited clustered microstructures on the surface like the plasma treated membranes. To probe this potential thermal degradation mechanism, we performed a radiative heating experiment by exposing our membrane to an infrared lamp. Following exposure, we used SEM to probe changes in the membrane and found that the nodules on clustered as well and the top layer eventually delaminated similar to plasma, Figure 15E.

4.4. CONCLUSIONS:

The ability to use plasma as a quick and efficient means to create omniphobic distillation membranes was explored. Following a brief oxygen plasma treatment, we found that microstructures formed on the surface of commercial PTFE membranes leading to superhydrophobic behavior from the membranes. Wetting resistance to low surface tension liquids was probed with a simple ethanol/water contact angle study. The plasma treated PTFE exhibited high resistance against low surface liquids as the contact angle remained above 120° with solutions that contained up to 40% ethanol whereas untreated PTFE's contact angle began to drop below 120° with solutions of 20% ethanol. Electrical impedance spectroscopy provided high resolution liquid entry pressure tests and demonstrated that the plasma treated PTFE membranes had enhanced pressure wetting resistance with both water and ethanol/water solutions. In addition to enhanced wetting resistance, the plasma treated membranes showed potentially higher fluxes in pressure driven distillation, but further studies must be done to fully understand how plasma treatment of the membranes enhances pressure driven distillation fluxes. Overall, we showed that plasma can be used to create omniphobic distillation membranes.

Furthermore, our studies informed the mechanism in which polymers are textured with plasma by suggesting that in addition to initial surface roughness, the polymers are also experiencing thermal degradation from the plasma. By understanding the mechanism in which the structures are formed, this study can potentially inform the design of future distillation membranes that exhibit antiwetting behavior.

5. Design of catalytic PTFE membranes for pressure driven distillation through atomic layer deposition

The work in this section was done at the Center of Integrated Nanotechnologies at the Sandia National Laboratory as part of the 2024 CINT Research Initiative Program. Atomic layer deposition, scanning electron microscopy, x-ray photoelectron spectroscopy and liquid entry pressure measurements were done by E.A. Hjelvik. S.D. Marks and M. Ticknor acquired data for grazing incidence wide angle x-ray scattering experiments. B. A. Knutson acquired data for J. Roback

5.1. INTRODUCTION

To combat fouling, there is increased interest in creating reactive membranes surfaces. In particular, the combination of advanced oxidation processes and membrane surface coatings has recently been pursued. Advanced oxidation processes (AOPs) are defined as methods that can generate hydroxyl radicals and other reactive oxygen species in water feed streams. Significant advances in the integration of photocatalysts as an AOP in water treatment to replace traditional methods of disinfection have been made. When properly activated, catalysts can generate free radicals in the feed stream which can degrade contaminants and in turn reduce membrane surface fouling. However, there is concern about the ability to activate the catalysts as well as their subsequent removal from the wastewater feed stream.[100]

As established in Chapter 2, modifying the surface of membranes has been found to reduce adhesion of foulants on membrane surfaces. Yu et al reported that treating polypropylene hollow fiber membranes with a NH_3 plasma treatment, which decreased

membrane hydrophobicity, led to improved performance of the membranes and reduced biofouling behavior.[34] Li et al grafted copolymers to a polyethersulfone membrane and reported that the total and irreversible fouling on the membranes decreased after grafting the polymer thin films.[101] Overall, it has been accepted that hydrophilic surfaces can better resist fouling. However, this fact is debated. Hou et al created a superhydrophobic PVDF membrane for use in membrane distillation and found that the superhydrophobic membrane resisted fouling from humic acid better than the pristine membrane. Ioannou et al found that through a two-step plasma treatment process of PTFE, which created a superhydrophobic surface, there was improved antifouling ability against bovine serum albumin.[88] To reconcile these contradicting studies, it has been suggested that antifouling ability is less to do with the overall hydrophobicity but the actual surface roughness. Horseman et al found that hydrophilic surfaces are less prone to colloidal fouling but they also observed that increasing roughness on hydrophilic surface led to a decrease in fouling propensity while increased roughness on hydrophobic surface led to an increase.[36] Overall, membrane surfaces can be engineered to aid in fouling and some groups have begun to explore the potential of integrating functional chemistries into the surfaces. For example, Hirsch et al found that through the plasma enhanced magnetron sputter of silver nanoparticles on RO membranes, they could achieve antifouling and antimicrobial properties.[102] Since functional surface chemistries could aid in both antifouling and potential in situ cleaning, there has been an interest in creating catalytic membranes, where catalytic materials are integrated into the membranes so they can serve as antifouling films but also aid in advanced oxidation processes.[102,103]

Catalytic membrane methods

Multiple groups have investigated combining the benefits of surface engineering and catalytic AOPs through coating membranes with catalytic materials. Generally, the processes to create catalytic membranes can be separated into blending or surface approaches. Blending involves the integration of catalytic materials in membrane casting solutions. The solutions are used to create membranes through phase conversion, electrostatic spinning or sol gel processes.[103–105] While blending has been extensively proven to create catalytic membranes, it does suffer in that these processes are time consuming, require significant chemical use, and have low product yield.[106] From all of these factors, the scalability of blending methods is questionable. Therefore, there has been interest in methods that allow for quick and scalable creation of catalytic membranes, and surface functionalization methods have been pursued.

Surface functionalization is where catalytic materials are integrated onto membrane surfaces. Generally, surface functionalization can be separated into coating methods or bottom-up synthesis approaches and offer quick, robust and controllable means to create catalytic membranes. For coating methods, spin coating is often pursued. In spin coating a catalytic solution is distributed onto a surface through centrifugal force and gravitational effects. Spin coating is an attractive method for creating catalytic films on membranes. Thickness can be easily controlled with spin coating and solution parameters.[107,108] However, spin coating is only applicable to coating simple geometry membranes, thus limiting the type of membranes that can be made into catalytic methods. On the other hand, bottom up-synthesis approaches are the most promising for creating catalytic membranes. In bottom-up synthesis, reactive catalyst precursor chemistries are

introduced to the membrane surface and eventually create catalytic films on the membrane top surface. Chemical vapor deposition, where substrates are continuously exposed to gaseous chemical precursors to grow materials on the surface, has been proven to create photocatalytic TiO_2 coatings on ceramic membranes.[109]

Overall, the ability to fabricate catalytic membranes has been thoroughly proven in a variety of different methods, with CVD and similar bottom-up synthesis approaches offering scalable methods that have means to provide controlled stable coatings. However, the application of these processes to distillation membranes is not simple. The challenge of creating catalytic distillation membranes comes from the introduction of a hydrophilic top surface to the hydrophobic membrane. As established in Chapter 4 section 4.1, liquid entry pressure, or wetting in a membrane, can occur from a decrease in hydrophobicity. In methods such as CVD the membranes are continuously exposed to the chemical precursors, and it is difficult to control the penetration of the chemicals through the membrane's pores. Additionally, as established in Chapter 3, hydrophobic membranes are typically comprised of chemistries that make it difficult to introduce the needed functional to grow catalytic materials. Therefore, these challenges must be addressed to realize the potential of bottom up synthesis approaches to create catalytic distillation membranes. Recently, there have been studies that investigate using atomic layer deposition (ALD) to grow materials on just the top surface of porous polymer material and chemically inert materials like PTFE.[110,111]

Atomic layer deposition, ALD, is a renowned surface chemistry technique, commonly used in the semiconductor industry, that can fabricate atomically thin layers of material on surfaces through the introduction of two self-limiting half reactions in the gas phase.

ALD reactions are done in a vacuum system and in the case of metal oxides a gaseous metal precursor and an oxygen source, typically water, are separately introduced into the system with dosing and purging steps, Figure SI 5. Usually, the metal precursor will react with OH groups on the surface, becoming covalently bound to the surface then the water will react with the precursor driving the formation of the oxide material. The two reactions are typically self-limiting in nature which allows for sequential steps of introducing the chemicals to the surface and atomic level control of the film growth. [112–114]

Pathak et al, proved the ability to control ALD reactions to the top surface of a isometric polycarbonate membranes, offering control of the pore size and wall composition of the polycarbonate membranes.[110] Particularly, they found that short dose times were crucial to keep the chemistries to the top surface as well as prevent sequential infiltration synthesis, which is an technique similar to ALD but the precursors can travel into the polymer network. Then Krumpolec et al, found that plasma modification of PTFE prior to ALD allowed for nucleation of materials on the surface via ALD.[115] To date there are few studies that utilize atomic layer deposition (ALD) to coat membranes with catalytic materials. Therefore, in this work we were interested in using ALD as a means to create catalytic distillation membranes without losing potential distillation performance.

5.2. MATERIALS AND METODS

5.2.1. Membrane and chemicals

Commercial PTFE membranes (Pall) were modified and tested. The membranes had a nominal pore diameter of 0.02 μm and arrived as flat sheet membranes in a dry state. Prior to modification and testing, samples were cut from flat sheets. For atomic layer

deposition reactions, titanium tetrachloride (Sigma Aldrich) and deionized (DI) water were used as reaction precursors. Sodium chloride (NaCl, Fisher Chemical) dissolved in DI water was used as the feed solution in liquid entry pressure tests. Methylene blue was dissolved in DI water and diluted to 5mg/mL for catalytic degradation tests.

5.2.2. Atomic layer deposition

Plasma assisted atomic layer deposition was performed at 165 C in a Picosun Sunale R150 ALD. Two reactions were programed for deposition onto the PTFE surface. The first was a remote oxygen plasma step followed by introduction of trimethylaluminum. For the plasma-TMA cycle, five cycles of remote oxygen plasma with a RF power of 2000 W, a pulse time of 30 seconds, and a purge time of 10 seconds were performed, then five cycles of TMA with a pulse time of 0.1 seconds and purge time of 6 seconds were performed. The second reaction was the TiO_2 with titanium tetrachloride and water. $TiCl_4$ was dosed into the ALD chamber with a pulse time of 0.1 seconds and a purge time of 6.0 seconds. Then water was dosed with a pulse of 0.2 seconds and purge of 8.0 seconds.

5.2.3. Materials characterization

Membrane morphology and surface topography was viewed with scanning electron microscopy (SEM) on a Hitachi SU8010 microscope. Prior to SEM imaging, platinum sputtered onto the PTFE membranes until a thickness of 3 nm was achieved on the surface.

X-ray photoelectron survey spectra were acquired from 0–1200 eV using a Kratos Supra X-ray photoelectron spectrometer. Polymer samples were isolated on the sample

plate to ensure consistent charging through the samples. The Al K alpha X-ray source was operated at 1486.7 kV and 15 mA current emission. Charge neutralization parameters were determined through use of continuous scans of the carbon 1s peak. Survey spectra were used to calculate the atomic percent of elements on the surface

Membrane surface wettability was observed through dropping a 10 μL droplet of water onto the surface following modification.

Grazing incidence wide angle scattering spectra were acquired using a Xenocs Xeuss 3.0 on the 1000TiO_2-PTFE samples. Samples were mounted onto a silica substrate and placed in the instrument. The x-ray was set at low angle of 0.2° to ensure measurement was just of the top surface of the membrane rather than the bulk.

The presence and morphology of TiO_2 on the membrane surface was investigated using X-ray absorption computed tomography (XCT) in both pure absorption and phase contrast modalities from a Zeiss Xradia Ultra 810 lab instrument with the large field of view (LFOV) optics. The PTFE active layer was separated from the support layer then enclosed in Kapton tape from both sides. The PTFE was then sliced with a razor blade into a wedge with a wide base and very thin point (<100 μm). 2-part epoxy was used to affix this wedge to a sample pin for imaging. The thin point extended slightly above the pin to isolate it for imaging while maintaining stability during rotation.

In pure absorption mode, the sample was rotated through 1301 projections spanning 180° with 15 seconds of X-ray exposure at each projection. The same number of projections were used in phase contrast mode but with 25 seconds of X-ray exposure at each to account for the drop in detector counts when phase optics are introduced to the

X-ray path. Detector pixels in LFOV are 64 nm and camera binning of 2 was used for all measurements to yield reconstructed voxel sizes of 128 x 128 x 128 nm^3 and a subsequent resolution of ~500 nm.

5.2.4. Model dye degradation to probe catalytic activity

The photocatalytic performance of the TiO_2-PTFE membranes with increasing cycles of ALD and a pristine PTFE as a control was evaluated by measuring the decrease in concentration of methylene blue using a UV spectrophotometer (Cary UV-) following exposure to UV light irradiation (365nm, x watts, light intensity xx). Membranes were cut into 5/8” circle, and mounted into petri dishes with Kapton tape to ensure a flat surface. The membranes were immersed in a solution of 5mg/L MB. Prior to commencing the UV lamp, the membranes sat in the solution of dyes in the dark for 1 hour to come to light absorption equilibrium, then for an additional 1 hour to establish the behavior of the membranes in the dark. Absorbance measurements were taken at each of these points with a UV Vis spectrometer (Cary 4000). Once UV lighting commenced, absorbance measurements were taken every 30 minutes for two hours. After the initial UV exposures, the samples were left in the dark for 16 hours and their absorbance was taken. Similarly, UV exposure was commenced

5.2.5. Liquid entry pressure

Liquid entry pressure measurements were taken to establish wetting resistance of the membranes following ALD fabrication. The membranes were cut into xx circles and loaded into a stainless-steel dead-end membrane cell. The feed side was loaded with a 5mM NaCl solution and was gently tapped to ensure no bubbles. The cell was hooked up to a nitrogen gas cylinder and the pressure slowly increased to 50 psi and sat for 30

minutes. Following this initial increase, the pressure was increased every 10-15 minutes by 10 psi. Once water was seen on the permeate end of the stainless steel, the pressure was recorded, and a needle valve was used to allow release the gas from the system.

5.3. RESULTS AND DISCUSSION

5.3.1. Atomic layer deposition of TiO_2 on PTFE membranes

TiO_2 was grown on PTFE membranes using a remote plasma atomic layer deposition process. PTFE is comprised of a carbon backbone decorated with four fluorine atoms, making it relatively chemically inert. To grow titanium on the PTFE, we functionalized the surface with a remote oxygen plasma treatment. As mentioned in Chapter 4, remote plasma allows for the introduction of reactive functional groups like oxygen to the surface. Following the preparation step, we ran 250, 500, and 1000 cycles of TiO_2 ALD on the PTFE surface. To check if the reaction was achieved, we performed basic surface wettability tests. Pristine PTFE has a contact angle of around 140° with the water droplet beading up on the surface. Following ALD processing, water spread across the surface with an immeasurable contact angle indicating a hydrophilic surface and a change to the surface chemistry.

Following depositions, we examined the membranes under scanning electron microscopy to observe any changes in the structure, Figure 16A. Untreated PTFE membranes are comprised of a fiber nodule structure, and as we increase ALD cycles we can see the both the fibers and nodules begin to increase in size, Figure 16B. At 250 cycles we see an increase in fiber thickness from pristine of approximately 81.8 nm. For 500 cycles we see an increase in thickness of 114.8 nm, in addition to the formation of

particles on the polymer fibers which was reported in.[111] Finally with 1000 cycles of ALD we see an increase in diameter of about 125.6 nm from pristine. We were surprised to see that the difference from pristine between 500 and 1000 was so similar as we are doubling the amount of material on the surface. However, we did find that in some areas on the 1000TiO_2 membrane there were thicker areas of material growth, Figure SI 6, which indicates that the deposition was not uniformly coating the membrane surface.

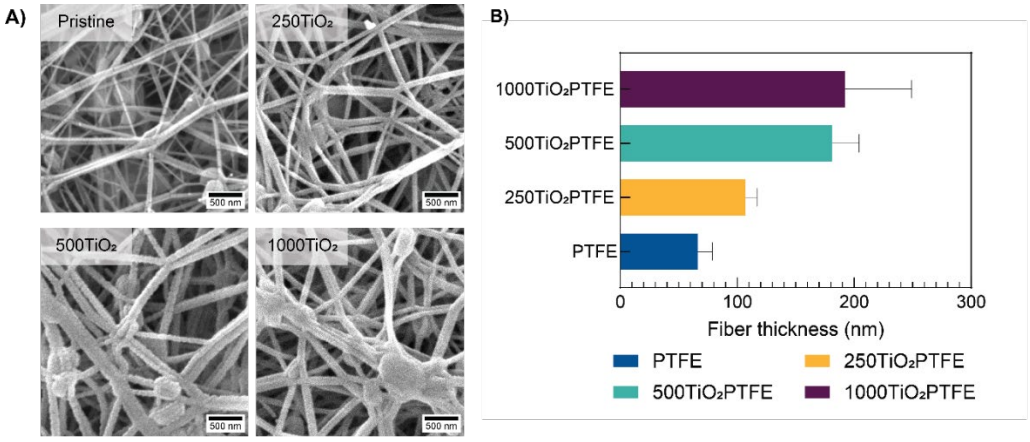

Figure 16: A) Scanning electron microscopy of ALD treated PTFE membranes. B) Summary of how thickness increases with increasing ALD cycles.

We confirmed the composition of the membranes with x-ray photoelectron spectroscopy, Figure 17A. For the XPS analysis, we chose four spots on the membrane and took the average and standard deviation of the percents. We see that with increasing cycles of ALD there is an increase in the titanium on the surface. At around 500 cycles, we start seeing a decrease in the fluorine peak. Interestingly, at 1000 cycles, we see some spots have virtually no fluorine on the survey spectra, whereas on others we still

see fluorine, Figure 17B. We hypothesize that this occurs due to an ununiform deposition of the TiO_2 and coincides with our observations with the SEM on the $1000TiO_2$.

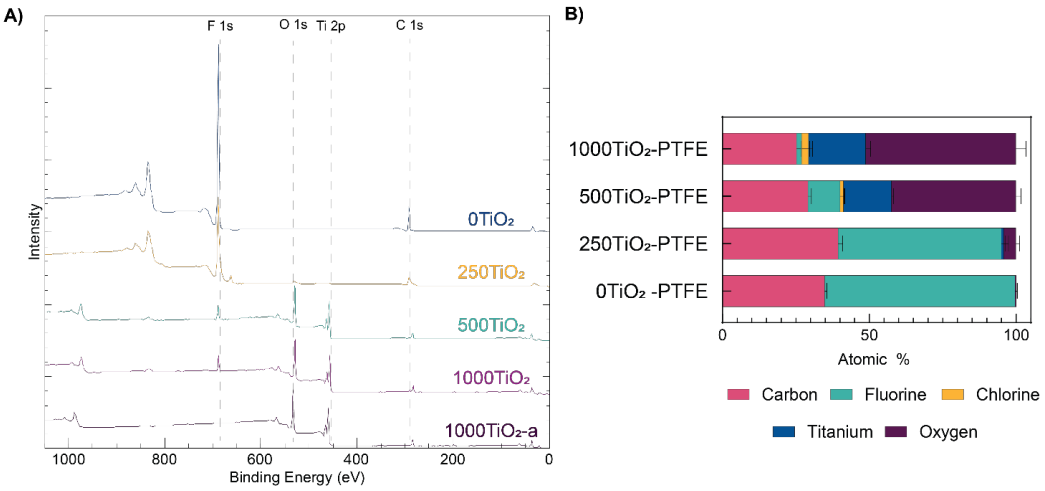

Figure 17: A) X-ray photoelectron survey spectra of TiO_2 membranes and B) summary of the atomic percents. Four spots were measured on the samples in triplicate. Some of the data was discarded due to severe sample charging on $0TiO_2$ and $250TiO_2$.

5.3.2. Impacts of TiO_2 deposition on PTFE membranes

While we were successful in the deposition of TiO_2 onto the PTFE we were concerned about the infiltration of the ALD precursors into the membrane. Since ALD is a conformal surface modification technique, it has been observed that when it coats isometric porous material the precursors can travel through the pore, thus coating the entire pore.[116] Distillation membranes selectivity and overall performance is reliant upon their hydrophobic nature which creates an air-liquid interface at the entry of the membrane pore. If the pore is entirely hydrophilic, water will pass through the membrane thus losing its selectivity.[46,97] As a result, we wanted to limit the penetration of the precursors into the membrane. Previous studies have shown that the top surface of a porous substrate can

be limited through short dosing times[110], therefore in our procedure we kept the dosing times to 0.1 seconds. We wanted to confirm the penetration of the TiO_2 into the membrane to ensure that the deposition remained on the top surface.

To determine the penetration of the TiO_2 into the PTFE membrane, we imaged the 1000TiO_2-PTFE membrane with X-ray absorption contrast computed tomography (XCT). Due to its ability to provide detailed cross-sectional images of materials pore network and morphology, XCT was an attractive candidate to analyze our samples.[117] We utilized the 1000 cycles sample as it theoretically should have the most material on the surface. At 5.4 keV, the TiO_2 has approximately an order of magnitude larger absorption coefficient than PTFE so the difference in material can be clearly resolved if they are distinctly layered.

Figure 18A shows the reconstructed volume of a sample after 500 cycles where the grayscale value is directly related to X-ray absorption – the whiter the voxel (3D pixel), the higher the X-ray absorption. Here, we see a clear thin layer of relatively highly absorbing material on the surface of the bulk PTFE layer which along with our XPS measurements in Figure 15 we can conclude is the TiO_2. Throughout the rest of the PTFE, the average grayscale remains nearly constant, indicating the lack of TiO_2 penetration. Thus, we can be reasonably confident that the TiO_2 forms a thin surface layer and does not penetrate deeper into the PTFE. Due to deformation during sample preparation, we cannot determine the true thickness of the TiO_2 but can estimate it to be ~1 μm, Figure 18B.

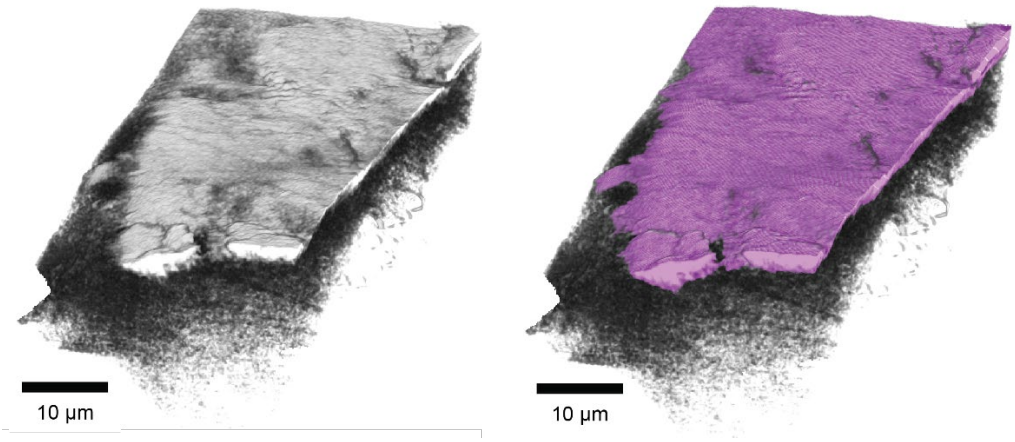

Figure 18: A) nano X-ray computed tomography of 1000TiO_2-PTFE images, the white top surface is associated with TiO_2 while the black volume is associated with PTFE. B) Histogram showing thickness variations of the TiO_2 layer per Figure 16A.

Since the TiO_2 is not seen through the entire membrane volume, we were interested in probing out the catalytic coating would impact overall wetting resistance with LEP measurements. LEP was performed in triplicate in a stainless-steel dead-end cell. For the unmodified PTFE, we report LEP values to be 180psi- 200 psi. Then as we increased cycles of ALD, we found that the TiO_2 PTFE exhibited LEPs 193, 186 and 137 for 250, 500 and 1000 cycles of LEP, respectively. Given the PTFE membranes were fibrous in nature, LEP can be approximated with the Purcell model, Equation SI Equation 1.0. Provided that we see a fiber increase and the catalytic material remains on the top surface of the membrane, we would have expected the LEP's to either increase or remain close to untreated PTFE's LEP.

We hypothesize that this trend could be due to a variety of factors. The first being, following LEP measurements, we observed that the 1000TiO_2 membrane exhibited surface cracking which may impact the wettability. However, we do not know if the surface

cracking is through the membrane which could cause the water to pass through the membrane. The second factor considers how TiO_2 may impact the thickness of the membrane airgap. Lopez et al and Deshmukh et al, observed that while distillation membranes permeabilities can be increased through decreasing the air-gap thickness, there is a notable higher risk of pore wetting with thinner membranes. This is due to a thermodynamic limit of wetting in air filled membranes. [22,97] Overall, there are a variety of factors that can explain the decrease in LEP, and further studies should be done to fully understand the wetting behavior of the catalytic membranes.

Prevalence of the surface cracks on the 1000TiO_2, Figure 19, is most likely a consequence of the ALD on the polymer surface. With ALD on polymer networks, there is a risk of the precursors infiltrating into the network, otherwise known as sequential infiltration synthesis, which in turn may impact overall mechanical properties.[43] To gain a full understanding of how the ALD processes were impacting the membranes, we were interested in obtaining nanoindentation measurements to determine the elastic moduli of the membranes. We found an increase in reduced modulus with increasing ALD cycles, from 4.7 MPa for the unmodified membrane to 310 MPa for the 1000 cycle membrane, attributed to the increased thickness of the rigid TiO2 coating layer. However, the exact details of the mechanical behavior likely arise from a complex interplay between fiber diameter, density, and adhesion. Table 2 gives the values for the reduced modulus, which is a composite measurement accounting for the moduli and Poisson's ratio of the sample and the indenter tip, for each of the membrane samples.

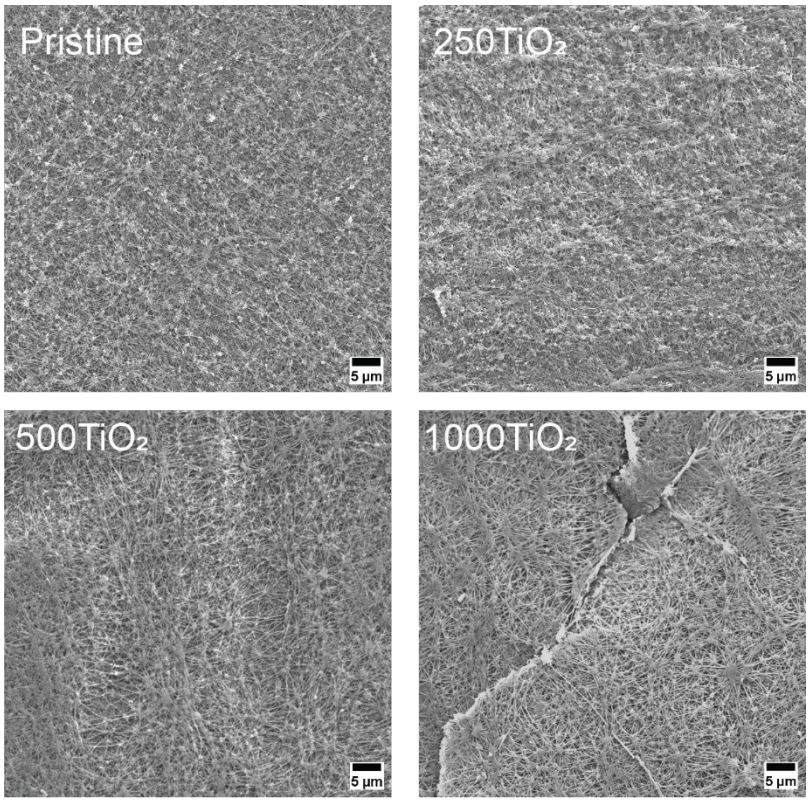

Figure 19: Evidence of cracking on the membrane top surface at 1000 cycles of ALD.

Table 2: Summary of changes in membrane parameters following atomic layer deposition of TiO_2

Sample	CA after ALD	CA before LEP	Fiber diameter (nm)	Modulus (MPa)	LEP (psi)
PTFE	NA	140	66.4±12.5	4.7±2.7	200
250TiO2	~50	110	107±10	6.8±6.2	193±5.7
500TiO2	<10	98	181±23	16.5±7.7	186±5.7
1000TiO2	<10	80	192±57.3	310±180	137±5.7

5.3.3. Utility as a catalytic membrane for desalination

TiO_2 is recognized as an ideal photocatalyst due to its flat band potential, stability, cost effectiveness and non-toxicity. [118,119] TiO_2 exhibits photocatalytic activity when exposed to direct light irradiation, ideally with a light that has a energy greater than or equal to the TiO_2 bandgap. During light exposure, photogenerated charge carriers (hole and electron) are formed.[120] Electrons transfer to the conduction band and holes, which remain at the valence band, are generated and trapped on the photocatalyst surface, which then produces reactive oxygen species like hydroxyl or oxygen radicals which can aid in the decomposition of contaminants. [120,121] TiO_2 bandgap changes based off the crystallite phase it is in and TiO_2 has three phases, anatase, rutile and brookite.[122] Photocatalytic activity is usually seen in anatase and rutile with anatase exhibiting higher photocatalytic behavior. Therefore, in the ALD of TiO_2 it was imperative that we achieved an anatase crystalline state. The reactions were done at 165 °C to ensure formation of TiO2 in the anatase phase, the phase of TiO_2 that is known to be photocatalytic. Polarized optical microscopy images of the coated membranes, indicated that with the introduction of TiO_2 there was polycrystalline films on the surface which were not observed on untreated PTFE, Figure SI 7. To further probe the crystallinity of the coatings, the structure of the TiO_2 layer was probed using grazing-incidence X-ray diffraction (GIXRD) using Cu k_α radiation.

The diffraction profile in Figure 20 represents the azimuthally integrated intensity measured on a 2D pixel-array detector. Pristine PTFE and TiO_2-coated PTFE specimens with the same length mounted to a low-background sample holder and measured in sequence. The strong reflection in both profiles at 1.3 $Å^{-1}$ arises from crystalline domains

of the PTFE membrane. The profile measured from the TiO_2-coated PTFE has clearly distinct scattering signatures arising from the coating. A broad amorphous peak centered at 0.95 $Å^{-1}$ arises from the amorphous TiO_2. The relatively weak reflection at 1.6 $Å^{-1}$ corresponds to the 002 reflection from crystalline TiO_2. The combine amorphous and crystalline scattering signatures indicates that the ALD process produces semicrystalline TiO_2 films at the surface of the PTFE films. [123]

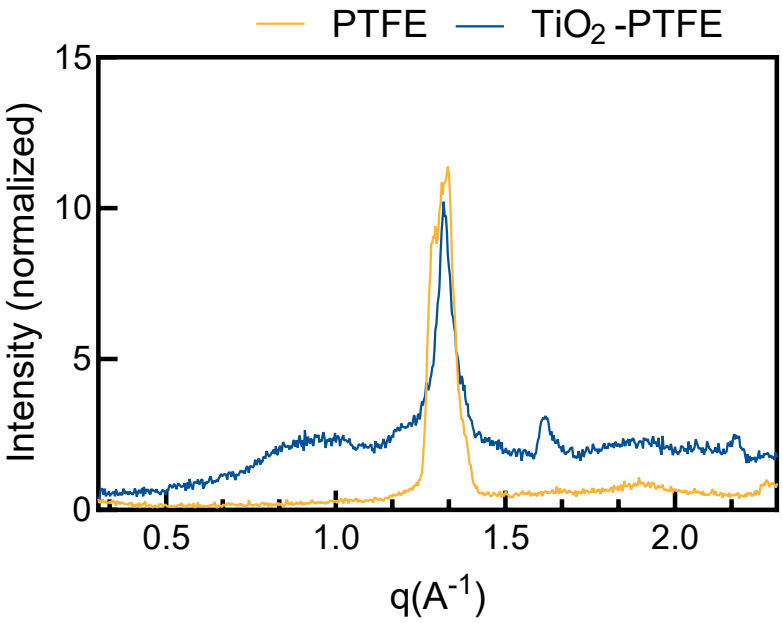

Figure 20: Grazing incidence wide angle x-ray scattering of pristine PTFE and 1000TiO_2 PTFE.

While we confirmed the TiO_2 on the PTFE membrane is in the anatase phase which should allow for photocatalytic degradation, we wanted to quantify the membranes' ability to degrade model contaminants. Photocatalytic performance was examined by examining the degradation of methylene blue (MB) under UV irradiation. As two controls we exposed a solution MB without a membrane and a untreated PTFE membrane submerged in MB.

Prior to UV exposure, we let the membranes sit in dark conditions for an hour to establish an adsorption equilibrium. After the initial hour, we took absorbance measurements to give us a baseline of how the membranes may impact the methylene blue. We let the samples sit in the dark for an additional hour and did not see any decrease in absorbance, Figure SI 8. Following the dark experiment, we exposed the membrane to a 365nm UV light for 2 hours, measuring the absorbance every 30 minutes. We observed that with increasing ALD cycles and exposure to UV irradiation, we saw a decrease in absorbance, Figure 21, with 1000TiO_2 having the highest degradation. The membrane with 250 cycles had a similar trend to untreated PTFE and MB. This may be due to not having enough TiO_2 on the surface. In addition to the two hours of UV irradiation, we let the membrane sit in the dark for another 16 hours and found that the absorbance values did not change. Following this 16-hour period, we exposed the solutions again to UV light and observed further degradation.

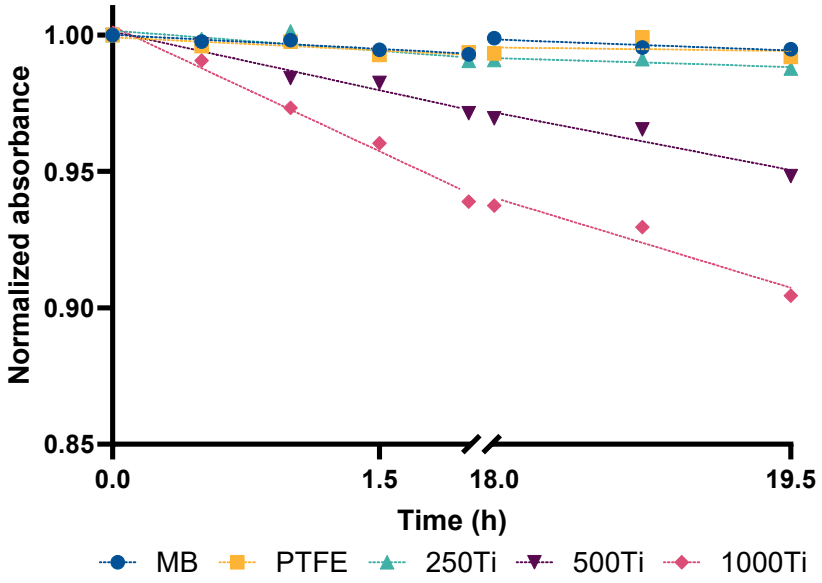

Figure 21: Photocatalytic degradation of methylene blue (MB) with the TiO_2 membranes. The initial UV irradiation experiment was two hours with absorbance being taken every 30 minutes. Following the first two hours, the membrane sat in the dark for 16 hours and then were exposed to UV light for an additional 1.5 hours.

5.4. CONCLUSIONS:

Atomic layer deposition has shown significant promise in its ability to create catalytic distillation membranes. We were able to limit the growth of the TiO_2 to the top surface of the membrane through limiting precursor dose times, then found that ALD offered control of photocatalytic activity through the number of ALD cycles during processing. In our membranes, we observed TiO_2 exhibited an anatase crystalline phase which has been associated with high photocatalytic activity, however we also observed potential amorphous phases of TiO_2. We expected to see this as our reaction was done at 165 C which is in the transition temperature range of where anatase crystals form. Therefore,

photocatalytic activity could potentially be further controlled through temperature variations in the ALD processes and ensuring full transition of amorphous TiO_2 to anatase and potentially rutile. The TiO_2 – PTFE membranes also exhibited high wetting resistances even though we were changing the surface hydrophilicity, but we do see a decrease in liquid entry pressure with increasing ALD cycles. We attributed this to the membrane potentially weakening due to changes in the mechanical properties, based off surface cracks on the surface observed in SEM and changes in nanoindentation, or due to changes in the membrane air gap. For future studies, the performance of these membranes in desalination processes should be further probed to further inform the use of ALD for catalytic membranes. Overall, this study has proved the ability to use ALD to create catalytic distillation membranes and has provided groundwork for informing the design of catalytic distillation membranes with ALD.

6. Informed design of asymmetric pores in hydrophobic membranes for pressure driven distillation

6.1. INTRODUCTION

Distillation membranes can be used in three distinct processes: membrane distillation, osmotic distillation and pressure driven distillation. All three processes utilize hydrophobic membranes, and as established in Chapter 2, when the membranes are submerged into a feed solution, liquid does not readily move through the membrane. Instead, an air-liquid interface is formed at the pore entry and different driving forces drive the liquid water to convert to vapor water allowing it to transport through the membrane.

In the case of membrane distillation (MD) it is a thermally driven process, meaning a temperature difference at the air liquid interface creates a partial vapor pressure difference thus leading to transport of vapor water through the membrane. The feed side of the membrane is usually hot while the permeate side is cold creating the temperature differential.[6,11,23] In osmotic distillation (OD), the driving force is created through a difference in concentration of solutes on the feed and permeate side leading to a buildup of osmotic pressure.[6] Then pressure driven distillation (PDD), the newest technology of the three, transport through the membrane is caused by an applied pressure on the feed side.

PDD offers many benefits over RO and is the most attractive distillation process as an alternative to RO. Similar to RO, pressure is applied to the feed side of the membrane which generates a difference in chemical potential between the feed and permeate side. [6] Since the transport of water in PDD is reliant upon the vapor transport of water through

an airgap, unlike liquid in RO processes, PDD sees almost complete rejection of nonvolatile contaminants. However, with its selectivity benefits over RO, PDD suffers from low permeabilities as established in Chapter 2.

To meet the high-pressure requirements that are commonly seen in RO sea and brackish water desalination, there is a need for high pressure resistances in PDD membranes. This comes in the form of membranes with high LEP's. Per Figure 22, to achieve high wetting resistances in a hydrophobic membrane with a contact angle of 140, the pore size of the membranes must be less than 100 nm.

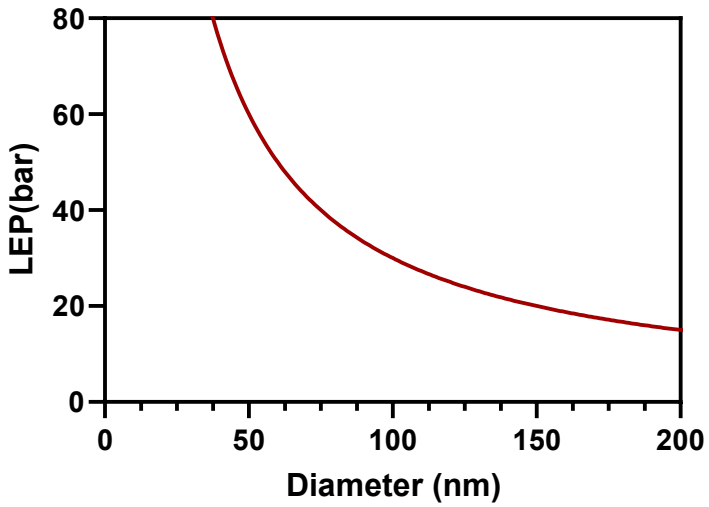

Figure 22: Liquid entry pressure reliance upon pore size, assuming a solution of water and hydrophobic membrane with a contact angle of 140°.

Pore sizes can increase transport resistances in PDD, and per equation 2.0 resistances in the system define the permeability in PDD. These resistances can be lowered, thus increasing the flux through the informed design of the membrane pores.

Therefore, for this project we explored how transport resistance in PDD could be reduced through the informed design of the membrane pores.

6.1.1. Asymmetric membranes and potential permeability increases

As established in Chapter 2, resistances in the air-gap membranes determine overall flux, and have an inverse relationship to permeability. The resistances that are typically encountered are interfacial and transmission. Transmission resistances can be separated into molecular diffusion, the interactions of the vapor with molecules in the pore, and Knudsen diffusion, interactions of the molecules with the pore itself.[6,20,21]

$$B_w^{MD} = \frac{\varepsilon P D_w M_w}{RTP_a \tau l} \qquad \text{Eq 5.0}$$

$$B_w^K = \frac{2}{3RT}\frac{\varepsilon r M_w}{\tau \delta}\sqrt{\frac{8RT}{\pi M_w}} \qquad \text{Eq 5.1}$$

$$B_T = (R_w^{MD} + R_w^K)^{-1} \qquad \text{Eq 5.2}$$

Equation 5: Simplified transmission resistance for air filled membranes.

Transmission resistances in Chapter 2 are defined in equation 2.3, which was derived to account for the effect of air molecules present in the nanopores and gives a more accurate calculation of flux in PDD. However, for the sake of looking at just physical parameters of the pore on resistances in PDD, we look at the simplified molecular diffusion and Knudsen permeability definitions, equation 5.0 and 5.1, respectively. In these equations, D_w is the diffusion coefficient of water, P is the total pressure in pore, P_a is the pressure of air in pore, τ is tortuosity of the pores, l is pore length, ε is porosity, and r is the maximum pore radius. The relationship between permeabilities and resistances is defined in equation 5.2, where permeability is the inverse sum of the resistances.[21]

For pores that are less than 100 nm, we only look at Knudsen resistances, as resistances from molecular diffusion typically dominate if pores that are greater than 150 nm. Looking at equation 5.1, reducing the pore length and increasing the pore size we can reduce transmission resistances. However, as previously established for PDD to be used as an alternative to RO, membranes with pore sizes less than 100 nm are required. Like RO membranes, PDD membranes can achieve higher permeabilities by decreasing the overall membrane thickness, however there is a thermodynamic wetting limit.

From liquid entry pressure (eq. 3.0) a thermodynamic wetting criterion was established to determine the critical distance between two opposed liquid-vapor interfaces, (the feed and permeate) in which the combination of the two membrane-solution interfaces present in vapor gap membranes is energetically unfavorable. It determined that there is a minimum pore length, as defined in Equation SI 2.0, for both low pressure (MD) and high pressure (PDD) applications and this pore length puts limits on the overall water permeability that is achieved with air-gap membranes.[22]

It has been suggested that asymmetric pores structure, Figure 23, could potentially reduce Knudsen resistances while also maintaining high pressure resistances. Asymmetric pores are defined as pores that have smaller pores on the active side that taper off into larger pore size towards the permeate side. When comparing the Knudsen permeability of a 150 nm pore and a 10 nm pore, we see that the 150 nm pore Knudsen permeability is 20 times higher than the 10 nm. However, if we consider an asymmetric pore with an active pore size of 10 nm that tapers into a 150 nm pore, we see that the Knudsen permeabilities of an asymmetric pore structure can be like a symmetric pore of 150 nm particularly at lower active pore lengths, Figure 24. We theoretically can achieve

high wetting resistances from our small pore size while also reducing the overall resistances thus increasing the Knudsen permeability. Therefore, we were interested in experimentally proving this ability of asymmetric pore structures in PDD.

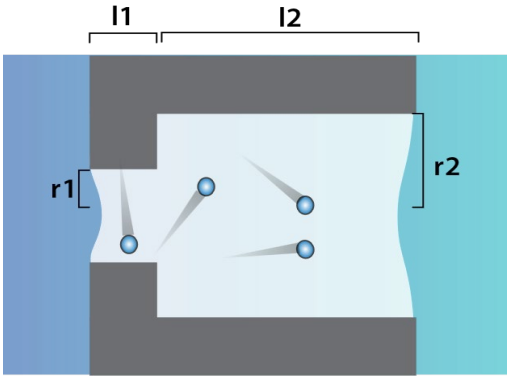

Figure 23: Schematic of asymmetric pore structure where r1 is the smaller pore radius that has a thickness of l1. The pore then moves into a larger pore, r2, of length l2.

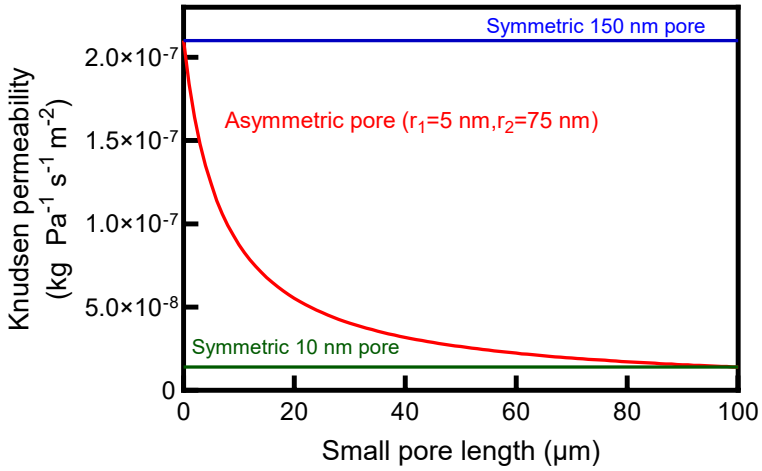

Figure 24: Knudsen permeability as a function of small pore length. Permeability for symmetric pores with a diameter of 10 nm and 150 nm is shown in green and blue respectively. Asymmetric pores with varying small pore length is shown in red.

6.2. MATERIALS AND METHODS

6.2.1. Membranes and chemicals

Isotropic and anisotropic anodic aluminum oxide (AAO) membranes (InRedox) were modified and tested. The anisotropic membranes had a total thickness of 60 μm. The active pore had a diameter that ranged from 10 nm-50 nm and had a length of 1.5 μm-5 μm. Then the support pore size was 150nm and made up the rest of the membrane length. The isotropic membranes had pore sizes that ranged from 10nm-100nm. Prior to modification, the membranes were placed in a oven set at 900 C to allow for annealing. Deionized (DI) water was obtained using a Millipore Synergy UV Remote Water Purification System. AAO membranes were hydroxylated with hydrogen peroxide (vendor) and then (Heptadecafluoro-1,1,2,2-tetrahydrodecyl) triethoxysilane (FAS) (Gelest) was chemically deposited onto the membranes to render then hydrophobic.

6.2.2. Chemical vapor deposition

Chemical vapor deposition of the FAS was performed in a ThermoScientific vacuum oven. Prior to deposition, membranes were hydroxylated in boiling hydrogen peroxide and rinsed with DI water. Once they were dried, membranes were placed into a petri dish in the preheated (100C-120C) vacuum oven. After 20 minutes of heating the membranes and glassware, 50 uL of the FAS was aliquoted into a vial and placed into the petri dish. The membrane, FAS and petri were covered to keep the FAS concentrated on the membrane. The vacuum chamber was pumped down to 21 inHg, and the vacuum was pulled for 15 minutes before closing the chamber. The reaction sat overnight, under vacuum and air was introduced to the chamber. The membranes were allowed to cool prior to characterization.

6.2.3. Materials characterization

Contact angle was measured with a Biolin Scientific tensiometer using the sessile drop technique. For all measurements, a droplet of DI water (less than 10 uL) was deposited onto the active side of the membrane surface using a pipette.

Membrane morphology and surface topography was viewed with a field emission scanning electron microscopy (FESEM) on a JEOL JSM-7401F microscope. Prior to SEM imaging, platinum was sputtered onto membranes until a thickness of 3 nm was achieved on the surface.

Attenuated total reflectance Fourier transform infrared (ATR-FTIR) spectra were acquired from 400–4000 cm-1 using a ThermoScientific Nicolet iS50 FTIR with a Smart iTX attachment with ATR capacities and an ATR diamond crystal. Measurements were taken of the membranes before and after FAS deposition.

X-ray photoelectron survey spectra were acquired from 0–1200 eV using a Kratos Supra X-ray photoelectron spectrometer. The Al K alpha X-ray source was operated at 1486.7 kV and 15 mA current emission. Survey spectra were used to calculate the atomic percent of elements on the surface

6.2.4. Liquid entry pressure

Liquid entry pressure measurements were taken to establish wetting resistance of the AAO membranes. The membranes were loaded into a stainless-steel dead-end membrane cell (InRedox). The feed side was loaded with a 5mM NaCl solution and was gently tapped to ensure no bubbles. The cell was connected to a nitrogen gas cylinder and the pressure slowly increased to 50 psi and sat for 30 minutes. Following this initial

increase, the pressure was increased every 10-15 minutes by 10 psi. Once water was seen on the permeate end of the stainless steel, the pressure was recorded, and a needle valve was used to release the gas from the system. To ensure accuracy of measurements, LEP was video recorded to track any changes to the system during pressure equilibrium wait times.

6.3. RESULTS AND DISCUSSION

6.3.1. Materials system for testing asymmetric pores

To test the theory that asymmetric membranes can achieve high wetting resistance and increased permeability we utilized anisotropic (asymmetric) anodic aluminum oxide membranes. AAO membranes have uniform cylindrical pores and serve as an ideal experimental system to confirm model behavior, since we do not have to account for variables such as tortuosity. This allows us to just focus on how pore structure impacts permeabilities. Prior to modification we imaged the membranes with field emission scanning electron microscopy, Figure 25, to confirm that the active side had smaller pore sizes while the support tapered into a larger pore. Prior to testing the wetting resistance and permeability of the asymmetric AAO membranes, they needed to be rendered hydrophobic. Briefly, chemical vapor deposition is a vacuum deposition method that is commonly used in microfabrication to produce thin films.[124] Typically, a substrate, in this case the AAO membrane, is exposed to a volatile precursor. This precursor reacts with active chemistry, such as hydroxyls, on the substrates surface providing a covalently bound functional chemistry on the surface. [125]

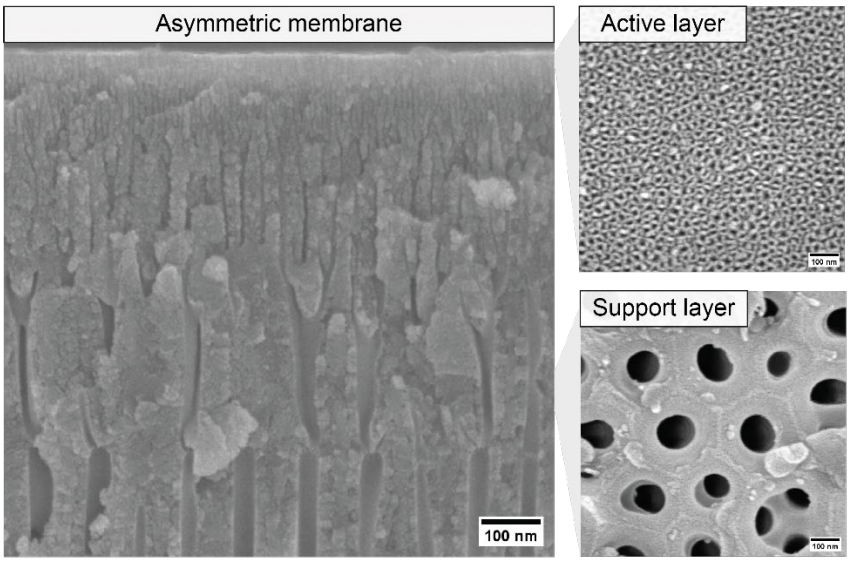

Figure 25: FESEM imaging of asymmetric AAO membranes. The smaller pore size on the active side was 20 nm and the larger pore size was 150 nm.

To render the AAO membranes hydrophobic we utilized a (Heptadecafluoro-1,1,2,2-tetrahydrodecyl) triethoxysilane, FAS, as the fluorinated carbon chain would impart hydrophobic behavior to the surface, Figure 26A. Due to its relatively low vapor pressure (<0.1 mmHg @ 25 C), we did have to heat the chamber to allow for deposition of the molecule. Prior to deposition, we submerged membranes into hot hydrogen peroxide to hydroxylate the surface.

Following hydroxylation, we performed CVD of the FAS on the membranes, and following an overnight deposition we found that the membranes were rendered hydrophobic as evidenced by the 150° contact angle on the active layer. Figure 26B. The support layers contact angle was 114°. The difference in contact angle on the support versus the active layer, can be due to only the active surface being exposed during deposition, and the FAS can only travel so far through the pores. Additionally, the smaller

pore size of the active layer may introduce a rougher surface thus giving a higher contact angle, as established in Chapter 4.

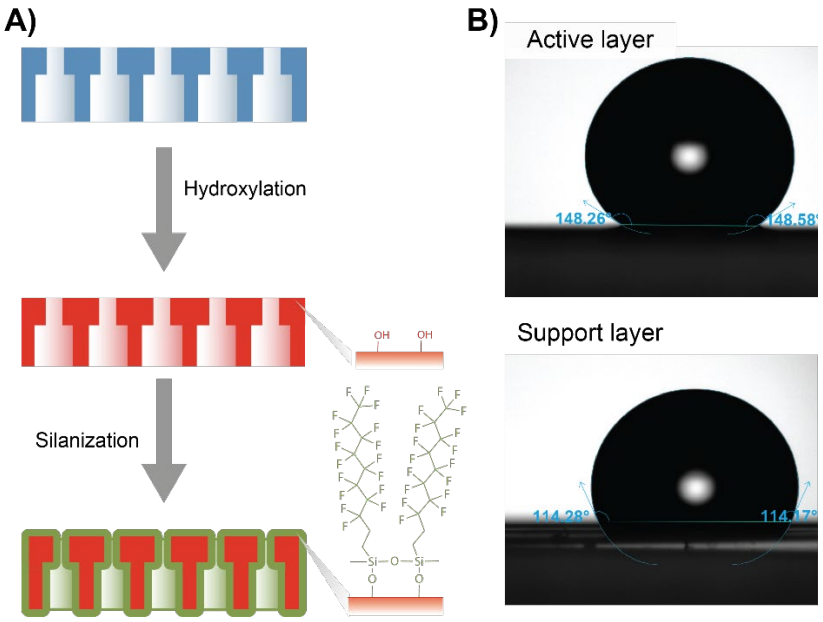

Figure 26: A) Fabrication procedure of hydrophobic AAO membranes. B) Contact angles on the active and support layer of the membranes after FAS modification.

We confirmed the presence of the FAS on the membrane with both x-ray photoelectron spectroscopy (XPS) and infrared spectroscopy (IR), Figure 27A and 27B respectively. Given that CVD forms thin films on the surface we were interested in analyzing just the top surface of our sample. In the XPS spectra, on unmodified AAO we only see peaks for aluminum and oxygen, and following CVD we see the evolution of carbon, fluorine and silica all of which are present in the FAS molecule. To supplement our XPS data, we also looked at the bulk structure of the AAO following deposition with IR, and found that following deposition we see the formation of peaks in the fingerprint region which corresponds to different carbon bonds. We also see a strong peak between 1400 and

1000 which can be corresponded to a C-F peak. Overall, our data confirms that we were successful in our deposition of FAS onto the AAO membranes.

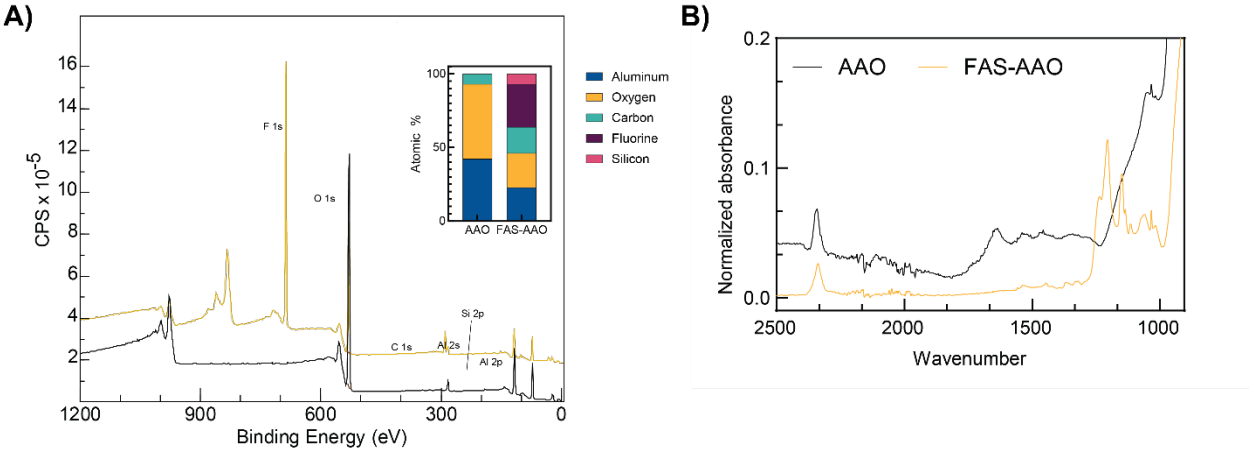

Figure 27: A) XPS survey spectra and summary of atomic % of AAO and AAO modified with FAS. B) FTIR of AAO and AAO modified with FAS.

6.3.2. Experimental set up for confirming pore performance

To test the performance of the membranes we were focused on testing their wettability and their overall flux. To test the wettability, we focused on characterizing the liquid entry pressure of the asymmetric membranes. Given the high contact angle and the small pore size (10-30nm), and assuming a pure water solution, we theoretically should achieve liquid entry pressures of 800-1000 psi. Liquid entry pressure measurements are performed in a dead-end membrane cell, where we load water into the feed side and pressurize the feed side with a two-stage gas regulator. The pressure that we begin to see water pushing through the permeate side is our recorded LEP.

In our initial tests of the asymmetric membranes, we were successful in achieving pressures of 400 psi without wetting, however the maximum pressure our regulators were

able output to meet was limited to 500 psi. We also found that in our LEP studies the amount of time between increases in pressure would impact the measurements. We found that longer wait times between pressure increases would ensure a pressure equilibrium and provide a more accurate measure of LEP. We sometimes found inconsistent LEP results during the pressure equilibrium times but were able to account for these through video monitoring of the LEP tests.

As for permeability, considering equation 2.3, we expect that the asymmetric membranes will have a flux that is three times faster than a symmetric membrane with small pore sizes. We were unable to test the flux of the asymmetric membranes, however, there is an established method to test PDD flux. With the dead-end cell we use for LEP, membranes are placed into the cell. Instead of pure water, the feed is loaded with a low concentration NaCl solution. The cell is then placed in a water bath that is heated which allows for faster flux. A permeate tube is connected to the permeate side and then closely monitored via video for a 16-21 hour period of time.

6.3.3. Future work

To further realize this work, liquid entry pressures should be done with regulators that have higher maximum allowable pressure inputs and flux tests should be done to corroborate theoretical flux values. As mentioned previously, there were inconsistencies in LEP data which may be caused from a variety of factors including defects in the membrane Figure SI 9, flawed fabrication methods, improper membrane loading, bubbles in the feed tube, too quick pressure increment increases, and many more. Additionally, LEP does not account for any potential partial pore wetting, where water begins to intrude through the pores without going through the entire membrane. A concern for the

asymmetric membranes is smaller pore is experiencing wetting prior to the maximum LEP, so there is a need to examine partial wetting instead of just full wetting. There has been work to study wetting with electrical impedance spectroscopy, and we utilized it in Chapter 4 to study the wetting behavior of the plasma treated membranes.

Overall, this work was done to prove the impact of pore structure on PDD permeability. We were successful in creating membranes that would offer ideal testing environment to prove that asymmetric membranes can help reduce Knudsen resistances and had promising initial liquid entry pressure measurements. The study could be further improved through more careful investigation of pore wetting and performing chemical vapor depositions with proper hydroxylation and utilizing a more robust CVD chamber. A custom vapor deposition chamber was designed and built solely by E.A. Hjelvik for this work, Figure SI 10.

7. Future directions and conclusions

The goal of this thesis was to study and improve distillation membrane design. We successfully applied well established surface chemistry techniques such as plasma cleaning and atomic layer deposition to enhance distillation membranes anti-wetting and anti-fouling coatings.

Plasma cleaning is a historically well-established method that can aid in various processes. Recently, plasma has found a significant application in desalination for its ability to alter surface chemistry and morphology. In our studies, we were able to prove that we could create microstructures on a PTFE membrane which imparted an antiwetting characteristic to the membranes through a simple low power plasma process. Plasma could also aid in other fabrication methods such as CVD of silanes on membranes as it is a proven technique to hydroxylate the surface. However, plasma could also potentially assist in addressing physical parameters that could hinder permeability in distillation meters.

Particularly, plasma could assist in low porosities of hydrophobic membranes as the direct ion bombardment could introduce more porosity onto the membranes. We observed that this is the case in track etch polycarbonate membranes after it was exposed to a brief plasma treatment, Figure SI 11, so further studies could probe how to design membranes with increased porosity with plasma. Additionally, plasma also offers the ability to modify just the top surface of a membrane. We were recently interested in creating PDD membranes with a thin vapor gap, and this was achieved through “masking” the membrane pore with an non-reactive aminosilane chemistry, sputtering the top surface of the membrane with platinum and relying on a shadowing effect to coat the very

top surface of the membrane and then making the membrane hydrophobic with CVD. Plasma theoretically could assist in eliminating the need for sputtering through the ablation and activation of just the top surface of the membrane with a remote plasma step, as remote plasmas have a limited penetration depth due to having a short mean free path.[82]

Atomic layer deposition is a powerful technique that can help modify the top surfaces of membranes imparting potential control over the pore size, top surface chemistry and potentially overall selectivity of the membranes. In our studies with atomic layer deposition, we proved that hydrophobic membranes could be successfully modified where they can serve as both distillation membranes and catalytic membranes. To further realize the ability for ALD in fabricating catalytic membranes, more studies should be done to control density of the catalytic material, test the flux of the membranes in both PDD and MD, and probe changes in mechanical properties and how it may impact overall performance.

Outside of catalytic membrane fabrication, ALD offers significant advantages for membrane fabrication in its ability to modify just the top surface. As mentioned in Chapter 5, the ALD reaction was limited to the top surface of the membrane by utilizing shorter dosage times in the ALD reaction. The short precursor dose times allows for two benefits, prevention of the entire membrane pore being coated and prevention of infiltration of the precursors into the polymer network. However, the latter could also be potentially studied to create catalytic membranes or improve membrane thermal or chemical resistance. Due to its ability to be limited to the top surface of a porous material, ALD offers an attractive method to create asymmetric membranes or membranes with thin vapor gap layers. ALD

overall offers significant advantages in membrane fabrication in that there is the ability to grow low-cost materials, control pore size and top surface chemistry.

In addition to probing different fabrication methods, we probed the oxidation resistance and permeability of distillation membranes, to provide a direct comparison towards RO polyamide membranes. As established in Chapter 2 and summarized in Table 1, distillation membranes have significantly higher oxidation resistances than polyamide membranes due to their chemical structures. In polyamide, the amide linkage is susceptible to chemical attacks which calls into question the long-term usability of polyamide membranes. Hydrophobic polymers used in distillation are typically comprised of chemistries that are not susceptible to chemical attack such as fluorine or hydrocarbon chemistry. We were interested in probing if these membranes would ever be impacted by desalination disinfection chemicals and exposed them in static conditions to high concentrations of ozone and sodium hypochlorite. Overall, we found highly fluorinated polymers like PTFE, did not experience any changes in performance and its structure was not impacted. PVDF was similar, but also showed in XPS studies that there was defluorination occurring which may lead to eventual failure. Then polypropylene membranes which are comprised of only hydrocarbons showed the most severe degradation. Overall, this study provided important information about how membrane chemistry will impact its overall ability to be used as a long-term membrane. However, due to recent EPA filings there is a need to find high oxidation resistant membranes that do not rely on PFAS chemicals in processing. ALD may also offer an opportunity in this area, as the infiltration of precursors into the polymer network has been shown to improve thermal stability of membranes.

The final project of this thesis probed into improving PDD fluxes through the inclusion of an asymmetric pore structure. This structure would allow for high wetting resistances while also reducing Knudsen resistances in the pore thus improving the flux. We were unable to complete this project due to inconsistencies in LEP which were found to be due to uncontrollable circumstances that prevented the project from moving forward. However, future studies could include studying the asymmetric wettability with electrical impedance spectroscopy and have potentially better hydrophobic fabrications using a more robust CVD system that includes gas purging and better vacuum. Overall, distillation membranes have potential in addressing the drawbacks of RO polyamide membranes but still have their own significant drawbacks before their potential can be realized. This thesis provides the groundwork of how surface chemistry technologies can be applied to improve distillation membrane design and then also provides a more in depth analysis of how distillation membranes chemical structure can be designed to impart oxidation resistance and how pore structure can be designed to improve fluxes.

References

(1) UN-Water. *Scarcity*. UN-Water. https://www.unwater.org/water-facts/scarcity/ (accessed 2021-12-14).

(2) Elimelech, M.; Phillip, W. A. The Future of Seawater Desalination: Energy, Technology, and the Environment. *Science* **2011**, *333* (6043), 712–717. https://doi.org/10.1126/science.1200488.

(3) Werber, J. R.; Osuji, C. O.; Elimelech, M. Materials for Next-Generation Desalination and Water Purification Membranes. *Nat. Rev. Mater.* **2016**, *1* (5), 16018. https://doi.org/10.1038/natrevmats.2016.18.

(4) Greenlee, L. F.; Lawler, D. F.; Freeman, B. D.; Marrot, B.; Moulin, P. Reverse Osmosis Desalination: Water Sources, Technology, and Today's Challenges. *Water Res.* **2009**, *43* (9), 2317–2348. https://doi.org/10.1016/j.watres.2009.03.010.

(5) Nickerson, T. R.; Antonio, E. N.; McNally, D. P.; Toney, M. F.; Ban, C.; Straub, A. P. Unlocking the Potential of Polymeric Desalination Membranes by Understanding Molecular-Level Interactions and Transport Mechanisms. *Chem. Sci.* **2023**, *14* (4), 751–770. https://doi.org/10.1039/D2SC04920A.

(6) Lopez, K. P.; Wang, R.; Hjelvik, E. A.; Lin, S.; Straub, A. P. Toward a Universal Framework for Evaluating Transport Resistances and Driving Forces in Membrane-Based Desalination Processes. *Sci. Adv. 9* (1), eade0413. https://doi.org/10.1126/sciadv.ade0413.

(7) Elimelech, M.; Phillip, W. A. The Future of Seawater Desalination: Energy, Technology, and the Environment. *Science* **2011**, *333* (6043), 712–717. https://doi.org/10.1126/science.1200488.

(8) Yao, Y.; Zhang, P.; Jiang, C.; DuChanois, R. M.; Zhang, X.; Elimelech, M. High Performance Polyester Reverse Osmosis Desalination Membrane with Chlorine Resistance. *Nat. Sustain.* **2021**, *4* (2), 138–146. https://doi.org/10.1038/s41893-020-00619-w.

(9) Werber, J. R.; Deshmukh, A.; Elimelech, M. The Critical Need for Increased Selectivity, Not Increased Water Permeability, for Desalination Membranes. *Environ. Sci. Technol. Lett.* **2016**, *3* (4), 112–120. https://doi.org/10.1021/acs.estlett.6b00050.

(10) Nguyen, D. T.; Lee, S.; Lopez, K. P.; Lee, J.; Straub, A. P. Pressure-Driven Distillation Using Air-Trapping Membranes for Fast and Selective Water Purification. *Sci. Adv.* **2023**, *9* (28), eadg6638. https://doi.org/10.1126/sciadv.adg6638.

(11) Alkhudhiri, A.; Darwish, N.; Hilal, N. Membrane Distillation: A Comprehensive Review. *Desalination* **2012**, *287*, 2–18. https://doi.org/10.1016/j.desal.2011.08.027.

(12) Howard, J. A.; Ingold, K. U. Absolute Rate Constants for Hydrocarbon Autoxidation. VI. Alkyl Aromatic and Olefinic Hydrocarbons. *Can. J. Chem.* **1967**, *45* (8), 793–802. https://doi.org/10.1139/v67-132.

(13) McKeen, L. W. 11 - Fluoropolymers. In *Film Properties of Plastics and Elastomers (Third Edition)*; McKeen, L. W., Ed.; Plastics Design Library; William Andrew Publishing: Boston, 2012; pp 255–313. https://doi.org/10.1016/B978-1-4557-2551-9.00011-6.

(14) Brown, E. N.; Rae, P. J.; Dattelbaum, D. M.; Clausen, B.; Brown, D. W. In-Situ Measurement of Crystalline Lattice Strains in Polytetrafluoroethylene. *Exp. Mech.* **2008**, *48* (1), 119–131. https://doi.org/10.1007/s11340-007-9075-3.

(15) O'Hagan, D. Understanding Organofluorine Chemistry. An Introduction to the C–F Bond. *Chem. Soc. Rev.* **2008**, *37* (2), 308–319. https://doi.org/10.1039/B711844A.

(16) Dalvi, V. H.; Rossky, P. J. Molecular Origins of Fluorocarbon Hydrophobicity. *Proc. Natl. Acad. Sci. U. S. A.* **2010**, *107* (31), 13603–13607. https://doi.org/10.1073/pnas.0915169107.

(17) McKean, D. C.; Duncan, J. L.; Batt, L. CH Stretching Frequencies, Bond Lengths and Dissociation Energies. *Spectrochim. Acta Part Mol. Spectrosc.* **1973**, *29* (6), 1037–1049. https://doi.org/10.1016/0584-8539(73)80143-6.

(18) Lippert, E. The Strengths of Chemical Bonds, von T. L. Cottrell. Butterworths Publications Ltd., London 1958. 2. Aufl., X, 317 S., Geb.t—/32/—. *Angew. Chem.* **1960**, *72* (16), 602–602. https://doi.org/10.1002/ange.19600721618.

(19) Lee, J.; Karnik, R. Desalination of Water by Vapor-Phase Transport through Hydrophobic Nanopores. *J. Appl. Phys.* **2010**, *108* (4), 044315. https://doi.org/10.1063/1.3419751.

(20) Lee, J.; Laoui, T.; Karnik, R. Nanofluidic Transport Governed by the Liquid/Vapour Interface. *Nat. Nanotechnol.* **2014**, *9* (4), 317–323. https://doi.org/10.1038/nnano.2014.28.

(21) Straub, A. P.; Elimelech, M. Energy Efficiency and Performance Limiting Effects in Thermo-Osmotic Energy Conversion from Low-Grade Heat. *Environ. Sci. Technol.* **2017**, *51* (21), 12925–12937. https://doi.org/10.1021/acs.est.7b02213.

(22) Deshmukh, A.; Lee, J. Membrane Desalination Performance Governed by Molecular Reflection at the Liquid-Vapor Interface. *Int. J. Heat Mass Transf.* **2019**, *140*, 1006–1022. https://doi.org/10.1016/j.ijheatmasstransfer.2019.06.044.

(23) Choudhury, M. R.; Anwar, N.; Jassby, D.; Rahaman, Md. S. Fouling and Wetting in the Membrane Distillation Driven Wastewater Reclamation Process – A Review. *Adv. Colloid Interface Sci.* **2019**, *269*, 370–399. https://doi.org/10.1016/j.cis.2019.04.008.

(24) Warsinger, D. M.; Swaminathan, J.; Guillen-Burrieza, E.; Arafat, H. A.; Lienhard V, J. H. Scaling and Fouling in Membrane Distillation for Desalination Applications: A Review. *Desalination* **2015**, *356*, 294–313. https://doi.org/10.1016/j.desal.2014.06.031.

(25) Maximous, N.; Nakhla, G.; Wan, W. Comparative Assessment of Hydrophobic and Hydrophilic Membrane Fouling in Wastewater Applications. *J. Membr. Sci.* **2009**, *339* (1), 93–99. https://doi.org/10.1016/j.memsci.2009.04.034.

(26) Israelachvili, J.; Pashley, R. The Hydrophobic Interaction Is Long Range, Decaying Exponentially with Distance. *Nature* **1982**, *300* (5890), 341–342. https://doi.org/10.1038/300341a0.

(27) Meyer, E. E.; Rosenberg, K. J.; Israelachvili, J. Recent Progress in Understanding Hydrophobic Interactions. *Proc. Natl. Acad. Sci.* **2006**, *103* (43), 15739–15746. https://doi.org/10.1073/pnas.0606422103.

(28) Wang, Z.; Lin, S. Membrane Fouling and Wetting in Membrane Distillation and Their Mitigation by Novel Membranes with Special Wettability. *Water Res.* **2017**, *112*, 38–47. https://doi.org/10.1016/j.watres.2017.01.022.

(29) Hou, D.; Christie, K. S. S.; Wang, K.; Tang, M.; Wang, D.; Wang, J. Biomimetic Superhydrophobic Membrane for Membrane Distillation with Robust Wetting and

Fouling Resistance. *J. Membr. Sci.* **2020**, *599*, 117708. https://doi.org/10.1016/j.memsci.2019.117708.

(30) Lu, X.; Peng, Y.; Ge, L.; Lin, R.; Zhu, Z.; Liu, S. Amphiphobic PVDF Composite Membranes for Anti-Fouling Direct Contact Membrane Distillation. *J. Membr. Sci.* **2016**, *505*, 61–69. https://doi.org/10.1016/j.memsci.2015.12.042.

(31) Shan, H.; Liu, J.; Li, X.; Li, Y.; Tezel, F. H.; Li, B.; Wang, S. Nanocoated Amphiphobic Membrane for Flux Enhancement and Comprehensive Anti-Fouling Performance in Direct Contact Membrane Distillation. *J. Membr. Sci.* **2018**, *567*, 166–180. https://doi.org/10.1016/j.memsci.2018.09.038.

(32) Li, J.-H.; Li, M.-Z.; Miao, J.; Wang, J.-B.; Shao, X.-S.; Zhang, Q.-Q. Improved Surface Property of PVDF Membrane with Amphiphilic Zwitterionic Copolymer as Membrane Additive. *Appl. Surf. Sci.* **2012**, *258* (17), 6398–6405. https://doi.org/10.1016/j.apsusc.2012.03.049.

(33) Hadidi, M.; Zydney, A. L. Fouling Behavior of Zwitterionic Membranes: Impact of Electrostatic and Hydrophobic Interactions. *J. Membr. Sci.* **2014**, *452*, 97–103. https://doi.org/10.1016/j.memsci.2013.09.062.

(34) Yu, H.-Y.; Hu, M.-X.; Xu, Z.-K.; Wang, J.-L.; Wang, S.-Y. Surface Modification of Polypropylene Microporous Membranes to Improve Their Antifouling Property in MBR: NH3 Plasma Treatment. *Sep. Purif. Technol.* **2005**, *45* (1), 8–15. https://doi.org/10.1016/j.seppur.2005.01.012.

(35) Sun, Q.; Su, Y.; Ma, X.; Wang, Y.; Jiang, Z. Improved Antifouling Property of Zwitterionic Ultrafiltration Membrane Composed of Acrylonitrile and Sulfobetaine Copolymer. *J. Membr. Sci.* **2006**, *285* (1), 299–305. https://doi.org/10.1016/j.memsci.2006.08.035.

(36) Horseman, T.; Wang, Z.; Lin, S. Colloidal Interactions between Model Foulants and Engineered Surfaces: Interplay between Roughness and Surface Energy. *Chem. Eng. J. Adv.* **2021**, *8*, 100138. https://doi.org/10.1016/j.ceja.2021.100138.

(37) Xu, B.; Feng, C.; Hu, J.; Shi, P.; Gu, G.; Wang, L.; Huang, X. Spin-Casting Polymer Brush Films for Stimuli-Responsive and Anti-Fouling Surfaces. *ACS Appl. Mater. Interfaces* **2016**, *8* (10), 6685–6692. https://doi.org/10.1021/acsami.5b12820.

(38) Skuse, C.; Alberto, M.; Luque-Alled, J. M.; Mercadillo, V. O.; Asuquo, E.; Gallego-Schmid, A.; Azapagic, A.; Gorgojo, P. Spray Coating of 2D Materials in the Production of Antifouling Membranes for Membrane Distillation. *J. Membr. Sci.* **2024**, *711*, 123162. https://doi.org/10.1016/j.memsci.2024.123162.

(39) Wang, K.; Hou, D.; Wang, J.; Wang, Z.; Tian, B.; Liang, P. Hydrophilic Surface Coating on Hydrophobic PTFE Membrane for Robust Anti-Oil-Fouling Membrane Distillation. *Appl. Surf. Sci.* **2018**, *450*, 57–65. https://doi.org/10.1016/j.apsusc.2018.04.180.

(40) Jia, Y.; Guan, K.; Mai, Z.; Fang, S.; Li, Z.; Zhang, P.; Zou, D.; Jiang, X.; He, G.; Matsuyama, H. Thin Continuous Membrane Coating with High Surface Energy for Comprehensive Antifouling Seawater Distillation. *Water Res.* **2023**, *244*, 120439. https://doi.org/10.1016/j.watres.2023.120439.

(41) Pourhakkak, P.; Taghizadeh, A.; Taghizadeh, M.; Ghaedi, M.; Haghdoust, S. Chapter 1 - Fundamentals of Adsorption Technology. In *Interface Science and Technology*; Ghaedi, M., Ed.; Adsorption: Fundamental Processes and Applications; Elsevier, 2021; Vol. 33, pp 1–70. https://doi.org/10.1016/B978-0-12-818805-7.00001-1.

(42) Huber, F.; Berwanger, J.; Polesya, S.; Mankovsky, S.; Ebert, H.; Giessibl, F. J. Chemical Bond Formation Showing a Transition from Physisorption to Chemisorption. *Science* **2019**, *366* (6462), 235–238. https://doi.org/10.1126/science.aay3444.

(43) Motta, A.; Seguini, G.; Perego, M.; Consonni, R.; Boccia, A. C.; Ambrosio, G.; Baratto, C.; Cerruti, P.; Lavorgna, M.; Tagliabue, S.; Wiemer, C. Sequential Infiltration Synthesis of Al2O3 in Biodegradable Polybutylene Succinate: Characterization of the Infiltration Mechanism. *ACS Appl. Polym. Mater.* **2022**, *4* (10), 7191–7203. https://doi.org/10.1021/acsapm.2c01073.

(44) Gong, B.; Peng, Q.; Jur, J. S.; Devine, C. K.; Lee, K.; Parsons, G. N. Sequential Vapor Infiltration of Metal Oxides into Sacrificial Polyester Fibers: Shape Replication and Controlled Porosity of Microporous/Mesoporous Oxide Monoliths. *Chem. Mater.* **2011**, *23* (15), 3476–3485. https://doi.org/10.1021/cm200694w.

(45) Bergsman, D. S.; Getachew, B. A.; Cooper, C. B.; Grossman, J. C. Preserving Nanoscale Features in Polymers during Laser Induced Graphene Formation Using Sequential Infiltration Synthesis. *Nat. Commun.* **2020**, *11* (1), 3636. https://doi.org/10.1038/s41467-020-17259-5.

(46) Kim, B.-S.; Harriott, P. Critical Entry Pressure for Liquids in Hydrophobic Membranes. *J. Colloid Interface Sci.* **1987**, *115* (1), 1–8. https://doi.org/10.1016/0021-9797(87)90002-6.

(47) Servi, A. T.; Kharraz, J.; Klee, D.; Notarangelo, K.; Eyob, B.; Guillen-Burrieza, E.; Liu, A.; Arafat, H. A.; Gleason, K. K. A Systematic Study of the Impact of Hydrophobicity on the Wetting of MD Membranes. *J. Membr. Sci.* **2016**, *520*, 850–859. https://doi.org/10.1016/j.memsci.2016.08.021.

(48) Guo, J.; Jiang, M.; Li, X.; Farid, M. U.; Deka, B. J.; Zhang, B.; Sun, J.; Wang, Z.; Yi, C.; Wong, P. W.; Jeong, S.; Gu, B.; An, A. K. Springtail-Inspired Omniphobic Slippery Membrane with Nano-Concave Re-Entrant Structures for Membrane Distillation. *Nat. Commun.* **2024**, *15* (1), 7750. https://doi.org/10.1038/s41467-024-52108-9.

(49) Asadolahi, M.; Fashandi, H. Creating Nature-Inspired Surface Roughness and Modifying Surface Chemistry of PVDF Electrospun Fibers Using Low-Pressure Plasma towards Omniphobic Membrane for Long-Term Distillation. *Sep. Purif. Technol.* **2024**, *330*, 125442. https://doi.org/10.1016/j.seppur.2023.125442.

(50) Williams, A. P.; Cook, E. R.; Smerdon, J. E.; Cook, B. I.; Abatzoglou, J. T.; Bolles, K.; Baek, S. H.; Badger, A. M.; Livneh, B. Large Contribution from Anthropogenic Warming to an Emerging North American Megadrought. *Science* **2020**, *368* (6488), 314–318. https://doi.org/10.1126/science.aaz9600.

(51) *Water Reuse: Potential for Expanding the Nation's Water Supply Through Reuse of Municipal Wastewater*; National Academies Press: Washington, D.C., 2012. https://doi.org/10.17226/13303.

(52) Liu, B.; Pimentel, A. L.; Watts, M. J.; Murphy, J. R.; Linden, K. G. Ozonation Greatly Improves Ceramic Membrane Microfiltration Efficiency during Wastewater Reuse: Mechanisms and Performance. *Environ. Sci. Water Res. Technol.* **2022**, *8* (7), 1535–1546. https://doi.org/10.1039/D2EW00105E.

(53) Nguyen, D. T.; Lopez, K. P.; Lee, S.; Lee, J.; Hernandez, M. T.; Straub, A. P. Water Desalination via Pressure-Driven Distillation with Chlorine-Resistant and Large-Area Polymeric Membranes. *Environ. Sci. Technol. Lett.* **2023**, *10* (8), 711–717. https://doi.org/10.1021/acs.estlett.3c00391.

(54) Szczuka, A.; Berglund-Brown, J. P.; Chen, H. K.; Quay, A. N.; Mitch, W. A. Evaluation of a Pilot Anaerobic Secondary Effluent for Potable Reuse: Impact of Different Disinfection Schemes on Organic Fouling of RO Membranes and DBP Formation. *Environ. Sci. Technol.* **2019**, *53* (6), 3166–3176. https://doi.org/10.1021/acs.est.8b05473.

(55) Chuang, Y.-H.; Szczuka, A.; Shabani, F.; Munoz, J.; Aflaki, R.; Hammond, S. D.; Mitch, W. A. Pilot-Scale Comparison of Microfiltration/Reverse Osmosis and Ozone/Biological Activated Carbon with UV/Hydrogen Peroxide or UV/Free Chlorine AOP Treatment for Controlling Disinfection Byproducts during Wastewater Reuse. *Water Res.* **2019**, *152*, 215–225. https://doi.org/10.1016/j.watres.2018.12.062.

(56) Do, V. T.; Tang, C. Y.; Reinhard, M.; Leckie, J. O. Effects of Chlorine Exposure Conditions on Physiochemical Properties and Performance of a Polyamide Membrane—Mechanisms and Implications. *Environ. Sci. Technol.* **2012**, *46* (24), 13184–13192. https://doi.org/10.1021/es302867f.

(57) Do, V. T.; Tang, C. Y.; Reinhard, M.; Leckie, J. O. Degradation of Polyamide Nanofiltration and Reverse Osmosis Membranes by Hypochlorite. *Environ. Sci. Technol.* **2012**, *46* (2), 852–859. https://doi.org/10.1021/es203090y.

(58) Powell, J.; Luh, J.; Coronell, O. Amide Link Scission in the Polyamide Active Layers of Thin-Film Composite Membranes upon Exposure to Free Chlorine: Kinetics and Mechanisms. *Environ. Sci. Technol.* **2015**, *49* (20), 12136–12144. https://doi.org/10.1021/acs.est.5b02110.

(59) McCurry, D. L.; Ishida, K. P.; Oelker, G. L.; Mitch, W. A. Reverse Osmosis Shifts Chloramine Speciation Causing Re-Formation of NDMA during Potable Reuse of Wastewater. *Environ. Sci. Technol.* **2017**, *51* (15), 8589–8596. https://doi.org/10.1021/acs.est.7b01641.

(60) Schreiber, I. M.; Mitch, W. A. Nitrosamine Formation Pathway Revisited: The Importance of Chloramine Speciation and Dissolved Oxygen. *Environ. Sci. Technol.* **2006**, *40* (19), 6007–6014. https://doi.org/10.1021/es060978h.

(61) Lee, S.; Straub, A. P. Opportunities for High Productivity and Selectivity Desalination via Osmotic Distillation with Improved Membrane Design. *J. Membr. Sci.* **2020**, *611*, 118309. https://doi.org/10.1016/j.memsci.2020.118309.

(62) Liu, W.; Wang, R.; Straub, A. P.; Lin, S. Membrane Design Criteria and Practical Viability of Pressure-Driven Distillation. *Environ. Sci. Technol.* **2023**, *57* (5), 2129–2137. https://doi.org/10.1021/acs.est.2c07765.

(63) Deshmukh, A.; Boo, C.; Karanikola, V.; Lin, S.; Straub, A. P.; Tong, T.; Warsinger, D. M.; Elimelech, M. Membrane Distillation at the Water-Energy Nexus: Limits, Opportunities, and Challenges. *Energy Environ. Sci.* **2018**, *11* (5), 1177–1196. https://doi.org/10.1039/C8EE00291F.

(64) Merle, T.; Pronk, W.; von Gunten, U. MEMBRO3X, a Novel Combination of a Membrane Contactor with Advanced Oxidation (O3/H2O2) for Simultaneous Micropollutant Abatement and Bromate Minimization. *Environ. Sci. Technol. Lett.* **2017**, *4* (5), 180–185. https://doi.org/10.1021/acs.estlett.7b00061.

(65) Bamperng, S.; Suwannachart, T.; Atchariyawut, S.; Jiraratananon, R. Ozonation of Dye Wastewater by Membrane Contactor Using PVDF and PTFE Membranes. *Sep. Purif. Technol.* **2010**, *72* (2), 186–193. https://doi.org/10.1016/j.seppur.2010.02.006.

(66) Rabuni, M. F.; Nik Sulaiman, N. M.; Aroua, M. K.; Hashim, N. A. Effects of Alkaline Environments at Mild Conditions on the Stability of PVDF Membrane: An Experimental Study. *Ind. Eng. Chem. Res.* **2013**, *52* (45), 15874–15882. https://doi.org/10.1021/ie402684b.

(67) Zhang, Y.; Zhao, P.; Li, J.; Hou, D.; Wang, J.; Liu, H. A Hybrid Process Combining Homogeneous Catalytic Ozonation and Membrane Distillation for Wastewater Treatment. *Chemosphere* **2016**, *160*, 134–140. https://doi.org/10.1016/j.chemosphere.2016.06.070.

(68) Li, K.; Xu, W.; Wen, G.; Zhou, Z.; Han, M.; Zhang, S.; Huang, T. Aging of Polyvinylidene Fluoride (PVDF) Ultrafiltration Membrane Due to Ozone Exposure in

Water Treatment: Evolution of Membrane Properties and Performance. *Chemosphere* **2022**, *308*, 136520. https://doi.org/10.1016/j.chemosphere.2022.136520.

(69) Puspitasari, V.; Granville, A.; Le-Clech, P.; Chen, V. Cleaning and Ageing Effect of Sodium Hypochlorite on Polyvinylidene Fluoride (PVDF) Membrane. *Sep. Purif. Technol.* **2010**, *72* (3), 301–308. https://doi.org/10.1016/j.seppur.2010.03.001.

(70) Awanis Hashim, N.; Liu, Y.; Li, K. Stability of PVDF Hollow Fibre Membranes in Sodium Hydroxide Aqueous Solution. *Chem. Eng. Sci.* **2011**, *66* (8), 1565–1575. https://doi.org/10.1016/j.ces.2010.12.019.

(71) Morent, R.; De Geyter, N.; Leys, C.; Gengembre, L.; Payen, E. Comparison between XPS- and FTIR-Analysis of Plasma-Treated Polypropylene Film Surfaces. *Surf. Interface Anal.* **2008**, *40* (3–4), 597–600. https://doi.org/10.1002/sia.2619.

(72) Gijsman, P.; Fiorio, R. Long Term Thermo-Oxidative Degradation and Stabilization of Polypropylene (PP) and the Implications for Its Recyclability. *Polym. Degrad. Stab.* **2023**, *208*, 110260. https://doi.org/10.1016/j.polymdegradstab.2023.110260.

(73) Brewis, D. M.; Mathieson, I.; Sutherland, I.; Cayless, R. A.; Dahm, R. H. Pretreatment of Poly(Vinyl Fluoride) and Poly(Vinylidene Fluoride) with Potassium Hydroxide. *Int. J. Adhes. Adhes.* **1996**, *16* (2), 87–95. https://doi.org/10.1016/0143-7496(95)00053-4.

(74) Ross, G. J.; Watts, J. F.; Hill, M. P.; Morrissey, P. Surface Modification of Poly(Vinylidene Fluoride) by Alkaline Treatment1. The Degradation Mechanism. *Polymer* **2000**, *41* (5), 1685–1696. https://doi.org/10.1016/S0032-3861(99)00343-2.

(75) Ni, T.; Zhao, S.; Kong, L.; Lin, J. Omniphobic Membranes: Fundamentals, Materials, and Applications. **2021**. https://doi.org/10.1039/9781839165436-00184.

(76) Cassie, A. B. D.; Baxter, S. Wettability of Porous Surfaces. *Trans. Faraday Soc.* **1944**, *40*, 546. https://doi.org/10.1039/tf9444000546.

(77) Karanikola, V.; Boo, C.; Rolf, J.; Elimelech, M. Engineered Slippery Surface to Mitigate Gypsum Scaling in Membrane Distillation for Treatment of Hypersaline Industrial Wastewaters. *Environ. Sci. Technol.* **2018**, *52* (24), 14362–14370. https://doi.org/10.1021/acs.est.8b04836.

(78) Wu, X.-Q.; Wu, X.; Wang, T.-Y.; Zhao, L.; Truong, Y. B.; Ng, D.; Zheng, Y.-M.; Xie, Z. Omniphobic Surface Modification of Electrospun Nanofiber Membrane *via* Vapor Deposition for Enhanced Anti-Wetting Property in Membrane Distillation. *J. Membr. Sci.* **2020**, *606*, 118075. https://doi.org/10.1016/j.memsci.2020.118075.

(79) Deng, L.; Ye, H.; Li, X.; Li, P.; Zhang, J.; Wang, X.; Zhu, M.; Hsiao, B. S. Self-Roughened Omniphobic Coatings on Nanofibrous Membrane for Membrane Distillation. *Sep. Purif. Technol.* **2018**, *206*, 14–25. https://doi.org/10.1016/j.seppur.2018.05.035.

(80) Palumbo, F.; Lo Porto, C.; Favia, P. Plasma Nano-Texturing of Polymers for Wettability Control: Why, What and How. *Coatings* **2019**, *9* (10), 640. https://doi.org/10.3390/coatings9100640.

(81) Thanu, D. P. R.; Srinadhu, E. S.; Zhao, M.; Dole, N. V.; Keswani, M. Chapter 8 - Fundamentals and Applications of Plasma Cleaning. In *Developments in Surface Contamination and Cleaning: Applications of Cleaning Techniques*; Kohli, R., Mittal, K. L., Eds.; Elsevier, 2019; pp 289–353. https://doi.org/10.1016/B978-0-12-815577-6.00008-6.

(82) Schiller, M.; Kulisch, W. Plasma Properties at the Transition from Remote to Direct Plasma. *Surf. Coat. Technol.* **1998**, *98* (1), 1590–1599. https://doi.org/10.1016/S0257-8972(97)00302-2.

(83) Gogolides, E.; Constantoudis, V.; Kokkoris, G.; Kontziampasis, D.; Tsougeni, K.; Boulousis, G.; Vlachopoulou, M.; Tserepi, A. Controlling Roughness: From Etching to Nanotexturing and Plasma-Directed Organization on Organic and Inorganic Materials. *J. Phys. Appl. Phys.* **2011**, *44* (17), 174021. https://doi.org/10.1088/0022-3727/44/17/174021.

(84) Di Mundo, R.; Palumbo, F.; d'Agostino, R. Nanotexturing of Polystyrene Surface in Fluorocarbon Plasmas: From Sticky to Slippery Superhydrophobicity. *Langmuir* **2008**, *24* (9), 5044–5051. https://doi.org/10.1021/la800059a.

(85) Di Mundo, R.; De Benedictis, V.; Palumbo, F.; d'Agostino, R. Fluorocarbon Plasmas for Nanotexturing of Polymers: A Route to Water-Repellent Antireflective Surfaces. *Appl. Surf. Sci.* **2009**, *255* (10), 5461–5465. https://doi.org/10.1016/j.apsusc.2008.09.020.

(86) Ellinas, K.; Gogolides, E. Ultra-Low Friction, Superhydrophobic, Plasma Micro-Nanotextured Fluorinated Ethylene Propylene (FEP) Surfaces. *Micro Nano Eng.* **2022**, *14*, 100104. https://doi.org/10.1016/j.mne.2022.100104.

(87) Ioannou, D.; Hou, Y.; Shah, P.; Ellinas, K.; Kappl, M.; Sapalidis, A.; Constantoudis, V.; Butt, H.-J.; Gogolides, E. Plasma-Induced Superhydrophobicity as a Green Technology for Enhanced Air Gap Membrane Distillation. *ACS Appl. Mater. Interfaces* **2023**, *15* (14), 18493–18504. https://doi.org/10.1021/acsami.3c00535.

(88) Ioannou, D.; Shah, P.; Ellinas, K.; Kappl, M.; Sapalidis, A.; Butt, H.-J.; Gogolides, E. Antifouling Plasma-Treated Membranes with Stable Superhydrophobic Properties for Membrane Distillation. *ACS Appl. Polym. Mater.* **2023**, *5* (12), 9785–9795. https://doi.org/10.1021/acsapm.3c01512.

(89) Lo Porto, C.; Di Mundo, R.; Veronico, V.; Trizio, I.; Barucca, G.; Palumbo, F. Easy Plasma Nano-Texturing of PTFE Surface: From Pyramid to Unusual Spherules-on-Pyramid Features. *Appl. Surf. Sci.* **2019**, *483*, 60–68. https://doi.org/10.1016/j.apsusc.2019.03.220.

(90) Xu, J.; Moon, H.; Xu, J.; Lim, J.; Fischer, T.; McNally, H. A.; Sintim, H. O.; Lee, H. One-Step Large-Scale Nanotexturing of Nonplanar PTFE Surfaces to Induce Bactericidal and Anti-Inflammatory Properties. *ACS Appl. Mater. Interfaces* **2020**, *12* (24), 26893–26904. https://doi.org/10.1021/acsami.0c04729.

(91) Palumbo, F.; Di Mundo, R.; Cappelluti, D.; d'Agostino, R. SuperHydrophobic and SuperHydrophilic Polycarbonate by Tailoring Chemistry and Nano-Texture with Plasma Processing. *Plasma Process. Polym.* **2011**, *8* (2), 118–126. https://doi.org/10.1002/ppap.201000098.

(92) Gryta, M. Application of Polypropylene Membranes Hydrophilized by Plasma for Water Desalination by Membrane Distillation. *Desalination* **2021**, *515*, 115187. https://doi.org/10.1016/j.desal.2021.115187.

(93) Inagaki, N. Plasma. In *Plasma Surface Modification and Plasma Polymerization*; CRC Press, 1996.

(94) Joshi, S. G.; Childress, A. E.; McGaughey, A. L. Onset, Rate, and Depth of Wetting Front Progression in Membrane Distillation. *J. Membr. Sci.* **2025**, *713*, 123253. https://doi.org/10.1016/j.memsci.2024.123253.

(95) Chen, Y.; Wang, Z.; Jennings, G. K.; Lin, S. Probing Pore Wetting in Membrane Distillation Using Impedance: Early Detection and Mechanism of Surfactant-Induced Wetting. *Environ. Sci. Technol. Lett.* **2017**, *4* (11), 505–510. https://doi.org/10.1021/acs.estlett.7b00372.

(96) Wang, Z.; Chen, Y.; Sun, X.; Duddu, R.; Lin, S. Mechanism of Pore Wetting in Membrane Distillation with Alcohol vs. Surfactant. *J. Membr. Sci.* **2018**, *559*, 183–195. https://doi.org/10.1016/j.memsci.2018.04.045.

(97) Lopez, K. P.; Nguyen, M.; McNally, D. P.; Neefe, S. R.; Ban, C.; Straub, A. P. Pore Wetting and Compaction in Pressure-Driven Distillation: Insights from Impedance Spectroscopy. *ACS EST Eng.* **2024**. https://doi.org/10.1021/acsestengg.4c00644.

(98) Zanini, S.; Barni, R.; Pergola, R. D.; Riccardi, C. Modification of the PTFE Wettability by Oxygen Plasma Treatments: Influence of the Operating Parameters and Investigation of the Ageing Behaviour. *J. Phys. Appl. Phys.* **2014**, *47* (32), 325202. https://doi.org/10.1088/0022-3727/47/32/325202.

(99) Lai, C.-L.; Liou, R.-M.; Chen, S.-H.; Huang, G.-W.; Lee, K.-R. Preparation and Characterization of Plasma-Modified PTFE Membrane and Its Application in Direct Contact Membrane Distillation. *Desalination* **2011**, *267* (2), 184–192. https://doi.org/10.1016/j.desal.2010.09.024.

(100) Giwa, A.; Yusuf, A.; Balogun, H. A.; Sambudi, N. S.; Bilad, M. R.; Adeyemi, I.; Chakraborty, S.; Curcio, S. Recent Advances in Advanced Oxidation Processes for Removal of Contaminants from Water: A Comprehensive Review. *Process Saf. Environ. Prot.* **2021**, *146*, 220–256. https://doi.org/10.1016/j.psep.2020.08.015.

(101) Li, D.; Wu, J.; Yang, S.; Zhang, W.; Niu, X.; Chen, Y.; Ran, F. Hydrophilicity and Anti-Fouling Performance of Polyethersulfone Membrane Modified by Grafting Block Glycosyl Copolymers *via* Surface Initiated Electrochemically Mediated Atom Transfer Radical Polymerization. *New J. Chem.* **2018**, *42* (4), 2692–2701. https://doi.org/10.1039/C7NJ04161F.

(102) Hirsch, U. M.; Teuscher, N.; Rühl, M.; Heilmann, A. Plasma-Enhanced Magnetron Sputtering of Silver Nanoparticles on Reverse Osmosis Membranes for Improved Antifouling Properties. *Surf. Interfaces* **2019**, *16*, 1–7. https://doi.org/10.1016/j.surfin.2019.04.003.

(103) Yu, S.; Wang, Y.; Sun, F.; Wang, R.; Zhou, Y. Novel Mpg-C3N4/TiO2 Nanocomposite Photocatalytic Membrane Reactor for Sulfamethoxazole Photodegradation. *Chem. Eng. J.* **2018**, *337*, 183–192. https://doi.org/10.1016/j.cej.2017.12.093.

(104) Xu, Z.; Wu, T.; Shi, J.; Teng, K.; Wang, W.; Ma, M.; Li, J.; Qian, X.; Li, C.; Fan, J. Photocatalytic Antifouling PVDF Ultrafiltration Membranes Based on Synergy of Graphene Oxide and TiO2 for Water Treatment. *J. Membr. Sci.* **2016**, *520*, 281–293. https://doi.org/10.1016/j.memsci.2016.07.060.

(105) Song, J.; Wang, X.; Yan, J.; Yu, J.; Sun, G.; Ding, B. Soft Zr-Doped TiO2 Nanofibrous Membranes with Enhanced Photocatalytic Activity for Water Purification. *Sci. Rep.* **2017**, *7* (1), 1636. https://doi.org/10.1038/s41598-017-01969-w.

(106) Li, N.; Lu, X.; He, M.; Duan, X.; Yan, B.; Chen, G.; Wang, S. Catalytic Membrane-Based Oxidation-Filtration Systems for Organic Wastewater Purification: A Review. *J. Hazard. Mater.* **2021**, *414*, 125478. https://doi.org/10.1016/j.jhazmat.2021.125478.

(107) Zhao, Y.; Lu, D.; Xu, C.; Zhong, J.; Chen, M.; Xu, S.; Cao, Y.; Zhao, Q.; Yang, M.; Ma, J. Synergistic Oxidation - Filtration Process Analysis of Catalytic CuFe2O4 - Tailored Ceramic Membrane Filtration via Peroxymonosulfate Activation for Humic Acid Treatment. *Water Res.* **2020**, *171*, 115387. https://doi.org/10.1016/j.watres.2019.115387.

(108) Chen, S.-L.; Wang, A.-J.; Dai, C.; Benziger, J. B.; Liu, X.-C. The Effect of Photonic Band Gap on the Photo-Catalytic Activity of Nc-TiO2/SnO2 Photonic Crystal Composite Membranes. *Chem. Eng. J.* **2014**, *249*, 48–53. https://doi.org/10.1016/j.cej.2014.03.075.

(109) Romanos, G. E.; Athanasekou, C. P.; Likodimos, V.; Aloupogiannis, P.; Falaras, P. Hybrid Ultrafiltration/Photocatalytic Membranes for Efficient Water Treatment. *Ind. Eng. Chem. Res.* **2013**, *52* (39), 13938–13947. https://doi.org/10.1021/ie303475b.

(110) Pathak, R.; Rozyyev, V.; Shevate, R.; Mane, A. U.; Elam, J. W. Controlling Nanoscale Pore Size and Wall Composition in Polycarbonate Membranes via Atomic Layer Deposition and Sequential Infiltration Synthesis: Implications for High

Water Permeance. *ACS Appl. Nano Mater.* **2023**, *6* (19), 17869–17880. https://doi.org/10.1021/acsanm.3c03161.

(111) Xu, Q.; Yang, Y.; Wang, X.; Wang, Z.; Jin, W.; Huang, J.; Wang, Y. Atomic Layer Deposition of Alumina on Porous Polytetrafluoroethylene Membranes for Enhanced Hydrophilicity and Separation Performances. *J. Membr. Sci.* **2012**, *415–416*, 435–443. https://doi.org/10.1016/j.memsci.2012.05.031.

(112) George, S. M. Atomic Layer Deposition: An Overview. *Chem. Rev.* **2010**, *110* (1), 111–131. https://doi.org/10.1021/cr900056b.

(113) Johnson, R. W.; Hultqvist, A.; Bent, S. F. A Brief Review of Atomic Layer Deposition: From Fundamentals to Applications. *Mater. Today* **2014**, *17* (5), 236–246. https://doi.org/10.1016/j.mattod.2014.04.026.

(114) Yasmeen, S.; Ryu, S. W.; Lee, S.-H.; Lee, H.-B.-R. Atomic Layer Deposition Beyond Thin Film Deposition Technology. *Adv. Mater. Technol.* **2023**, *8* (20), 2200876. https://doi.org/10.1002/admt.202200876.

(115) Krumpolec, R.; Cameron, D. C.; Homola, T.; Černák, M. Surface Chemistry and Initial Growth of Al2O3 on Plasma Modified PTFE Studied by ALD. *Surf. Interfaces* **2017**, *6*, 223–228. https://doi.org/10.1016/j.surfin.2016.10.005.

(116) Elam, J. W.; Xiong, G.; Han, C. Y.; Wang, H. H.; Birrell, J. P.; Welp, U.; Hryn, J. N.; Pellin, M. J.; Baumann, T. F.; Poco, J. F.; Satcher, J. H. Atomic Layer Deposition for the Conformal Coating of Nanoporous Materials. *J. Nanomater.* **2006**, *2006* (1), 064501. https://doi.org/10.1155/JNM/2006/64501.

(117) Bossa, N.; Chaurand, P.; Vicente, J.; Borschneck, D.; Levard, C.; Aguerre-Chariol, O.; Rose, J. Micro- and Nano-X-Ray Computed-Tomography: A Step Forward in the Characterization of the Pore Network of a Leached Cement Paste. *Cem. Concr. Res.* **2015**, *67*, 138–147. https://doi.org/10.1016/j.cemconres.2014.08.007.

(118) Singh, J.; Khan, S. A.; Shah, J.; Kotnala, R. K.; Mohapatra, S. Nanostructured TiO2 Thin Films Prepared by RF Magnetron Sputtering for Photocatalytic Applications. *Appl. Surf. Sci.* **2017**, *422*, 953–961. https://doi.org/10.1016/j.apsusc.2017.06.068.

(119) Tayade, R. J.; Natarajan, T. S.; Bajaj, H. C. Photocatalytic Degradation of Methylene Blue Dye Using Ultraviolet Light Emitting Diodes. *Ind. Eng. Chem. Res.* **2009**, *48* (23), 10262–10267. https://doi.org/10.1021/ie9012437.

(120) Nakata, K.; Fujishima, A. TiO2 Photocatalysis: Design and Applications. *J. Photochem. Photobiol. C Photochem. Rev.* **2012**, *13* (3), 169–189. https://doi.org/10.1016/j.jphotochemrev.2012.06.001.

(121) Jantawasu, P.; Sreethawong, T.; Chavadej, S. Photocatalytic Activity of Nanocrystalline Mesoporous-Assembled TiO2 Photocatalyst for Degradation of Methyl Orange Monoazo Dye in Aqueous Wastewater. *Chem. Eng. J.* **2009**, *155* (1), 223–233. https://doi.org/10.1016/j.cej.2009.07.036.

(122) Liu, G.; Wang, X.; Chen, Z.; Cheng, H.-M.; Lu, G. Q. (Max). The Role of Crystal Phase in Determining Photocatalytic Activity of Nitrogen Doped TiO2. *J. Colloid Interface Sci.* **2009**, *329* (2), 331–338. https://doi.org/10.1016/j.jcis.2008.09.061.

(123) Chu, L.; Qin, Z.; Yang, J.; Li, X. Anatase TiO2 Nanoparticles with Exposed {001} Facets for Efficient Dye-Sensitized Solar Cells. *Sci. Rep.* **2015**, *5* (1), 12143. https://doi.org/10.1038/srep12143.

(124) Sun, L.; Yuan, G.; Gao, L.; Yang, J.; Chhowalla, M.; Gharahcheshmeh, M. H.; Gleason, K. K.; Choi, Y. S.; Hong, B. H.; Liu, Z. Chemical Vapour Deposition. *Nat. Rev. Methods Primer* **2021**, *1* (1), 1–20. https://doi.org/10.1038/s43586-020-00005-y.

(125) Carlsson, J.-O.; Martin, P. M. Chapter 7 - Chemical Vapor Deposition. In *Handbook of Deposition Technologies for Films and Coatings (Third Edition)*; Martin, P. M., Ed.; William Andrew Publishing: Boston, 2010; pp 314–363. https://doi.org/10.1016/B978-0-8155-2031-3.00007-7.

(126) Akbari, R.; Antonini, C. Contact Angle Measurements: From Existing Methods to an Open-Source Tool. *Adv. Colloid Interface Sci.* **2021**, *294*, 102470. https://doi.org/10.1016/j.cis.2021.102470.

(127) Ul-Hamid, A. *A Beginners' Guide to Scanning Electron Microscopy*; Springer International Publishing: Cham, 2018. https://doi.org/10.1007/978-3-319-98482-7.

(128) Zhou, W.; Apkarian, R. P.; Wang, Z. L.; Joy, D. Fundamentals of Scanning Electron Microscopy.

(129) Smith, B. C. *Fundamentals of Fourier Transform Infrared Spectroscopy*; CRC Press, 2011.

(130) Ismail, A. A.; van de Voort, F. R.; Sedman, J. Chapter 4 Fourier Transform Infrared Spectroscopy: Principles and Applications. In *Techniques and Instrumentation in Analytical Chemistry*; Paré, J. R. J., Bélanger, J. M. R., Eds.; Instrumental Methods in Food Analysis; Elsevier, 1997; Vol. 18, pp 93–139. https://doi.org/10.1016/S0167-9244(97)80013-3.

(131) Gengenbach, T. R.; Major, G. H.; Linford, M. R.; Easton, C. D. Practical Guides for X-Ray Photoelectron Spectroscopy (XPS): Interpreting the Carbon 1s Spectrum. *J. Vac. Sci. Technol. A* **2021**, *39* (1), 013204. https://doi.org/10.1116/6.0000682.

(132) Greczynski, G.; Hultman, L. A Step-by-Step Guide to Perform x-Ray Photoelectron Spectroscopy. *J. Appl. Phys.* **2022**, *132* (1), 011101. https://doi.org/10.1063/5.0086359.

(133) Stevie, F. A.; Donley, C. L. Introduction to X-Ray Photoelectron Spectroscopy. *J. Vac. Sci. Technol. A* **2020**, *38* (6), 063204. https://doi.org/10.1116/6.0000412.

Appendix 1: Overview of materials characterization methods

Static Contact angle

Static contact angle is a method that determines surface hydrophilicity. Contact angle can also be referred to as a wetting angle. As established in equation 4.0, the wettability of a surface is determined by the interfacial energies between solid-gas, liquid-gas and liquid-solid. For our studies, we utilized a static contact angle measurement, where we would drop a 10μL of water on the surface and measure the contact angle. If the angle was less than 90° it would be considered hydrophilic and if it is more than 90° it is hydrophobic. Contact angle is usually used as a first step in determining changes to a surface.[126]

Scanning electron microscopy

Scanning electron microscopy (SEM) was utilized to image membrane samples and provided a qualitative image of how our membranes were being impacted by our treatments. In SEM, a sample is exposed with a beam of electrons that interact with the atoms of the sample. These interactions lead to the production of different signals like secondary electrons and back scattered electrons. Secondary electrons signals are created due to inelastic interactions between the beam electrons and the valence electrons of the sample and backscatter electrons signals are from the elastic interactions between the beam and the samples atoms nucleus. Backscattered electrons can provide information about variations in local chemical contribution. Figure 28 provides a schematic of the electron processes The images in this thesis were done with secondary electron imaging. [127,128]

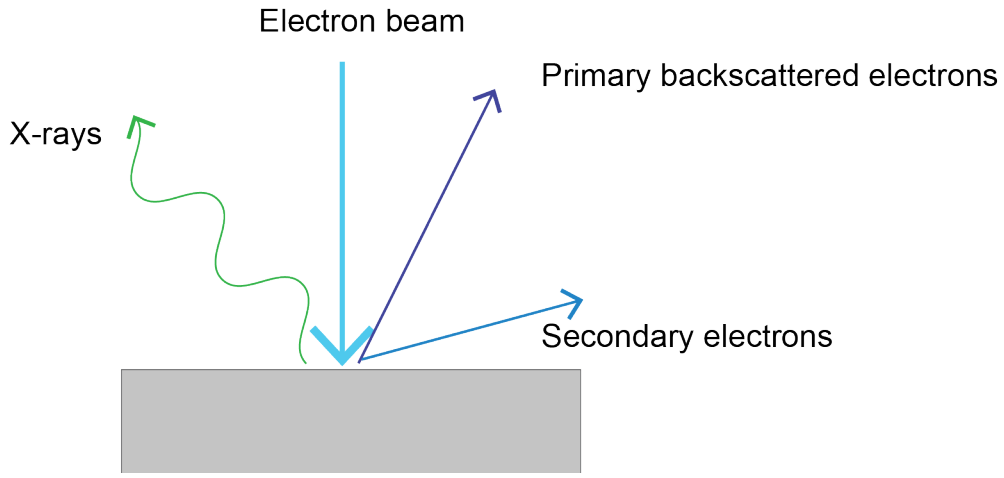

Figure 28: Schematic detailing electron processes in scanning electron microscopy. An electron beam hits the sample and excites the electrons leading to emission of different energies, X-rays, primary back scattering, and secondary electrons.

X-ray photoelectron spectroscopy

X-ray photoelectron spectroscopy (XPS) is an x-ray-based technique that studies the surface composition of materials. Samples are irradiated by x-ray leading to the excitation of atoms on the surface of the material leading to the eventual ejection of electrons from the atoms, otherwise known as photoemission, Figure 29. The kinetic energy of the ejected electrons is measured, and binding energy is calculated based off the kinetic energy measured, initial x-ray energy, and work function of the detector, Equation SI 3. The energy of the emitted electrons is reliant upon the binding environment. XPS analysis can be separated into survey or core analysis. In survey analysis, information about the overall composition of the sample can be deduced. Figures 17A and 27A illustrate what a survey XPS spectra looks like, then Figures 9A and 15A are atomic percent summaries based on the information provided from XPS surveys. In core analysis, information about the binding state of atoms can be determined. Figures 9 C-E are carbon core scans of

polymer membranes. XPS is limited to the first 10 nm of a material's surface due to a limited photoelectron escape depth. The electrons that are emitted in XPS can only travel a short distance through a sample before losing energy.[131,132]

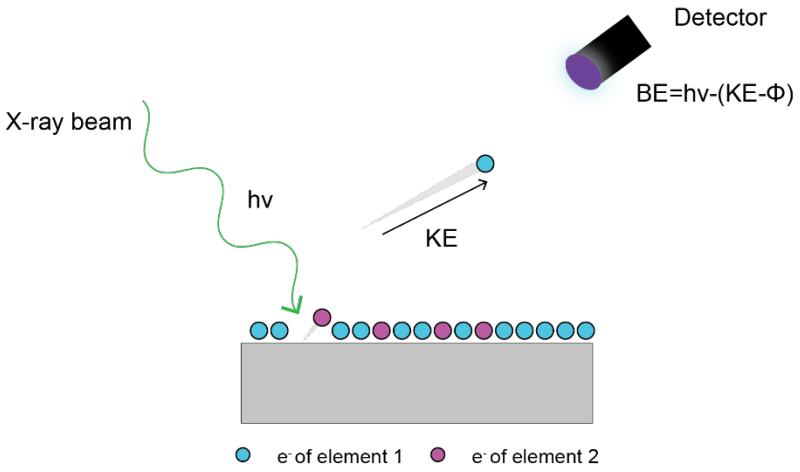

Figure 29: Schematic of x-ray photoelectron spectroscopy. X-ray's excite electrons on surface of material and they leave the surface with a specific kinetic energy. The electrons are collected at the detector which calculates the binding energy.

Fourier transform infrared spectroscopy

Fourier transform infrared spectroscopy (FTIR) measures how infrared light interacts with materials. When exposed to light, molecules can absorb it at different wavelengths. When a material absorbs IR light the molecules within the material experience a net change in its dipole moment as the molecules move. Dipole moments occur in molecules due to differences in atom polarity. The peaks that appear in IR are due to this change in dipole moment. For IR analysis in this thesis, most of the measurements were done with attenuated total reflectance IR. In ATR-FTIR, the sample is placed on a crystal, IR light passes through a crystal, this reflects internally at the crystal-sample interface, IR light

goes into the sample and is absorbed causing a dipole moment. ATR-FTIR analyzes a penetration depth between 0.5 and 5 μm and provides information on the bulk structure of a material. [129,130]

Grazing incidence wide angle x-ray scattering

Grazing incidence wide angle x-ray scattering (GIWAXS) investigates structural properties like crystallinity of thin films and surfaces. In GIWAXS, x-rays hit a sample at a low angle from the surface to ensure that the x-ray is interacting with the top surface rather than penetrating the bulk sample. The x-ray scatters on the near surfaces as it encounters different crystalline regions on the surface and is collected by a detector which provides analysis of the diffraction data. Typically, information about the crystalline, texture and phase transitions can be gathered from the GIWAXS data.

Nano x-ray computed tomography

Nano x-ray computed tomography (XCT) provides information about the internal structure of materials at nanometer resolution. In XCT, x-rays penetrate through a sample and sample properties such as composition, structure and density will cause different interactions of the x-ray through the sample. The x-rays are detected and then an image is able to be produced. [117]

Appendix 2: List of coauthorships and contributions

1. Lopez, K. P.; Wang, R.; Hjelvik, E. A.; Lin, S.; Straub, A. P. Toward a Universal Framework for Evaluating Transport Resistances and Driving Forces in Membrane-Based Desalination Processes. *Science Advances* *9* (1), eade0413. https://doi.org/10.1126/sciadv.ade0413.

   E.A. Hjelvik provided explanation on summary of transport through air membranes and provided support in the creation of Figure 3A

2. Mungan, A. L.; Hjelvik, E. A.; Straub, A. P.; Korak, J. A. A Hybrid Anion Exchanger with Nanoscale Zero Valent Iron for Trace Hexavalent Chromium Removal from Drinking Water. *Environ. Sci.: Adv.* **2024**. https://doi.org/10.1039/D4VA00246F.

   E.A. Hjelvik provided XPS (core and survey) and SEM-EDS analysis of resin samples and aided in synthesis of zerovalent iron synthesis

3. Roth, R. S.; Birnhack, L.; Avidar, M.; Hjelvik, E. A.; Straub, A. P.; Epsztein, R. Effect of Solution Ions on the Charge and Performance of Nanofiltration Membranes. *npj Clean Water* **2024**, *7* (1), 25. https://doi.org/10.1038/s41545-024-00322-9.

   E.A. Hjelvik provided XPS core analysis of Na and Cl on polyamide samples.

4. Lee, S.; Larris, O.; Hjelvik, E. A.; Straub, A. P. High Pressure Resistance in Omniphobic Distillation Membranes with Re-Entrant Nanostructures. *NanoLetters*, **Submitted**

   E.A. Hjelvik provided XPS survey analysis on membranes

Supplementary information

Figures

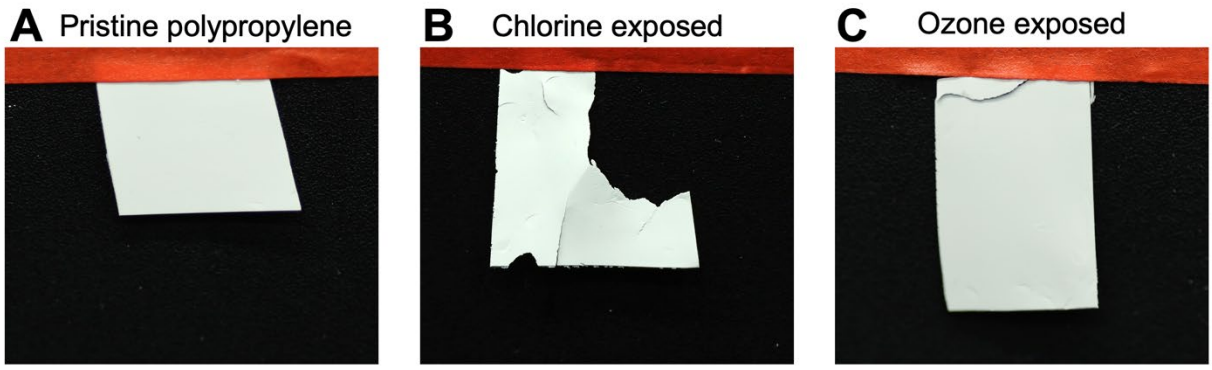

Figure SI 1: Digital photographs of (A) pristine polypropylene (PP) membranes, (B) PP membranes after exposure to XX chorine, and (C) PP membrane after exposure to XX ozone.

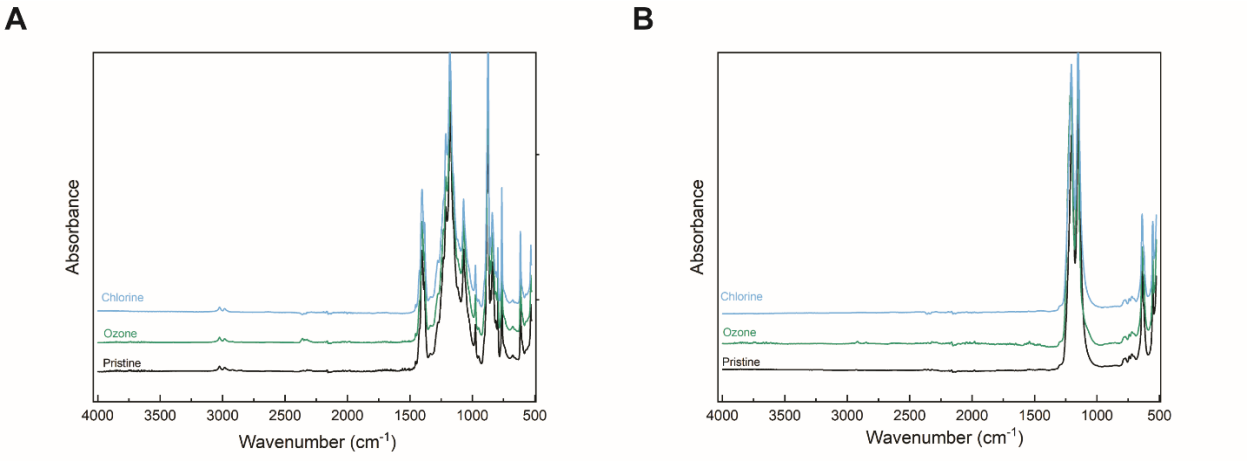

Figure SI 2: Attenuated total reflectance Fourier transform infrared (ATR-FTIR) spectroscopy scans of (A) polyvinylidene fluoride and (B) polytetrafluoroethylene

membranes before and after exposure to ozone and chlorine. ATR-FTIR spectra reflects membranes after 10000 ppm chlorine for 72 h or 15 ppm ozone for 3 h.

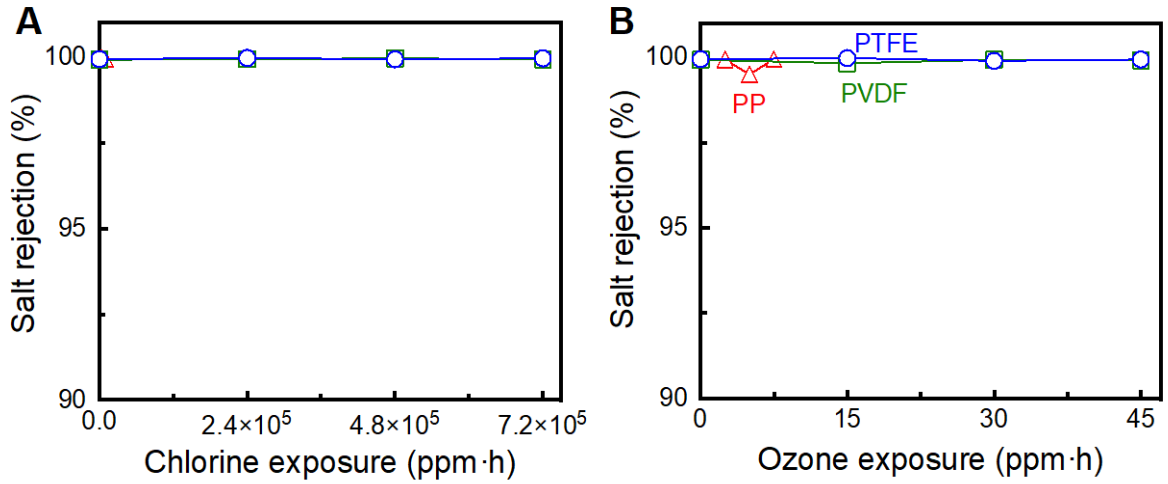

Figure SI 3: Water flux as a function of oxidant exposure for polytetrafluorethylene (PTFE), polyvinylidene fluoride (PVDF), and polypropylene (PP) membranes after exposure to a 10000 ppm chlorine solution (A) and a 15 ppm ozone solution (B) through a direct contact membrane distillation cell. Temperatures were 60 ºC and 20 ºC through the feed and permeate channels, respectively.

Table SI 1: Summary of membrane properties. Nominal pore size, thickness, porosity, and support material information were obtained from the manufacturers. Static water contact angle was measured as described in the materials and methods.

	PTFE	**PVDF**	**PP**
Structure	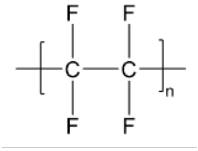	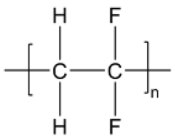	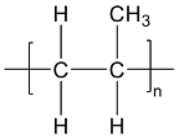
Nominal Pore Size (µm)	0.2	0.22	0.2
Total Thickness (µm)	76-152	125	170
Contact Angle (°)	131 ± 1.49	121 ± 1.51	140 ± 0.971
Porosity (%)	70-90	75	<90
Support Material	Polypropylene	-	-

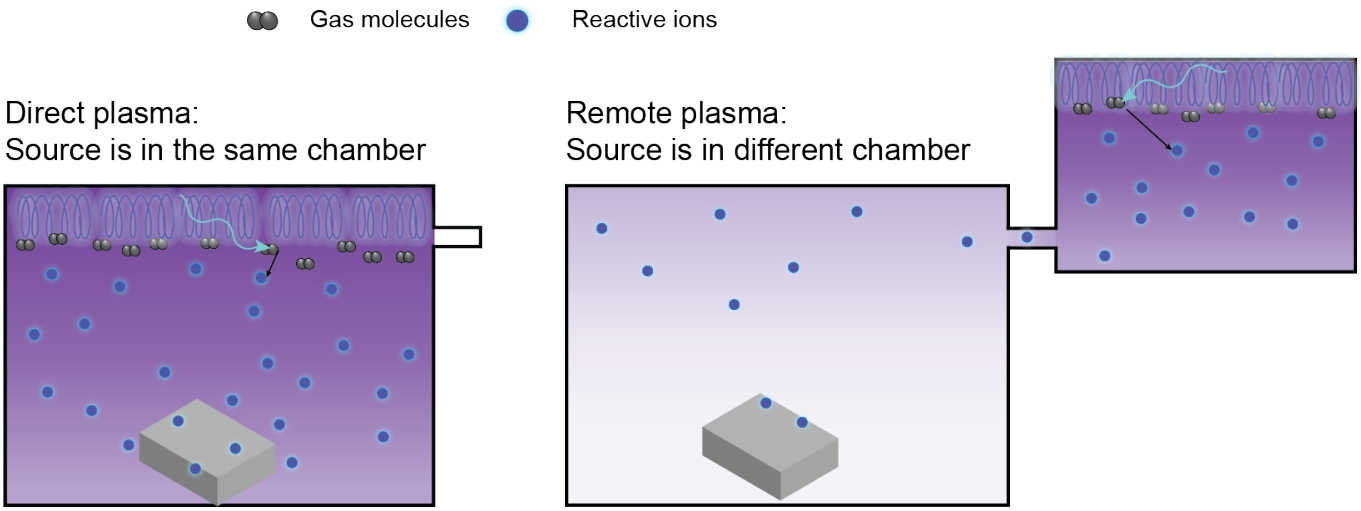

Figure SI 4: Direct vs remote plasma. Direct plasma occurs in the same chamber as the sample while remote plasma occurs in a different chamber then diffuses into the material chamber.

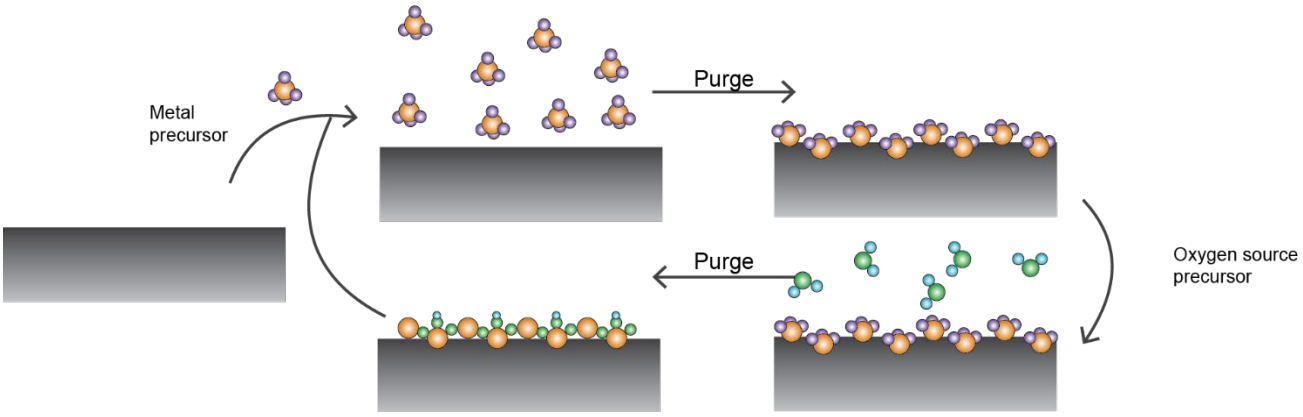

Figure SI 5: Schematic of atomic layer deposition.

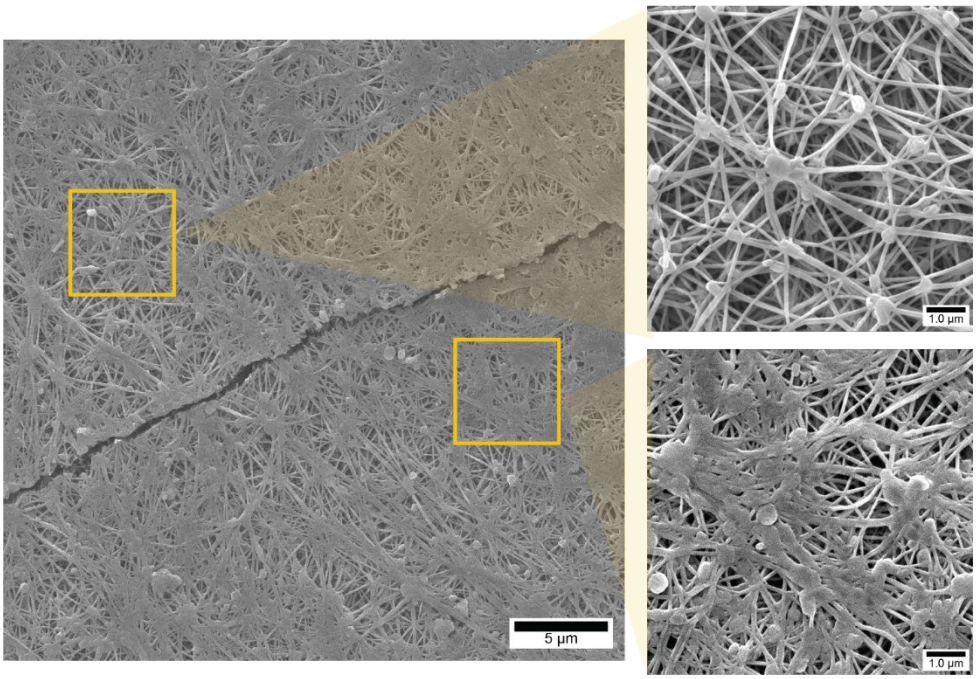

Figure SI 6: 1000TiO_2-PTFE membrane shows uneven growth of TiO_2 on the membrane surface.

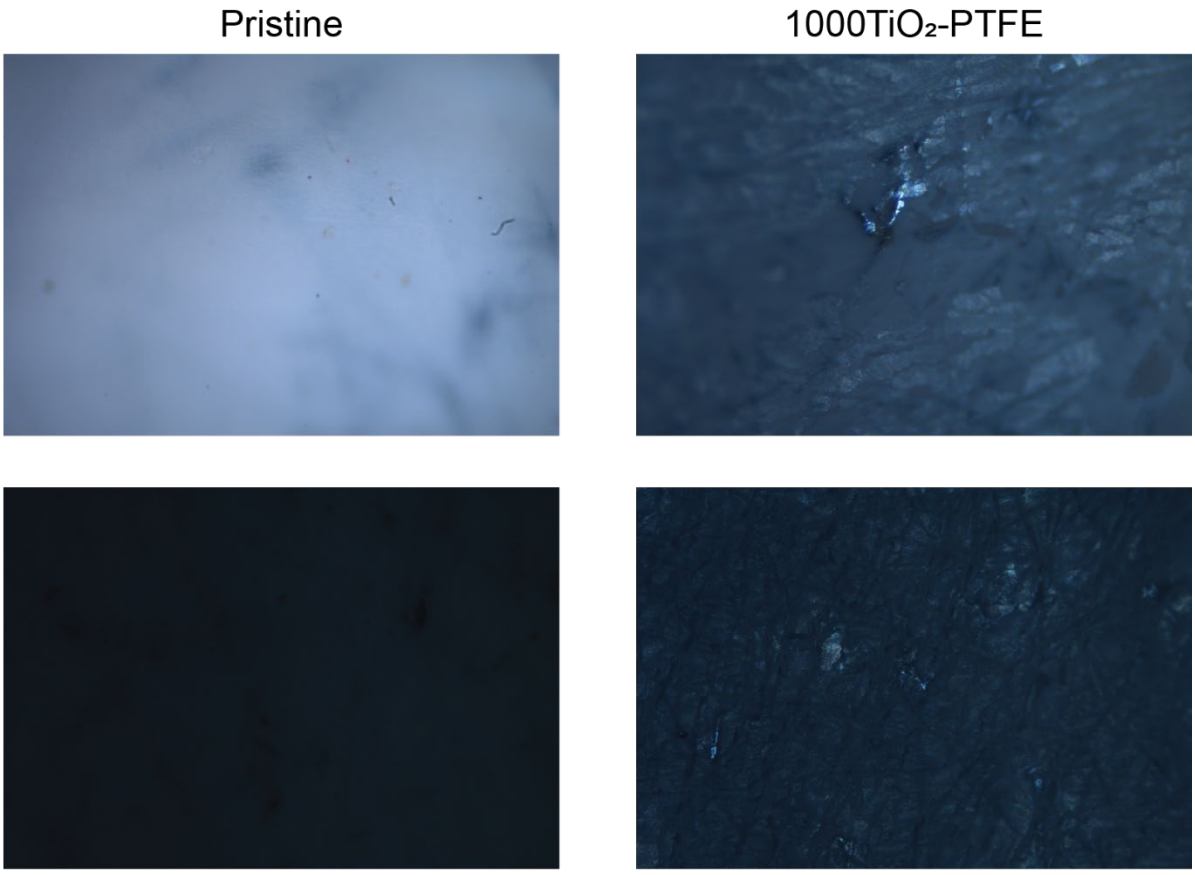

Figure SI 7: Polarized optical microscopy images of pristine PTFE (left) and 1000TiO2-PTFE (right).

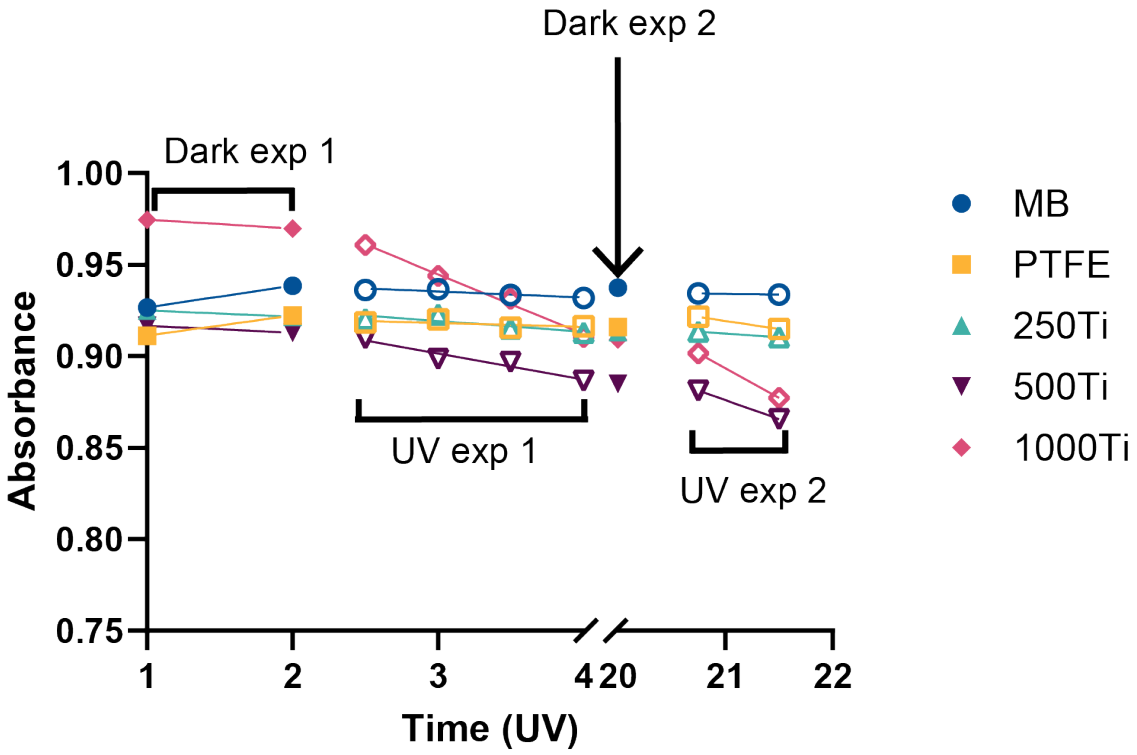

Figure SI 8: Raw UV absorbance data of MB study.

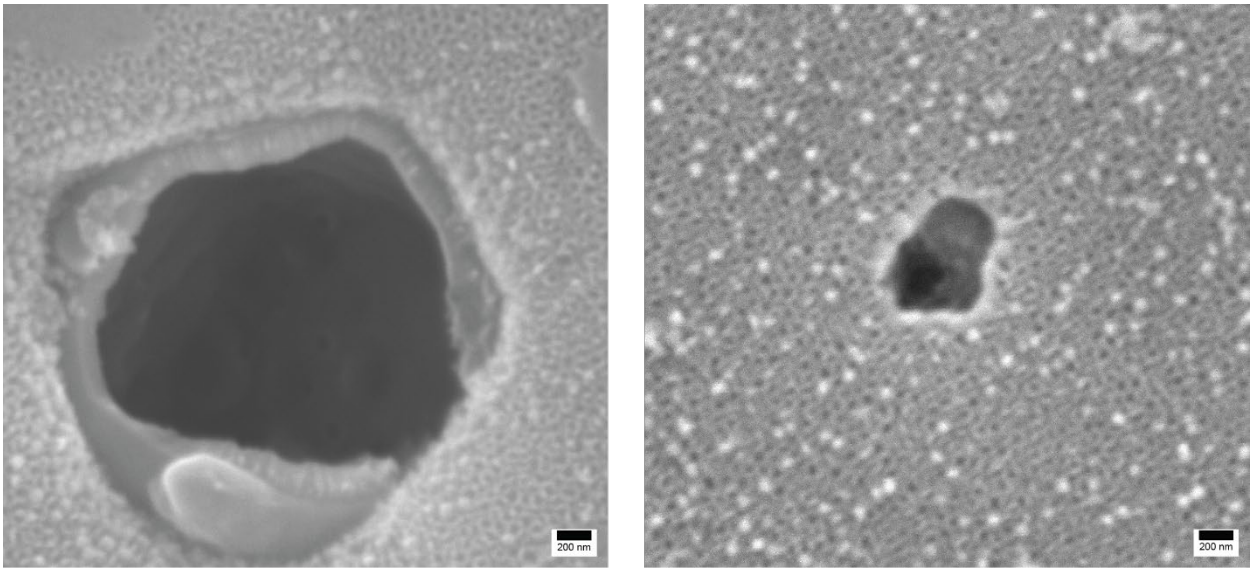

Figure SI 9: Defects observed in asymmetric AAO membranes.

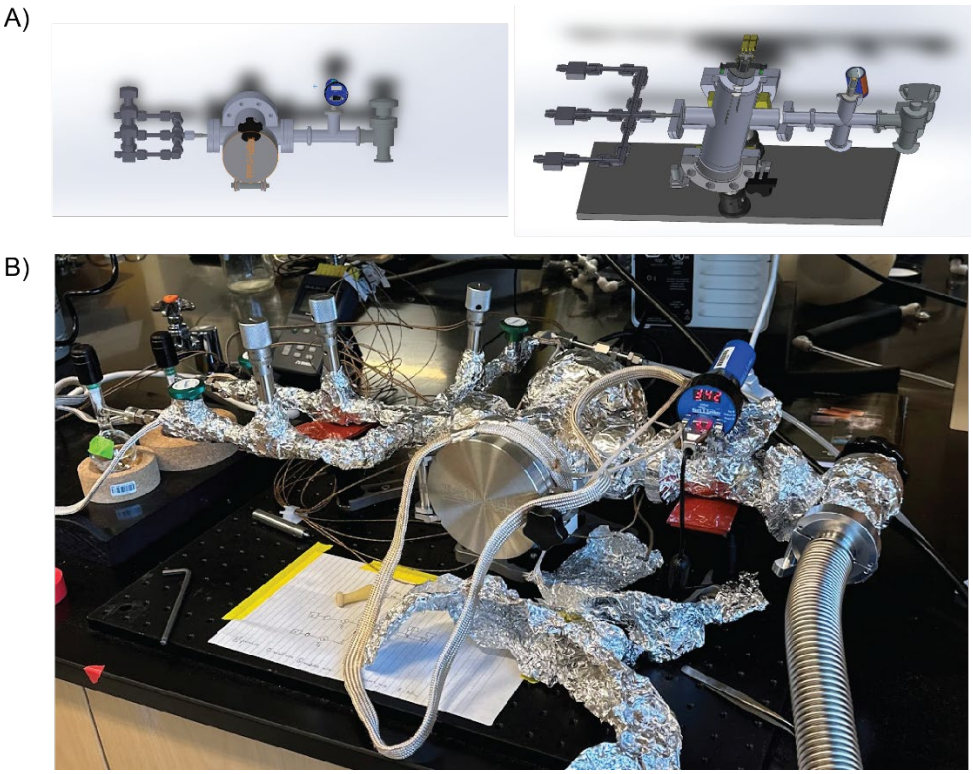

Figure SI 10: A) Design iterations of custom chemical vapor deposition system. B) Built custom chemical vapor deposition system.

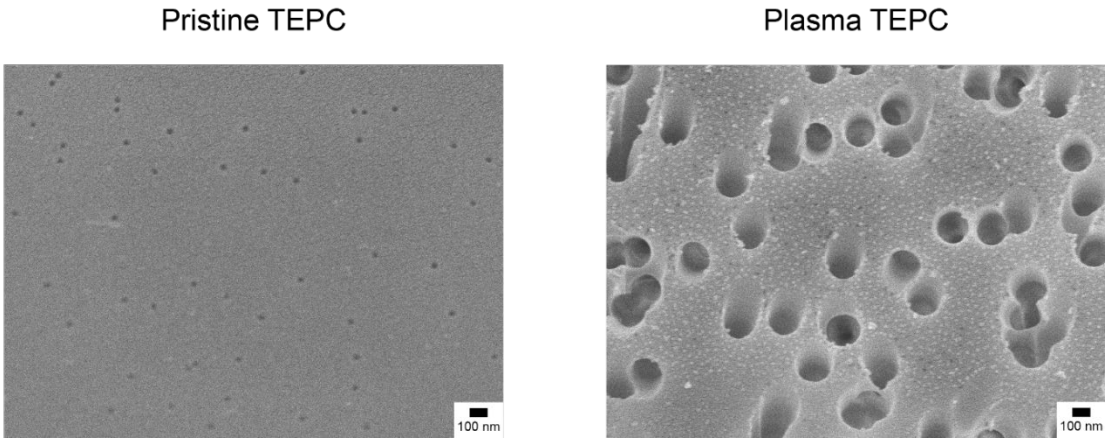

Figure SI 11: Changes in tracked etched polycarbonate after plasma treatment.

Equations

Purcell wetting

For polymeric membranes such as PTFE, PVDF, and PP where the pore is considered voids between fibers, models such as the Purcell model, equation 4.0, are more accurate. Similarly to the Young-Laplace LEP, the Purcell model is based upon the contact angle (θ_{eq}), surface tension of the solution ($\gamma_{LV,}$), and pore radius (r). But to account for how the pore is impacted by polymer fiber radius, R, and the angle below horizontal at which the liquid meniscus pins prior to break-through. [47]

$$LEP = \frac{-2\gamma_{LV}}{r}\frac{\cos(\theta_{eq}+\alpha)}{1+\frac{R}{r(1-\cos\alpha)}} \quad \text{Eq .SI 1}$$

Equation SI 1: Purcell liquid entry pressure for fibrous membranes

Thermodynamic wetting criterion of air-gap membranes:

The thermodynamic wetting criterion can be used to determine the membrane thickness and pore size in which the two liquid-vapor menisci present in air-gap membranes do not touch: where *l* is the length of the pore, r is the pore radius, α is the equilibrium contact angle on the membrane surface, and θ is the geometric angle between the liquid-vapor interface and a line normal to the interface which depends on the mechanical equilibrium established between the hydraulic pressure drop across the membrane and the traction force from surface tension.[22,97]

$$\frac{l}{r} > \frac{2}{3(cos\theta - cos\alpha)}\left[\frac{1}{1+sin\theta} + sin\theta\right] \quad \text{Eq . SI 2}$$

Equation SI 2: Wetting criterion for air filled that establishes minimum pore lengths

Relationship between binding energy and kinetic energy in XPS

BE is defined as the binding energy, hv corresponds to the photo energy, KE is the kinetic energy and ϕ is the instrument work function.[133]

$$BE = h\nu - (KE - \phi)$$

Equation SI 3: Equation relating binding energy and kinetic energy in x-ray photoelectron spectroscopy.